NEW METHODS FOR DYNAMIC NUCLEAR POLARIZATION IN INSULATING SOLIDS: THE OVERHAUSER EFFECT AND TIME DOMAIN TECHNIQUES

by

Thach V. Can

M.Sc., Physics (2011)
Florida State University

Submitted to the Department of Chemistry
in Partial Fulfillment of the Requirement for the Degree of
Doctor of Philosophy in Chemistry

at the
Massachusetts Institute of Technology
June 2017

Signature redacted

Signature of Author_____
Department of Chemistry
April 28, 2017

Signature redacted

Certified by_____
Robert G. Griffin
Professor of Chemistry
Thesis Supervisor

Signature redacted

Accepted by_____
Robert W. Field
Haslam and Dewey Professor of Chemistry
Chairman, Department Committee on Graduate Students

This doctoral thesis has been examined by a committee of the department of chemistry as follows:

Signature redacted

Professor Keith A. Nelson
Chairman

Signature redacted

Professor Robert G. Griffin
Thesis Supervisor

Signature redacted

Professor Troy Van Voorhis
Thesis Committee Member

New Methods for Dynamic Nuclear Polarization in Insulating Solids: the Overhauser Effect and Time Domain Techniques

by

Thach V. Can
Submitted to the Department of Chemistry
on May 12th, 2017 in Partial Fulfillment of the Requirement for the
Degree of Doctor of Philosophy in Chemistry

Abstract

Dynamic nuclear polarization (DNP) is now established as a powerful technique for improving the sensitivity of NMR signals by several orders of magnitude, enabling otherwise impossible experiments. Unfortunately, the enhancements obtained at high magnetic fields (> 9 T) are only a small fraction of the theoretical limit due to the fact that current DNP mechanisms, including the cross effect and solid effect, utilize continuous wave (CW) microwave irradiation, and scale unfavorably with B_0. This has motivated us to develop new DNP methods that do not suffer from the same field dependences.

Our first attempt resulted in the observation of the Overhauser effect in insulating solids doped with 1,3-bisdiphenylene-2-phenylallyl (BDPA) or sulfonated-BDPA (SA-BDPA) radical. As opposed to all other CW DNP mechanisms, the enhancement of the OE in insulating solids scales favorably with B_0, increasing in magnitude in going from 5 T, to 9.4 T, to 14.1 T, and to 18.8 T. This finding sheds a new light on the seemingly well-understood Overhauser effect.

Our second approach is to perform time domain or pulsed DNP, which differs fundamentally from CW DNP, and like CP and INEPT transfers, is in principle independent of B_0. In particular, we have investigated the performance of two related pulse sequences including the nuclear orientation via electron spin locking (NOVEL) and integrated solid effect (ISE) at magnetic fields ranging from 0.35 T to 3.35 T. The NOVEL pulse sequence relies on a matching condition between the nuclear Larmor frequency and the electron Rabi frequency, resulting in a fast polarization transfer from electron to protons (hundreds of ns time scale). Furthermore, we showed that adding amplitude modulation to the microwave field, analogous to a ramped CP experiment, led to longer mixing time (μs time scale) but improved the enhancement by a factor of 1.4 to 2. Finally, we implemented a new version of the integrated solid effect (ISE) by modulating the microwave frequency instead of sweeping the B_0 which is technically challenging in high field superconducting magnets. In comparison to NOVEL, ISE gives similar DNP enhancement even far below the NOVEL condition. Our study sets the foundation for further development of time domain DNP at high fields.

Thesis Supervisor: Robert G. Griffin
Title: Professor of Chemistry and Director of the Francis Bitter Magnet Laboratory

Dedicated to my parents, Van Can and Oanh Nguyen.

Table of Contents

List of Figures

Acknowledgements

I would like to thank my thesis advisor, Professor Robert Griffin, for his guidance and support. The diverse and flexible research environment that he creates has been crucial to my academic development. I wish to carry on some of his relentless enthusiasm towards science.

A big part of my thesis was resulted from fruitful collaborations. I have been fortunate to work with and learn from many world-class scientists at Bruker BioSpin Corporation (Dr. Ralph Weber, Dr. Marc Caporini, Dr. Melanie Rosay, Leo Tometich, Dr. Ivan Sergeyev, Dr. James Kempf, and Dr. Kalina Ranguelova); at the National High Magnetic Field Laboratory (Dr. Johannes McKay, Peter Gorkov, Bianca Trociewitz, Dr. Thierry Dubroca, Dr. Han van Tol, and Prof. Stephen Hill); at Weizmann Institute of Science (Prof. Shimon Vega, and Dr. Frederic Mentink-Vigier); at Utrecht University (Prof. Marc Baldus); and at MIT (Dr. Joseph Walish, Dr. Graham Sazama, Dr. Derek Frantz, Dr. Sudheer Jawla, Prof. Timothy Swager, and Prof. Richard Temkin). In particular, I would like to express my special gratitude to Ralph, Marc Caporini, and Johannes. Ralph has been a great mentor in EPR spectroscopy and helped me with many pulsed DNP experiments. I had a great time working with Marc on the Overhauser effect. Working with him made me a more carful experimentalist and helped me gain a full handle on CW DNP experiments before delving into pulsed DNP. Johannes has taught me quite a few things about high frequency microwave in the short amount of time working together.

The interactions I have had with members of the Griffin's group (Qing Zhe Ni, Dr. Eugenio Daviso, Dr. Evgeny Markhasin, Dr. Albert Smith, Dr. Yongchao Su, Dr. Bjorn Corzilius, Dr. Loren Andreas, Dr. Michael Colvin, Dr. Kevin Donovan) have been an important part of my training as well. Qing, Eugenio, and Evgeny showed me the first demonstration of the power of DNP on their 380 MHz/250 GHz system. Seeing the DNP-enhanced signal blowing up to full screen made it easier my decision to study DNP. Andy made sure that I was able to run his 140 GHz system comfortably on my own before leaving the lab. I am also grateful for the technical staff (Ajay Thakkar, Jeff Bryant, Michael Mullins, Dr. David Ruben) and the administrative staff (Jillian Haggerty, Wanda Hernandez) for keeping everything in working order.

My wife, Qing Zhe Ni, has been a big influence since the first day we met at Florida State University. I thank her for always believing in me and encouraging me to grow to my full potential. Above all, she gives me a lot of love and support and together with Lily, a 5 lb.

little Pomeranian a.k.a. "the rat", they have been my biggest cheerleaders everyday in the lab.

I am indebted to my parents in law, Dr. DaQun Ni and Shijie Shen, for their love and support; and my son, Bright Can, for bringing so much joy and laughter to my life. Together with my wife, they have made USA my second home. I would also like to thank my extended family in Vietnam and China for their never-ending love. My group of friends in Vietnam (Thuy Thai, Hanh Le, Ha Nguyen, Phuong Nguyen, Hung Luong, Nam Nguyen, Tuyen Do, Lich Nguyen, and Thanh Nguyen) has always been rooting for me when I succeed and picking me up when I tumble.

I would like to thank Prof. Timothy Cross at the National High Magnetic Field Laboratory and Florida State University for teaching me my first NMR lessons and for his continuing support and advice.

Finally, I can't thank my parents enough for making sure that my education always comes first and at the same time giving me a lot of freedom. I thank my dad for inadvertently getting me interested in how things work and encouraging me to pursue science.

Chapter 1: Introduction

1.1 Motivation

Nuclear magnetic resonance (NMR) is a powerful, nondestructive technique used in physics, chemistry, structural biology, and material science. However, the technique is based on the polarization of a spin ensemble at thermal equilibrium dictated by the Boltzmann distribution, thus the sensitivity of NMR experiments is extremely low compared to other analytical methods such as infrared spectroscopy or X-ray diffraction. Moreover, the sensitivity of NMR signals from solid samples is attenuated further by other factors such as the limitation in sample volume, linebroadening by anisotropic couplings and the detection of nuclei with low gyromagnetic ratios.

Developments of solid-state NMR (ssNMR) in the last ~60 years have evolved heavily around improving the sensitivity. Revolutions of ssNMR in term of sensitivity date back to late 1950s with the introduction of cross polarization (CP) experiment by Hartmann and Hahn[1] around the same time with the invention of magic angle spinning (MAS) experiments by Andrew[2] and independently by Lowe[3]. In addition, advances in magnet technology provide higher and higher magnetic fields, recently reaching the GHz range for ^{1}H NMR frequencies. Finally, dynamic nuclear polarization (DNP) has revolutionized the field of MAS ssNMR in the last two decades and is, undoubtedly, going to do so in the coming years.

Dynamic nuclear polarization was first postulated by Overhauser[4] in 1953 and experimentally confirmed soon after by Carver and Slichter on ^{7}Li metal[5] and then on ^{23}Na metal, ^{23}Na in liquid ammonia[6]. In such experiments, the polarization of nuclei was enhanced by saturating the allowed electronic transitions. The effect, known as Overhauser effect, is mediated by time-dependent dipolar or scalar interactions. Until our recent discovery, it had long been a conventional wisdom that such effect is operative only in conductors or solutions where the electrons are mobile. In contrast, for dielectric solids, as it is the case for biological samples, DNP is mediated by the solid effect (SE), cross effect (CE) and thermal mixing (TM). The SE was discovered by Jeffries[7, 8] and was widely utilized to prepare polarized targets[9]. However, it was not used in contemporary DNP experiments until recently due to the B_0^{-2} dependence and the lack of high power microwave sources. The CE, first described by Kessenikh[10] and later by Hwang and Hill[11, 12], became dominant at high field especially after the development of biradicals[13]. The B_0^{-1}

dependence in CE makes it much more efficient at high magnetic field compared to SE. Thermal mixing[14-16] is the dominant mechanism when the interaction between electrons is large and the EPR spectrum is homogeneously broadened. As a result of the high concentration of radicals often leads to severe NMR linebroadening.

Recent advancements in instrumentations enable DNP/NMR experiments at magnetic fields up to 18.8 T (527 GHz / 800 MHz). As a result, there are mounting experimental data showing that the DNP enhancements of both CE and SE decrease with increasing the B_0 field. This is due to the fact that both CE and SE utilize continuous wave (CW) irradiation of microwave with field strength on the order of ~1 MHz which can be regarded as a small perturbation compared to the proton Larmor frequency. Thus, this thesis aims at developing new DNP methods for high frequency DNP. To this end, we have discovered the Overhauser effect in insulating solids, a CW DNP method that scales with the magnetic field. Furthermore, we focus on the development of time domain or pulsed DNP, a repertoire of pulse sequences utilizing intense microwave pulses instead of low power CW irradiation for polarization transfer. We have demonstrated very high DNP efficiency using nuclear orientation via electron spin locking (NOVEL) and frequency-swept integrated solid effect (FS-ISE) sequences at magnetic fields up to 3.35 T (94 GHz / 143 MHz of electron and proton Larmor frequency, respectively).

1.2 Thesis outline

In **Chapter 2**, we review the mechanisms of all the DNP processes that have been observed in insulating solids including those using low power, CW microwave irradiation (the solid effect, cross effect and Overhauser effect) as well as those microwave pulses (NOVEL, ISE, dressed state solid effect (DSSE), nuclear rotating frame DNP (NRF DNP)). Quantum mechanical descriptions to each mechanism are presented using model consisting of one electron and one nucleus except for the Overhauser effect, which is best described as a rate process. Such description serves as a phenomenological interpretation to the OE in insulating solids that we recently discovered and presented in **Chapter 3**. The rest of this thesis (**Chapters 4** to **8**) concerns with the development of time domain DNP techniques with focusing on the NOVEL and ISE pulse sequences. Our development started out at low field (0.35 T) with the demonstration of very high DNP efficiency using the constant-amplitude NOVEL (CA-NOVEL) sequence (**Chapter 4**) and ramped-amplitude NOVEL (RA-NOVEL) sequence (**Chapter 5**). **Chapter 6** deals with the FS-ISE pulse sequence, which is closely related to NOVEL. However, we showed that FS-ISE has a great flexibility in term of

the microwave field strength requirement. The results at X-band (0.35 T) have set a strong foundation for our further development of time domain DNP at higher fields including Q-band (1.2 T) in **Chapter 7** and W-band (3.35 T) in **Chapter 8**. Our results at various magnetic fields have a direct implication on and help navigate the future research toward the realization of time domain DNP at magnetic fields used in contemporary NMR applications.

1.3 References

[1] S.R. Hartmann, E.L. Hahn, Nuclear Double Resonance in the Rotating Frame, Phys. Rev., 128 (1962) 2042-2053.

[2] E.R. Andrew, A. Bradbury, R.G. Eades, Removal of Dipolar Broadening of Nuclear Magnetic Resonance Spectra of Solids by Specimen Rotation, Nature, 183 (1959) 1802-1803.

[3] I.J. Lowe, Free Induction Decays of Rotating Solids, Phys. Rev. Lett., 2 (1959) 285.

[4] A.W. Overhauser, Polarization of Nuclei in Metals, Phys. Rev., 92 (1953) 411.

[5] T.R. Carver, C.P. Slichter, Polarization of Nuclear Spins in Metals, Phys. Rev., 92 (1953) 212.

[6] T.R. Carver, C.P. Slichter, Experimental Verification of the Overhauser Nuclear Polarization Effect, Phys. Rev., 102 (1956) 975.

[7] C. Jeffries, D., Polarization of Nuclei by Resonance Saturation in Paramagnetic Crystals, Phys. Rev., 106 (1957) 164.

[8] C.D. Jeffries, Dynamic Orientation of Nuclei by Forbidden Transitions in Paramagnetic Resonance, Phys. Rev., 117 (1960) 1056.

[9] A. Abragam, M. Goldman, Principles of dynamic nuclear polarisation, Reports on Progress in Physics, 41 (1978) 395-467.

[10] A. Kessenikh, V., V. Lushchikov, I., A. Manenkov, A., Y. Taran, V., Proton Polarization in Irradiated Polyethylenes, Soviet Physics - Solid State, 5 (1963) 321-329.

[11] C. Hwang, F., D. Hill, A., New Effect in Dynamic Polarization, Phys. Rev. Lett., 18 (1967) 110.

[12] C. Hwang, F., D. Hill, A., Phenomenological Model for the New Effect in Dynamic Polarization, Phys. Rev. Lett., 19 (1967) 1011.

[13] K. Hu, H. Yu, T. Swager, R. Griffin, Dynamic nuclear polarization with biradicals., J. Am. Chem. Soc., 126 (2004) 10844-10845.

[14] R.A. Wind, M.J. Duijvestijn, d.L. van, C., A. Manenschijn, J. Vriend, Applications of dynamic nuclear polarization in 13C NMR in solids, Prog. Nucl. Magn. Reson. Spectrosc., 17 (1985) 33-67.

[15] M. Duijvestijn, J., R. Wind, A., J. Smidt, A quantitative investigation of the dynamic nuclear polarization effect by fixed paramagnetic centra of abundant and rare spins in solids at room temperature, Physica B+C, 138 (1986) 147-170.

[16] M. Goldman, Spin temperature and nuclear magnetic resonance in solids, Clarendon Press, Oxford, 1970.

Chapter 2: Mechanisms of Dynamic Nuclear Polarization in Insulating Solids

Adapted from T.V. Can, Q.Z. Ni, and R.G. Griffin, Journal of Magnetic Resonance 253 (2015) 23-35

Dynamic nuclear polarization (DNP) is a technique used to enhance signal intensities in NMR experiments by transferring the high polarization of electrons to their surrounding nuclei. The past decade has witnessed a renaissance in the development of DNP, especially at high magnetic fields, and its application in several areas including biophysics, chemistry, structural biology and materials science. Recent technical and theoretical advances have expanded our understanding of established experiments: for example, the cross effect DNP in samples spinning at the magic angle. Furthermore, new experiments suggest that our understanding of the Overhauser effect and its applicability to insulating solids needs to be re-examined. In this article, we summarize important results of the past few years and provide quantum mechanical explanations underlying these results.

2.1. Introduction

The history of dynamic nuclear polarization (DNP) dates from 1953 when Overhauser proposed that irradiation of electron paramagnetic resonance (EPR) transitions could result in the enhancement of the polarization of coupled nuclei. [1]. Shortly thereafter, Carver and Slichter performed the first DNP experiments that confirmed the Overhauser effect (OE). In particular, they observed enhanced ^{7}Li signal intensities obtained from Li metal dispersed in mineral oil [2]. The enhancement was also observed in solutions of Na^{+} in liquid NH_3 [3]. The first DNP mechanism documented for insulating solids was the solid effect (SE) and was described by Jefferies [4, 5] and Abragam and coworkers [6, 7]. Five years later, the cross effect DNP mechanism was observed by Kessennikh [8, 9], and subsequently discussed in more detail by Hill and Hwang [10, 11] and Wollan [12, 13]. The goal of many of these early efforts was to understand the physics underlying DNP and to develop experiments that produced polarized targets for neutron scattering experiments. Indeed, preparation of polarized targets remains an area of active interest in experimental particle physics, most recently using pulsed DNP methods (*vide infra*). For the interested reader there are excellent reviews of these early experiments [14-17]

In the 1980s and early 1990s, efforts to incorporate DNP into magic angle spinning (MAS) and other solid state NMR experiments were initiated by Wind [18] *et al.* , Yannoni [19-21] and Schaefer *et al.* [22]. These experiments used klystron microwave sources and were performed primarily at a magnetic field of 1.4 T (60 MHz/40 GHz ^{1}H/electron Larmor frequencies) although one experiment at 1.9 T was reported [23]. However, these experiments were limited to low fields because of the paucity of microwave sources operating above 40-50 GHz. In 1993 Becerra, et al. [24] introduced the gyrotron as a microwave source for DNP experiments at 5 T (140 GHz for electrons), with the specific aim of developing an experimental approach that would permit DNP at higher magnetic fields used for contemporary NMR experiments. These magnetic fields require microwave sources that ideally operate at the 10-100 watt level in the ~140-660 GHz frequency range, corresponding to magnetic fields of ~5-23 T and ^{1}H Larmor frequencies of ~200-1000 MHz. Subsequently, gyrotron based DNP/NMR spectrometers operating at 250 GHz/380 MHz and 460 GHz/700 MHz were successfully constructed [25-28]. In addition, DNP/NMR instruments operating at 263 GHz/400 MHz, 395 GHz/600 MHz and 527 GHz/800 MHz are now available commercially. The accessibility of this new instrumentation has stimulated a variety of new applications as well as investigations of new DNP mechanisms.

In this review, we discuss key aspects of several known DNP mechanisms including continuous wave (CW) and time domain DNP. We present recent experimental results together with some new quantum mechanical treatments. Our analysis builds on the work by Hu *et al.* [29]. However, we emphasize the use of perturbation theories (both time independent and time dependent; non-degenerate and degenerate). Furthermore, we include the effects of MAS in CE DNP that have been considered recently [30, 31]. Our discussion focuses primarily on the mechanisms of DNP in insulating solids at high fields. For other aspects of DNP such as instrumentation, radical development, applications, etc., we refer the reader to other reviews by Ni *et al.* [32], Barnes *et al.* [33], Maly *et al.* [34], and Nanni *et al.* [35].

The paper is organized as follows. In **Sections 2.1 and 2.2**, we discuss CW DNP mechanisms in which the microwave fields are treated as time-dependent harmonic perturbations, while the remaining terms in the Hamiltonian are viewed as static. Diagonalization of the static Hamiltonian is conveniently approximated using time independent perturbation theory, without obscuring any conclusions. In the case of CE DNP (**Section 2.2**), despite the magic angle spinning, the Hamiltonian can also be regarded as static at each rotor angle. **Section 2.3.1** deals with pulsed DNP methods using low microwave power including DNP in the nuclear rotating frame (NRF DNP) and the dressed state solid effect (DSSE) in which the microwave fields are treated as perturbations. In **Section 2.3.2**, we discuss two time-domain DNP experiments: nuclear orientation via electron spin locking (NOVEL) and the integrated solid effect (ISE), where the microwave fields are large and can no longer be treated as perturbations.

2.2. CW DNP

2.2.1. Narrow EPR spectrum

The first class of DNP mechanisms in insulating solids involves radical dopants that satisfy the inequality $\delta,\Delta < \omega_{0I}$, where δ,Δ and ω_{0I} are the homogenous electron paramagnetic resonance (EPR) linewidth, the breadth of the EPR spectrum and the nuclear Larmor frequency, respectively. In this case, DNP is mediated by the Overhauser effect and/or the solid effect. The influence of MAS can be conveniently ignored because the EPR spectrum is narrow and therefore the electron energy levels are only weakly modulated by the sample rotation. The molecular structures of four narrow-line polarizing agents are shown in **Figures 2.1a-d** and include 1,3-bisphenylene-2-phenylallyl (BDPA), sulfonated-

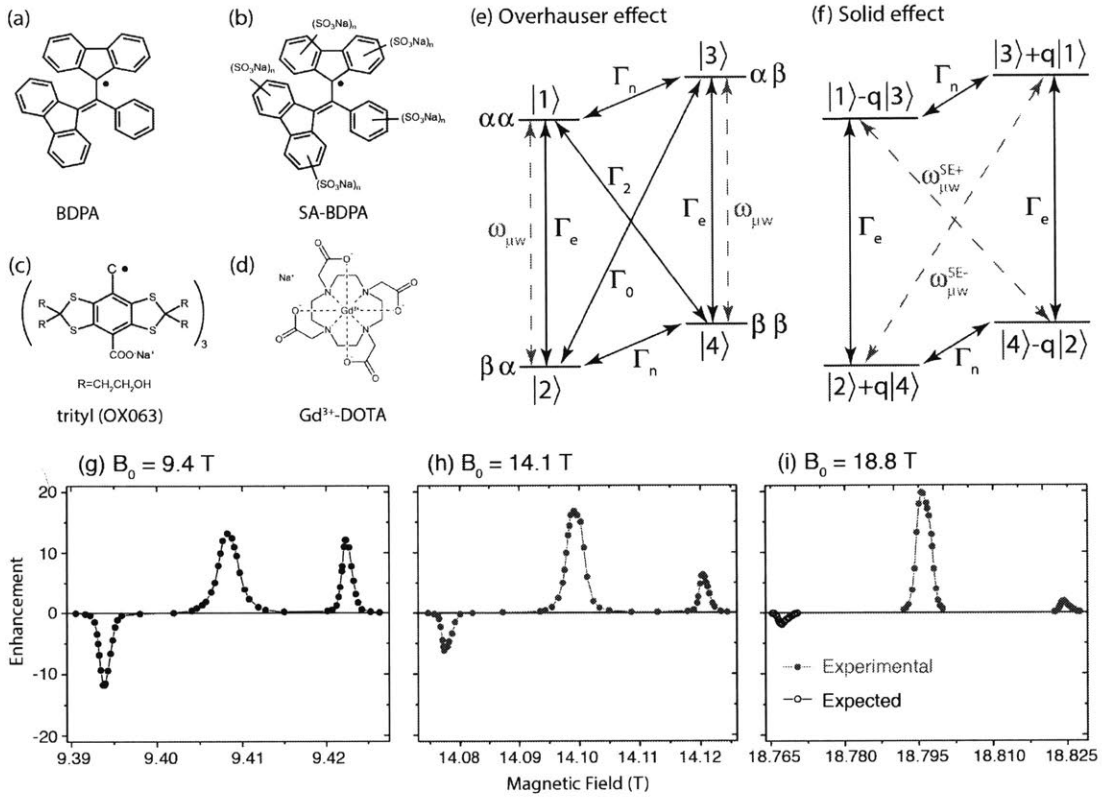

Figure 2.1: Molecular structures of radicals for the solid effect (a) BDPA, (b) sulfonated BDPA (SA-BDPA), (c) trityl-OX063 and (d) Gd^{3+}-DOTA.

(e) Energy level diagram for the Overhauser effect. The imbalance between the ZQ and DQ relaxation rates act to distribute the polarizations upon the microwave driven saturation of the EPR transition, resulting in the DNP enhancement. (f) Energy level diagram for the solid effect. Neither the ZQ or DQ relaxations are required. Instead, saturation of the ZQ or DQ transitions leads to the DNP enhancement.

^{1}H DNP enhancement Zeeman field profiles of BDPA in polystyrene are shown for (g) 9.4 T, (h) 14.1 T and (i) 18.8 T [36]. The positive enhancement due to the Overhauser effect is present at the center of each field profile and appears to scale with B_0. In contrast, the solid effect enhancements scales very closely to B_0^{-2}. At 18.8 T, the maximum enhancement of the Overhauser effect is one order of magnitude larger than that of the solid effect.

BDPA (SA-BDPA), trityl OX063 and Gd^{3+}-DOTA. These polarizing agents have a small g-anisotropy or, in the case of Gd^{3+} a narrow $-½ \rightarrow ½$ central EPR transition due to molecular symmetry. However, the EPR lines are broadened by the proton hyperfine couplings (BDPA and SA-BDPA), residual g-anisotropy (trityl OX063), or second order zero field splitting (Gd^{3+}-DOTA).

2.2.1.1. Overhauser effect

The Overhauser effect was the first DNP mechanism proposed for systems with mobile electrons, namely conducting solids and liquids. The effect is operative in a two-spin system consisting of one electron and one nucleus (**Figure 2.1e**), and relies on the presence of the zero quantum (ZQ) and double quantum (DQ) relaxation pathways with differing relaxation rates. The imbalance between the two rates, (Γ_0 and Γ_2 in Figure 1e) leads to an enhancement in nuclear polarization. In particular, upon microwave irradiation near the single quantum (SQ) EPR transition, the DQ and ZQ relaxation, mediated by molecular tumbling in liquids and translational motion of electrons in conducting solids, redistribute the populations via fluctuations of the anisotropic and isotropic couplings, respectively. This results in a Zeeman field profile that is symmetrically centered at the frequency of the EPR transition. In liquids, the DQ transition is generally the dominant relaxation pathway, and leads to the observation of negative DNP enhancements for ^{1}H. However in insulating solids, we recently observed a significant OE DNP with a *positive* enhancement, indicating that the ZQ term is dominant [36]. This is illustrated in Zeeman field profiles of **Figures 2.1g-i** where the positive enhancement in the center of the profiles is assigned to the OE. In addition, quantum mechanical simulations predict an OE even though the samples are insulators. In contrast to some other CW DNP mechanisms, the OE relies on allowed EPR transitions, requires much less microwave power, and appears to scale favorably with the magnetic field as is also illustrated in the panels in **Figure 2.1g-i**.

To date the OE in insulators has only been observed for BDPA and its derivative SA-BDPA. In addition, perdeuteration of BDPA resulted in an order of magnitude decrease in DNP efficiency but, more importantly, in a sign change of the OE enhancement from positive to *negative* as well. This result suggests that ^{1}H-e$^-$ hyperfine coupling is essential for the OE and ~ 5 MHz ^{1}H couplings are present in BDPA. This also provides an explanation of why the OE is not observed for the trityl radical. In particular, trityl was designed to eliminate all ^{1}H couplings in order to have a narrow line to enhance Overhauser effects in solution.

Efforts are underway to improve the efficiency of the OE with the synthesis of new narrow-line radicals with hyperfine couplings larger than those found in BDPA. Furthermore, theoretical and experimental research is needed to fully understand the origin of cross relaxation mechanisms responsible for the OE in insulating solids.

2.2.1.2. Solid effect

The solid effect (SE) is similar to the OE in that it involves a two-spin process between an electron spin *S* and nuclear spin *I*. The Zeeman field profiles for the SE (plus the OE) are shown in **Figure 2.1g-i** and the SE is responsible for the negative and positive signal enhancements at $\omega_{SE} = \omega_e \pm \omega_{0I}$. In the secular approximation, the static Hamiltonian for such a system can be written as

$$H = \omega_{0S} S_z - \omega_{0I} I_z + A S_z I_z + B S_z I_x \tag{2.1.1}$$

where the first two terms are the electron and nuclear Zeeman interactions, and the last two terms the secular and pseudo-secular hyperfine couplings, respectively. Using first order perturbation theory we rewrite *H* as

$$H = H^{(0)} + H^{(1)} \tag{2.1.2}$$

where the small perturbation $H^{(1)}$ is the pseudo-secular hyperfine coupling term in 2.1.1. The unperturbed Hamiltonian $H^{(0)}$ is already diagonal in the direct product basis set. The energy levels and the corresponding eigenstates of *H* can then be evaluated using perturbation theory. The direct product states are not eigenstates of *H* and there is a small but essential mixing of these states due to the pseudo-secular hyperfine coupling (**Figure 2.1f**). The degree to which the states are mixed is given by the factor *q* [37]

$$q \approx \frac{B}{2\omega_{0I}} \tag{2.1.3}$$

As a result, the nominally forbidden ZQ and DQ transitions become slightly allowed and can be driven by the microwave field, yielding an enhancement in the nuclear polarization that is positive or negative depending on the field position relative to the position of the EPR line. We refer to the plots shown in **Figures 2.1g-i** as Zeeman field profiles. Note that in this CW DNP experiment the coefficient of state mixing is proportional to ω_0^{-1}, and therefore the transition probability is $\sim \omega_0^{-2}$. Thus, the SE enhancements decrease significantly at higher fields, which is a characteristic of continuous wave (CW) DNP experiments. On the other hand, the transition rate can be improved by increasing the microwave field strength [38, 39]. Another approach is to use a radical whose EPR linewidth is progressively narrowed with the magnetic field as demonstrated by Corzilius *et al.* using high spin transition metal ions [40]. An enhancement of 144 at 5 T has been reported using trityl-OX063 radical [39].

The Hamiltonian can also be expressed as a direct sum

$$H = H_{13} \oplus H_{24} \tag{2.1.4}$$

where H_{13} and H_{24} are the Hamiltonians in the electron spin up and spin down subspaces, respectively. Accordingly, diagonalization of H in each subspace is straightforward, because H_{13} and H_{24} are both *2x2* matrices. This approach was used in the work by Hu *et al.* [29].

2.2.2. Cross effect

A third class of DNP experiments requires that the EPR spectra of the polarizing agents be inhomogenously broadened by the *g*-anisotropy and that the spectral breadth be large compared to the nuclear Larmor frequencies. Thus, in these "cross effect" (CE) experiments the inequality $\delta < \omega_{0I} < \Delta$ is satisfied [8, 9], and it is possible to have a <u>*three spin*</u> polarization transfer by satisfying the matching condition $\omega_{0I} = \omega_{0S_1} - \omega_{0S_2}$. Here, the subscripts refer to the nuclear Larmor frequencies and the two electrons whose Larmor frequencies are separated by the g-value differences, respectively. To date, the most efficient CE DNP is observed with biradicals containing two tethered nitroxide moieties, where the electron-electron coupling is 20-35 MHz [41-43]. Hu *et al.* presented a quantum mechanical description of the CE DNP in static samples [29]. Recent experimental data show that the effect of MAS is essential in understanding CE DNP. For example, there is significant signal quenching in DNP experiments during MAS but not for static samples [44]. It is therefore important to take into account the effect of sample spinning.

It is worth noting that in some circumstances the CE and SE are simultaneously present, such as, in static samples at low temperatures (~10 K) doped with either the monoradical TEMPOL [45] or the biradical TOTAPOL [46], but we refer the reader to the literature for a discussion of this case. Another topic that will not be discussed in detail in this article is the thermal mixing mechanism which requires that $\delta > \omega_{0I}$, that is a homogeneously broaden EPR spectrum. Thermal mixing has been studied recently with simulations by Hovav *et al.* [47], but to date it has not been of great practical importance for high field DNP since most of the EPR spectra are inhomogeneously broadened. Thus, at higher temperatures (~80-110 K) where most MAS experiments are being performed, the CE is dominant.

2.2.2.1. Cross effect DNP Zeeman field profiles

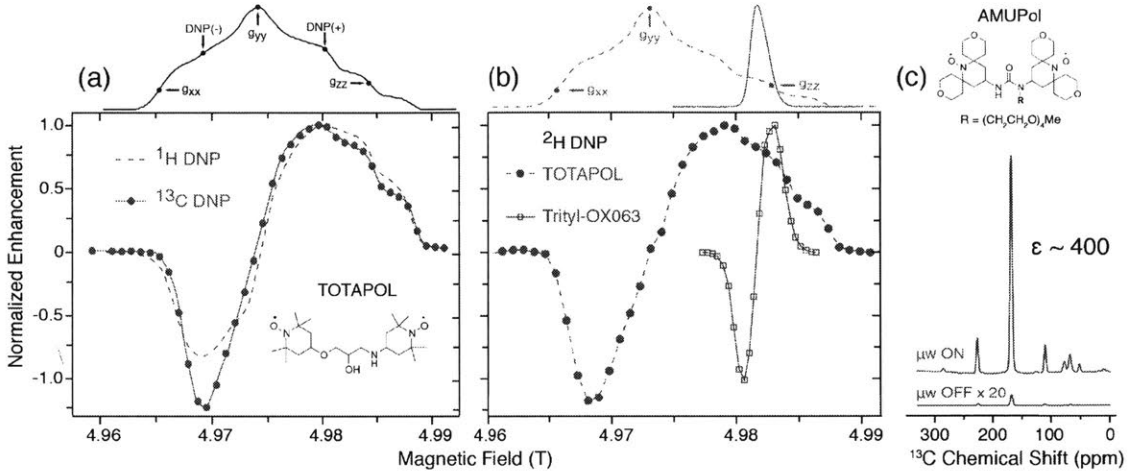

Figure 2.2: (a) ^{1}H and ^{13}C DNP field profiles of TOTAPOL. (b) ^{2}H DNP field profiles of TOTAPOL and trityl-OX063. For TOTAPOL, the maximum ^{1}H enhancement is obtained at the DNP(+) field position, whereas for other nuclei of lower gyromagnetic ratios such as ^{13}C and ^{2}H, the maximum enhancements are at the DNP(-) field position. In both cases, the asymmetry is ~ 20%. For low gamma nuclei, trityl-OX03, a narrow-line radical, still satisfies the CE condition and gives higher enhancement by a factor of ~ 4 compared to TOTAPOL. (c) Cross effect DNP at 380 MHz/250 GHz using biradical AMUPol. The sample contains 1 M ^{13}C, ^{15}N-urea in 60/30/10 (volume ratio) d8-glycerol/D_2O/H_2O glassy matrix doped with 10 mM AMUPol. We obtained an enhancement of 400 at 80 K. To date, AMUPol is the best biradical for CE DNP. The radical also gives significant enhancement at temperatures above 150 K. Figures (a) and (b) are from Maly *et al.* .[48] [49].

In order to establish the DNP mechanism that is present and to optimize the DNP enhancement, it is customary to record the enhancement as a function of the Zeeman field as illustrated in Figure 1 above and here we show Zeeman field profiles for the CE. In **Figure 2.2a** we show the ^{1}H and ^{13}C DNP field profiles of biradical TOTAPOL, and **Figure 2.2b** compares the ^{2}H DNP Zeeman field profiles obtained with TOTAPOL and the narrow-line monoradical trityl-OX063 [48, 49]. The enhancements were normalized to the maximum positive enhancement. For TOTAPOL, the ^{1}H, ^{13}C and ^{2}H field profiles span roughly the EPR line with the maximum positive and maximum negative enhancements appearing at the high and low field sides, respectively. For ^{1}H, the maximum enhancement is at the positive field position and the asymmetry between the maximum positive and the maximum negative enhancements is ~ 20%. ^{13}C and ^{2}H, which are both low-γ nuclei and relatively close in Larmor frequency, show almost identical field profiles. An asymmetry of ~20% was also observed for ^{13}C and ^{2}H, but the maximum enhancement is located at the negative field position. The reason for this difference is that the nuclear Zeeman frequencies for ^{13}C ($\omega_{0^{13}C}$ =53 MHz) and ^{2}H (ω_{0^2H} = 32.4 MHz) fit into the ~ 20 G field interval (~4.9690-4.9710

T, ~56 MHz) which is the region where the largest number of electrons per Gauss occurs in the EPR spectrum. In contrast the largest ^{1}H enhancement requires a separation of 211 MHz, which in turn requires a larger spectral breadth leading the profile shown in **Figure 2.2a**.

The ^{2}H DNP field profile of trityl-OX063 suggests that cross effect is the dominating mechanism, consistent with the fact that the EPR linewidth of trityl satisfies the CE condition for ^{2}H. This is also the case for other low-γ nuclei such as ^{17}O [50]. For these nuclei, the CE using trityl is more efficient than biradicals such as TOTAPOL due to the narrow EPR linewidth, which permits a larger fraction of the electrons to participate in the DNP processes. For example, Maly *et al.* obtained a factor of ~ 4 higher in the enhancement using trityl rather than TOTAPOL [49].

Figure 2.2c shows the enhancement $\varepsilon = 400$ obtained with the biradical AMUPol, the most efficient biradical currently available [43], at 380 MHz/250 GHz. Overall, AMUPol provides approximately twofold larger DNP enhancements when compared to TOTAPOL. The improvement in the DNP efficiency can be attributed to the shorter intramolecular tether between the electron pairs, which increases the e^{-}-e^{-} dipole coupling from ~23 MHz in TOTAPOL to ~35 MHz in AMUPol. In addition, the four methyl groups on the TEMPO rings are replaced by two tetrahydropyran rings which increases the electronic relaxation times [41] [43] [51]. Finally, the water solubility of AMUPol is greatly improved by addition of the polyethylene glycol chain.

2.2.2.2. The Hamiltonian

Figure 2.3a shows that the efficiency of the CE increases with spinning frequency ($\omega_r / 2\pi$) [52], necessitating a description that includes the MAS effect. This effect was observed initially by K. Hu [53] and has been explored more recently by Mentink-Vigier *et al.* using quantum mechanical simulations [30]. Concurrently, Thurber *et al.* independently presented a study of the CE in MAS experiments using a combination of theoretical analysis and simulations [31]. Both studies highlighted the importance of the dynamical behavior near the avoided level crossings (*vide infra*). The centerpiece of the simulations performed by both groups is the calculation of the time evolution of the quantum mechanical system. Due to the periodicity of the Hamiltonian in an MAS experiment, the time evolution can be evaluated by repeatedly applying the time evolution operator each rotor period. Calculation

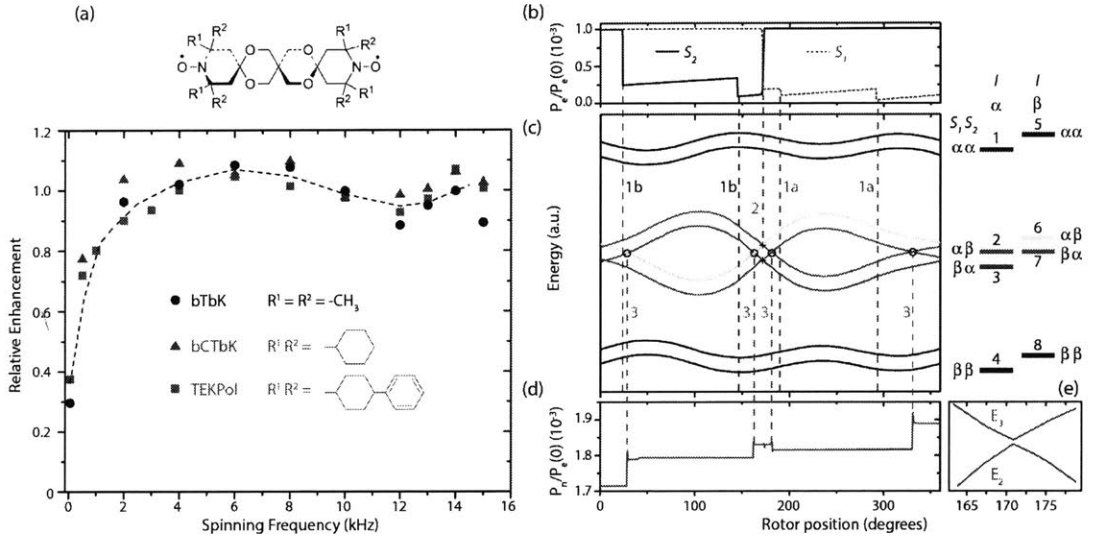

Figure 2.3: Cross effect DNP in a three-spin system consisting of two electrons S_1, S_2 and one nuclear spin I. (a) Enhancement as a function of the spinning frequency on bTbK, bCTbK and TEKPol biradicals [52]. All three radicals show a similar trend with a local minimum at ~ 12 kHz, and appear to increase at faster spinning. (b) Polarization of electrons during one rotor period. (c) The modulations of the energy levels during one rotor period due to anisotropic interactions including the *g*-anisotropy and the e^--e^- dipolar coupling. (d) Nuclear polarization during one rotor period. (e) Electron-electron avoided level crossing.
The dashed lines 1a and 1b indicate the flipping of the electron spins as the microwave frequency crosses one of the electron Larmor frequencies. The green dashed line 2 corresponds to the electron-electron avoided level crossing where the two electrons exchange their polarizations. The red dashed line 3 represents the three-spin avoided crossings at which DNP transfer occurs, as seen in the change of the nuclear polarization. Figures (b) to (e) were reproduced with slight modifications from the simulations by Mentink-Vigier *et al.* [30].

of the evolution operator during one rotor period was done in a stepwise manner and the orientation of the rotor was incremented (**Figure 2.3b-e**).

Here, we present an alternative approach based on a straightforward application of perturbation theory that can be used to understand important aspects of MAS CE. We begin with the Hamiltonian of a three-spin 1/2 system consisting of two electron spins S_1, S_2 and one nuclear spin I. We then decompose the Hamiltonian into an unperturbed part and a small perturbation from the pseudo-secular hyperfine coupling. The unperturbed Hamiltonian is block diagonal with four *2x2* blocks which can be diagonalized with minimum effort. The unperturbed energy levels give a good approximation of the electron-microwave crossing. The degeneracy at the central energy levels results in either electron-electron crossing or three-spin crossing. More detailed calculations are presented below.

After a secular approximation, the Hamiltonian has the form

$$H = \omega_{0S_1} S_{1z} + \omega_{0S_2} S_{2z} - \omega_{0I} I_z + \left(A_1 S_{1z} + A_2 S_{2z}\right) I_z + \left(B_1 S_{1z} + B_2 S_{2z}\right) I_x + d\left(3 S_{1z} S_{2z} - \vec{S}_1 \vec{S}_2\right) - 2J \vec{S}_1 \vec{S}_2 \quad (2.2.1)$$

where ω_{0S_1}, ω_{0S_2} and ω_{0I} are Larmor frequencies. A_1 and A_2 are secular hyperfine couplings between the electrons and the nucleus, and B_1 and B_2 are pseudo-secular hyperfine couplings between the electrons and the nucleus. d and J are the dipolar coupling and J-coupling between the two electrons, respectively. It is worth noting that in a MAS experiment, ω_{0S_1}, ω_{0S_2}, B_1, B_2 and d are time-dependent, ignoring the chemical shift anisotropy of the nucleus. The direct product basis set consists of eight states of the form $|IS_1S_2\rangle$ as illustrated in **Figure 2.3c**. Treating the pseudo-secular hyperfine coupling as a small perturbation, we write the Hamiltonian as

$$H = H^{(0)} + H^{(1)} \quad (2.2.2)$$

where $H^{(0)}$ is the unperturbed part and $H^{(1)}$ is the perturbation. $H^{(0)}$ is block diagonal and therefore can be written as direct sum of four *2x2* matrices, *i.e.*

$$H^{(0)} = H_{15} \oplus H_{23} \oplus H_{67} \oplus H_{48} \quad (2.2.3)$$

$H^{(1)}$ only connects the four center states. Consequently $H^{(1)}$ is reduced to a *4x4* matrix perturbing the four center states only.

$$H^{(1)} = H_{2367}{}^{(1)} = \begin{pmatrix} 0 & 0 & \frac{B_\Delta}{4} & 0 \\ 0 & 0 & 0 & -\frac{B_\Delta}{4} \\ \frac{B_\Delta}{4} & 0 & 0 & 0 \\ 0 & -\frac{B_\Delta}{4} & 0 & 0 \end{pmatrix} \quad (2.2.4)$$

where

$$B_\Delta = B_1 - B_2 \quad (2.2.5)$$

2.2.2.3. Level crossings

(a) Electron-microwave crossings

The electron-microwave crossing occurs when the applied microwave frequency is on resonance with one of the EPR transitions (single electron flip). In principle, diagonalization

of the unperturbed Hamiltonian gives a good approximation of this type of level crossings. The electron-microwave crossings read

$$\omega_{\mu w} = \omega_{0S_{1(2)}} \pm A_{1(2)} \pm (d - J) \tag{2.2.6}$$

which can be approximated as

$$\omega_{\mu w} \approx \omega_{0S_{1(2)}} \tag{2.2.7}$$

In other words, the three-spin system can be treated as non-interacting, and therefore flipping of a single electron occurs when the microwave frequency matches the Larmor frequency of either electron.

(b) Electron-electron crossings

The electron-electron crossings occur in the {23} and {67} subspaces (**Figure 2.3c**). This can be realized by treating the *d* and *J* terms in H_{23} and H_{67} as perturbations. The avoided level crossings correspond to the degeneracy of these subspaces in the absence of the *d* and *J* perturbation. It follows that

$$\omega_{\Delta} = \mp \frac{A_{\Delta}}{2} \approx 0 \tag{2.2.8}$$

where

$$A_{\Delta} = A_1 - A_2 \tag{2.2.9}$$

$$\omega_{\Delta} = \omega_{0S_1} - \omega_{0S_2} \tag{2.2.10}$$

The $\mp$ signs in (2.2.8) correspond to the degeneracy in H_{23} and H_{67}, respectively.

We then use degenerate perturbation theory, resulting in *1:1* mixing of states in the {23} and {67} subspaces due to the electron-electron couplings. As a consequence, the two electrons exchange polarization at these level crossings (**Figure 2.3c**). The rate at which electrons exchange polarization at these level crossings can be approximated using Landau-Zener theory as demonstrated by Thurber *et al.*. To see that the energy levels actually do not cross, hence the name *avoided level crossing*, we note that in the vicinity of the degeneracy point, H_{23} and H_{67} can be diagonalized analytically. For example, diagonalization of H_{23} gives the following eigenenergies

$$\tilde{E}_2 = \frac{1}{2}\left[\left(\omega_{0I} - \frac{D_d}{2}\right) \pm \sqrt{\left(\omega_{\Delta} + \frac{A_{\Delta}}{2}\right)^2 + D_0^2}\right] \tag{2.2.11}$$

$$\tilde{E}_3 = \frac{1}{2}\left[\left(\omega_{0I} - \frac{D_d}{2}\right) \mp \sqrt{\left(\omega_\Delta + \frac{A_\Delta}{2}\right)^2 + D_0^2}\right] \tag{2.2.12}$$

where

$$D_d = 2\left(d - J\right) \tag{2.2.13}$$

$$D_0 = -\left(d + 2J\right) \tag{2.2.14}$$

The + in (2.2.11) and − in (2.2.12) corresponds to positive $\omega_\Delta + A_\Delta / 2$. Whereas, the − in (2.2.11) and + in (2.2.12) corresponds to negative $\omega_\Delta + A_\Delta / 2$.

$$\lim_{\omega_\Delta + \frac{A_\Delta}{2} \to 0^+} \tilde{E}_2 = \lim_{\omega_\Delta + \frac{A_\Delta}{2} \to 0^-} \tilde{E}_3 = \frac{1}{2}\left[\left(\omega_{0I} - \frac{D_d}{2}\right) + D_0\right] \tag{2.2.15}$$

$$\lim_{\omega_\Delta + \frac{A_\Delta}{2} \to 0^-} \tilde{E}_2 = \lim_{\omega_\Delta + \frac{A_\Delta}{2} \to 0^+} \tilde{E}_3 = \frac{1}{2}\left[\left(\omega_{0I} - \frac{D_d}{2}\right) - D_0\right] \tag{2.2.16}$$

This means that the energy levels do not cross and the energy gap is approximately equal to the perturbation D_0 from the e^--e^- couplings as demonstrated in **Figure 2.3e**.

(c) Three-spin crossings

In general this type of level crossing does not coincide with the electron-electron crossing, *i.e.* the condition (2.2.8) is not fulfilled. Let us assume that

$$\omega_\Delta \pm \frac{A_\Delta}{2} \geq 0 \tag{2.2.17}$$

In this case, the two energy levels at the center are

$$\tilde{E}_3 = \frac{1}{2}\left[\left(\omega_{0I} - \frac{D_d}{2}\right) - \sqrt{\left(\omega_\Delta + \frac{A_\Delta}{2}\right)^2 + D_0^2}\right] \tag{2.2.18}$$

$$\tilde{E}_6 = \frac{1}{2}\left[\left(-\omega_{0I} - \frac{D_d}{2}\right) + \sqrt{\left(\omega_\Delta - \frac{A_\Delta}{2}\right)^2 + D_0^2}\right] \tag{2.2.19}$$

Imposing the degeneracy of the two levels in (2.2.18) and (2.2.19), we obtain

$$\omega_{0I} = \frac{1}{2}\left[\sqrt{\left(\omega_\Delta + \frac{A_\Delta}{2}\right)^2 + D_0^2} + \sqrt{\left(\omega_\Delta - \frac{A_\Delta}{2}\right)^2 + D_0^2}\right] \tag{2.2.20}$$

This condition can be simplified for small A_Δ.

$$\omega_{0I} \approx \sqrt{\omega_\Delta{}^2 + D_0^2} \tag{2.2.21}$$

Note that the matching conditions in (2.2.20) and (2.2.21) were established without any assumption on the size of the e^--e^- dipolar and *J* couplings. For biradicals that have been used for CE, the e^--e^- dipolar coupling is 20-35 MHz; the *J* coupling is usually negligible except for the case of BTurea (~ 20 MHz). Therefore, we can assume that e^--e^- dipolar and *J* couplings are very small compared to the nuclear Larmor frequency. In this case, the condition (2.2.21) can be simplified further.

$$\omega_\Delta \approx \sqrt{\omega_{0I}{}^2 - D_0^2} \approx \omega_{0I} - \frac{D_0^2}{2\omega_{0I}} \approx \omega_{0I} \tag{2.2.22}$$

The *1:1* state mixing due to $H^{(1)}$ given in (2.2.4) arises from degenerate perturbation theory, resulting in the change in the nuclear polarization.

The energy levels in equations (2.2.18) and (2.2.19) are obtained by diagonalizing the unperturbed Hamiltonians H_{23} and H_{67}. As a result, the perturbation $H^{(1)}$ is transformed to

$$\tilde{H}^{(1)} = \frac{B_\Delta}{4}\begin{pmatrix} 0 & 0 & \cos\frac{\gamma+\delta}{2} & -\sin\frac{\gamma+\delta}{2} \\ 0 & 0 & -\sin\frac{\gamma+\delta}{2} & -\cos\frac{\gamma+\delta}{2} \\ \cos\frac{\gamma+\delta}{2} & -\sin\frac{\gamma+\delta}{2} & 0 & 0 \\ -\sin\frac{\gamma+\delta}{2} & -\cos\frac{\gamma+\delta}{2} & 0 & 0 \end{pmatrix} \tag{2.2.23}$$

where γ and δ are given as

$$-\frac{\pi}{2} \le \gamma, \delta \le \frac{\pi}{2} \tag{2.2.24}$$

$$\gamma = \arctan\left(\frac{D_0}{\omega_\Delta + \frac{A_\Delta}{2}}\right) \approx \frac{D_0}{\omega_{0I}} \tag{2.2.25}$$

$$\delta = \arctan\left(\frac{D_0}{\omega_\Delta - \frac{A_\Delta}{2}}\right) \approx \frac{D_0}{\omega_{0I}} \tag{2.2.26}$$

We can see that three-spin crossings are due to the anti-diagonal terms which equal to

$$-\frac{B_\Delta}{4}\sin\frac{\gamma+\delta}{2} \approx -\frac{B_\Delta}{4}\frac{\gamma+\delta}{2} \approx -\frac{B_\Delta}{4}\frac{D_0}{\omega_{0I}} \qquad (2.2.27)$$

The energy gap would then be $\frac{B_\Delta}{2}\frac{D_0}{\omega_{0I}}$, a result that is consistent with previous works by Hu *et al.*[54], Thurber *et al.*[31], and Vanhouten *et al.*[55].

2.2.2.4. Paramagnet induced signal quenching

Another result associated with the MAS is the signal quenching effect due to the paramagnetic dopants. This was documented recently by Corzilius *et al.* [44] and Thurber *et al.*[56]. Corzilius *et al.* studied the effect of four different polarizing agents including both single (trityl-OX063, 4-amino TEMPO, Gd^{3+}-DOTA) and two electron (TOTAPOL) species.

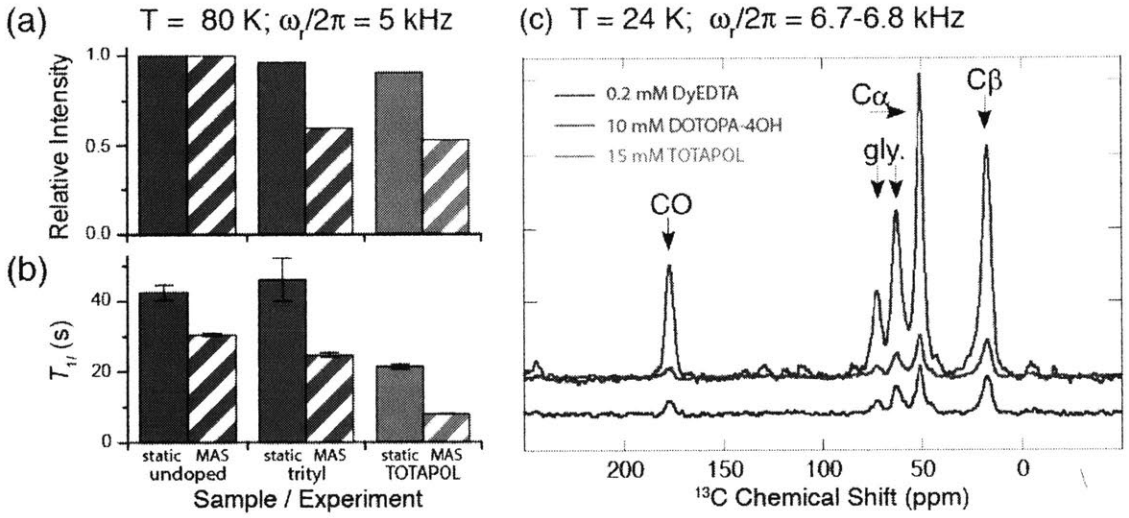

Figure 2.4: (a) Signal quenching in homogenous frozen DNP samples induced by the paramagnetic dopants [36]. (b) T_1 of ^1H appears to correlate with signal quenching effect [36]. (c) CE in the absent of microwave acts to reduce the NMR signal [56]. This effect was observed at very low temperature.

Figure 2.4a shows the signal losses during CP MAS and static experiments for both trityl and TOTAPOL. The signal quenching appears to associate with the enhanced spin-lattice relaxation (**Figure 2.4b**), which implies that the MAS modulation of the electron-nuclear dipole coupling is essential for the quenching. The signal quenching in CP MAS experiments could be due to: (i) the large shift in resonances of nuclei in close proximity with the magnetic dopants, (ii) the homogenous linebroadening originating from the modulation of the electron-nuclear coupling, and (iii) decrease in the CP efficiency as a consequence of the PRE effect on the $T_{1\rho}$ of ^1H.

The work by Thurber *et al.* only used cross effect radicals including biradical (TOTAPOL) and triradicals (DOTOPA-4OH and DOTOPA-Ethanol). A factor as large as ~6 in the signal loss was observed at very low temperature (~ 20K) and with sample spinning (**Figure 2.4c**). The effect at higher temperature (80 K) was smaller, consistent with the data from Corzilius *et al.* . Using quantum mechanical simulations, the authors suggest that the signal loss is due to the cross effect in the absence of microwaves and that the effect is dependent on the electron spin diffusion.

2.3. Pulsed DNP

2.3.1. Pulsed DNP using low microwave power

2.3.1.1. DNP in the nuclear rotating frame (NRF DNP)

This class of pulsed DNP mechanisms does not impose a defined resonance condition on the microwave power, and thus can operate at low microwave power. Accordingly, for this type of pulsed DNP sequences the microwave field is treated as a small perturbation, as was the case of CW DNP.

DNP in the nuclear rotating frame (NRF DNP) is conveniently described as the solid effect in the NRF. By transforming to the nuclear rotating frame, the mixing of states is no longer dependent on the magnetic field, but rather on the RF field strength, thereby eliminating the unfavorable field dependence of the conventional (lab frame) SE. The idea was first utilized by Bloembergen and Sokorin in a nuclear spin system [57], then by Wind [58] and, most recently, by Farrar [59] in an electron-nuclear system.

The Hamiltonian in the lab frame assumes the form

$$H = \omega_{0S} S_z - \omega_{0I} I_z + \vec{S} \cdot \vec{\vec{A}} \cdot \vec{I} - 2\omega_{1I} \cos(\omega_{rf} t) I_x \qquad (3.1.1)$$

In the nuclear rotating frame, after secular approximation with respect to I_z and redefining the transverse axis of spin S, the Hamiltonian simplifies to

$$H = \omega_{0S} S_z + B S_x I_z + A S_z I_z - \omega_{1I} I_x \qquad (3.1.2)$$

where A and B are the secular and pseudo-secular hyperfine coupling, respectively. We have assumed that the RF field is on resonance with the nuclear Larmor frequency.

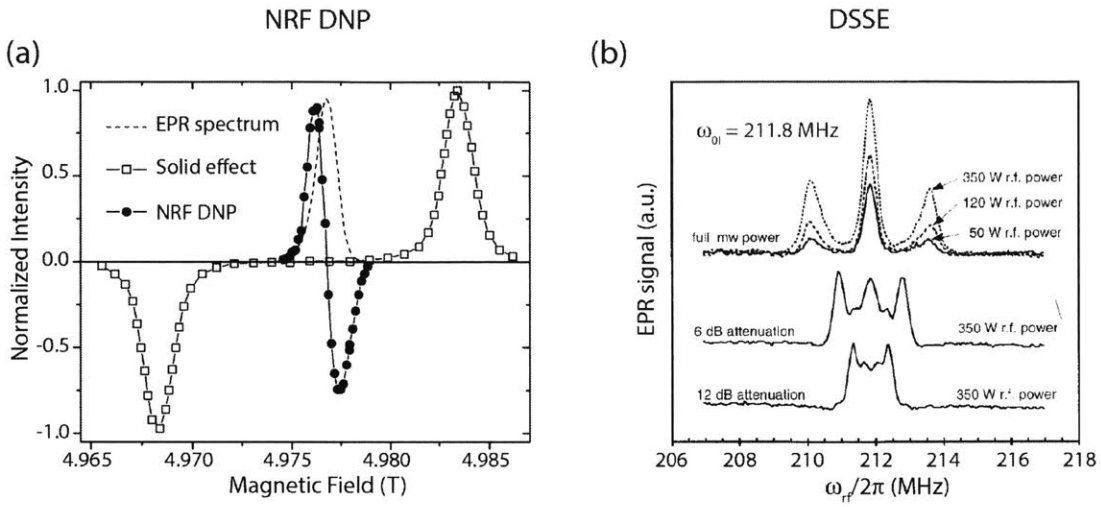

Figure 2.5: (a) EPR spectrum (dashed), SE DNP (open square) and NRF DNP (solid circle) field profiles of trityl radical at 139.5 GHz [59] [60]. Note that the separation between the negative and the positive enhancements is much narrower in NRF DNP compared to the SE DNP. Observation of the positive NRF DNP in the low field side, which is in opposite of SE DNP, can be explained by its dependence on the phase of the RF field.

(b) The loss in the electron polarization as a function of ω_{rf} in DSSE. The center peak is attributed to the ENDOR effect, whereas the two satellite peaks are attributed to DSSE. The experiment was performed on polystyrene doped with perdeuterated d_{21}-BDPA [61] in which the hyperfine coupling is negligible. The disposition of the satellite peak is proportional to the microwave field strength.

After a $-\pi/2$ rotation about I_y, the Hamiltonian is transformed to

$$H = \omega_{0S}S_z - BS_xI_x - AS_zI_x - \omega_{1I}I_z \tag{3.1.3}$$

As opposed to the lab frame SE DNP, NRF DNP does not require pseudo-secular hyperfine coupling. In other words, the secular approximation with respect to S_z is valid and the Hamiltonian can be truncated to

$$H = \omega_{0S}S_z - AS_zI_x - \omega_{1I}I_z \tag{3.1.4}$$

which is block diagonal in the direct product basis, and H is a direct sum of two $2x2$ matrices.

$$H = H_{13} \oplus H_{24} \tag{3.1.5}$$

Diagonalization of H is straightforward, and the matching condition is given as

$$\Omega_S = \omega_{\mu w} - \omega_{0S} = \pm\sqrt{\omega_{1I}^2 + \left(\frac{A}{2}\right)^2} \tag{3.1.6}$$

The mixing of states in each electronic subspace is defined by an angle θ

$$\theta = \arctan(\frac{A}{2\omega_{1I}}) \tag{3.1.7}$$

The state mixing is due to the secular hyperfine coupling, which is inversely proportional to the RF field instead of B_0 and is much larger than that for the SE. On the other hand, the separation between the positive and the negative enhancement conditions are much narrower compared to the lab frame SE. This feature is illustrated in **Figure 2.5a** for trityl radical. Note that the peaks of the lab frame SE and the NRF DNP appear to be opposite, which can be explained by the fact that the sign of the enhancement of NRF DNP is also dependent on the phase of the RF field.

2.3.1.2. Dressed state solid effect (DSSE)

The dressed state solid effect (DSSE) uses an RF field to drive the polarization transfer. Thus, the RF field is treated as a small, harmonic, time-dependent perturbation. The microwave field acts to create an electron spin dressed state, an analogy to the dressed atom states in optics [62]. In the microwave rotating frame, the Hamiltonian is written as

$$H = -\omega_{0I} I_z + \omega_{1S} S_x + A S_z I_z + B S_z I_x \tag{3.1.8}$$

After a secular approximation with respect to I_z, the Hamiltonian is truncated to

$$H = -\omega_{0I} I_z + A S_z I_z + \omega_{1S} S_x \tag{3.1.9}$$

which is block diagonal in the direct product basis set, *i.e.*,

$$H = H_{12} \oplus H_{34} \tag{3.1.10}$$

where H_{12} and H_{34} are the Hamiltonian in the nuclear spin up and spin down subspaces, respectively. After diagonalization, we obtain the following matching condition for the RF frequency

$$\Omega_{rf} = \omega_{rf} - \omega_{0I} = \pm\sqrt{\omega_{1S}^2 + \left(\frac{A}{2}\right)^2} \tag{3.1.11}$$

The matching condition (3.1.11) implies that during the DNP period the RF is applied far off resonance and the NMR signal is observed on resonance. Thus far, DSSE has only been

observed indirectly via the loss of the electron polarization [61]. In the case of d_{21}-BDPA, the secular hyperfine coupling is negligible and the matching conditions can be simplified to

$$\Omega_{rf} = \pm\omega_{1S} \tag{3.1.12}$$

This explains the result in **Figure 2.5b**, as the peak position appears to be displaced linearly with respect to the microwave field strength.

2.3.2. Pulsed DNP using high microwave power

In contrast to NRF DNP and DSSE, the microwave fields in the cases of nuclear orientation via electron spin locking (NOVEL) and the integrated solid effect (ISE) can no longer be treated as small perturbations. Both NOVEL and ISE rely on matching the Hartman-Hahn condition between the microwave rotating frame $(\omega_{1S}/2\pi)$ and the nuclear lab frame $(\omega_{0I}/2\pi)$. Even though ISE also functions with low microwave power, it performs optimally at the Hartman-Hahn condition, which requires strong microwave fields. In both cases the polarization is transferred coherently by the electron-nuclear dipolar coupling on the submicrosecond time scale, about three orders of magnitude faster than in conventional ^{1}H-^{13}C/^{15}N CP experiments. Both sequences were initially developed for the preparation of polarized targets using photoexcited triplet states of pentacene doped into host crystals of naphthalene or *ortho*- or *para*-terphenyl (**Figure 2.6a**). In the original experiments, the source of polarization was a photoexcited triplet state of pentacene generated by a laser pulse (**Figure 2.6b**). More recently, we have used NOVEL to enhance ^{1}H polarization in samples of polystyrene doped with BDPA. As illustrated in **Figure 2.7** the microwave field profile shows a sharp rise to a peak at $\omega_{1S} = \omega_{0I} = 15\,MHz$ followed by a long tail. There is a hint of a second maximum in the data at ~30 MHz (second harmonic), but it is not much above the S/N. Note that the breadth of the matching condition is broad, indicating that the electron couples strongly to the ^{1}H's in the lattice. Solid echoes were used to record the ^{1}H spectra, and the enhancement ε=100 was obtained with experiments at 300 K. In addition, we have performed similar experiments on systems containing nitroxide radicals and on frozen solutions of SA-BDPA and trityl. Therefore, the experiment appears to be robust and widely applicable even at this early stage.

2.3.2.1. Nuclear orientation via electron spin locking (NOVEL)

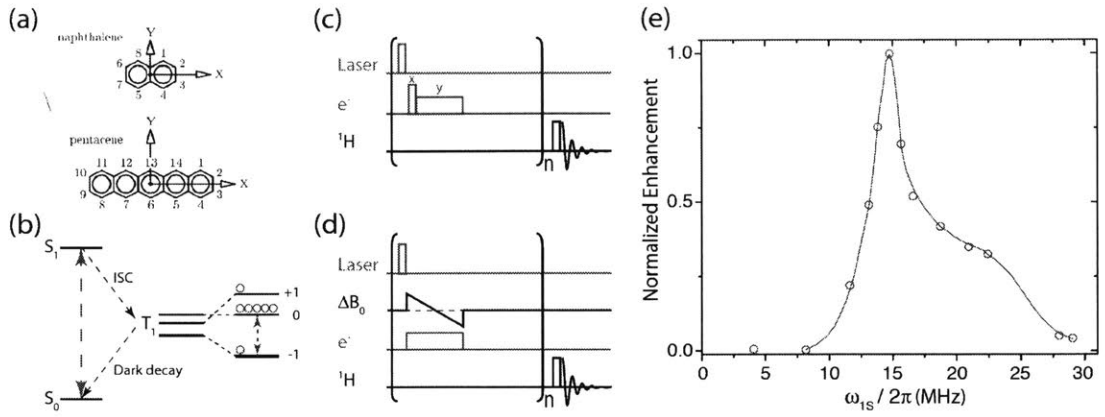

Figure 2.6: (a) Naphthalene doped with pentacene, a favorite sample for NOVEL and ISE pulsed DNP. (b) Photoexcited triplet state of pentacene created by a laser pulse. State with $S_z = 0$ is preferably populated due to the selection rules for the intersystem crossing (ISC) process. (c), (d) NOVEL and ISE pulse sequences on samples doped with pentacene. (e) NOVEL matching condition shows a sharp peak and a long tail at high microwave power indicative of higher order processes involving one electron and multiple nuclei [63].

The NOVEL sequence is an electron-nuclear analogue of cross polarization (CP) in NMR. In a heteronuclear spin system such as ^{1}H-^{13}C, the separation in energy levels due to the difference in the gyromagnetic ratios inhibits the polarization transfer. In a CP experiment, the separation is removed in the doubly rotating frame, leading to a matching in the energy levels, and thus enabling the polarization transfer between nuclei via dipolar coupling. For an electron-nuclear system, the difference in gyromagnetic ratios is so large that matching in a double rotating frame is difficult. However, matching between the electron rotating frame and the nuclear lab frame is possible and also allows efficient polarization transfer and generation of z-polarization. This idea was mentioned in the original Hartman-Hahn paper on cross polarization [64] and was implemented on an electron-nuclear system by Wenckenbach *et al.* in a NOVEL experiment. In the next section, we derive the matching condition, and for a more detailed discussion on the NOVEL sequence we refer the readers to the papers by Wenckebach *et al.* [65, 66]

In the laboratory frame, the Hamiltonian for the NOVEL experiment has the form

$$H = \omega_{0S} S_z - \omega_{0I} I_z + \vec{S} \cdot \vec{\vec{A}} \cdot \vec{I} + 2\omega_{1S} \cos(\omega_{\mu w} t) S_x \qquad (3.2.1)$$

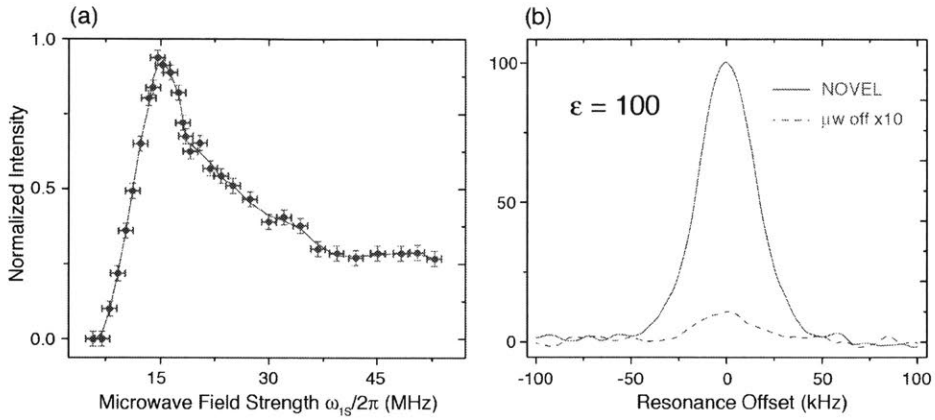

Figure 2.7: NOVEL experiment at 0.35 T and 300 K on a sample of protonated polystyrene doped with 2% BDPA (mass ratio). (a) The matching condition shows a maximum at $\omega_{1S} = \omega_{0I} \approx 15 MHz$ followed by a long tail at high field strength, similar to the published data in **Fig. 2.6e**. (b) Proton NMR spectra of the sample obtained with (red, solid line) and without (blue, dashed line) pulsed DNP. The spectra were acquired using solid echo sequence. A maximum enhancement of 100 was observed.

where the first two terms are the Zeeman interactions, the third is the electron-nuclear interaction, and the last is the microwave spin lock field. Upon transforming to the microwave rotating frame, the Hamiltonian can be truncated to

$$H = \Omega_S S_z - \omega_{0I} I_{zz} + A_{zx} S_z I_x + A_{zy} S_z I_y + A_{zz} S_z I_z + \omega_{1S} S_x \tag{3.2.2}$$

where Ω_S is the microwave offset

$$\Omega_S = \omega_{0S} - \omega_{\mu w} \tag{3.2.3}$$

Transformation to a tilted frame that combines the first and the last terms yields

$$H = \omega_{eff} S_z - \omega_{0I} I_z + \left(A_{zx} I_x + A_{zy} I_y + A_{zz} I_z\right)\left(S_z \cos\theta - S_x \sin\theta\right) \tag{3.2.4}$$

where

$$\omega_{eff} = \pm\sqrt{\Omega_S^2 + \omega_{1S}^2} \tag{3.2.5}$$

The sign of ω_{eff} depends on the phase as well as the offset of the microwave.

We now redefine the transverse axes of the nuclear spin by combining the terms containing I_x and I_y, yielding the Hamiltonian

$$H = \omega_{eff} S_z - \omega_{0I} I_z + \left(A I_z + B I_x\right)\left(S_z \cos\theta - S_x \sin\theta\right) \tag{3.2.6}$$

where A and B are secular and pseudo-secular hyperfine couplings, respectively.

$$A = A_{zz} \tag{3.2.7}$$

$$B = \sqrt{A_{zx}^2 + A_{zy}^2} \tag{3.2.8}$$

Using perturbation theory, we can write the Hamiltonian as

$$H = H^{(0)} + H^{(1)} \tag{3.2.9}$$

where the unperturbed Hamiltonian H_0 and the perturbation H_1 are given as

$$H^{(0)} = \omega_{eff} S_z - \omega_{0I} I_z + A\cos\theta I_z S_z \tag{3.2.10}$$

$$H^{(1)} = B I_x \left(S_z \cos\theta - S_x \sin\theta\right) - A\sin\theta I_z S_x \tag{3.2.11}$$

The inter-subspace splitting between the ZQ subspace and the DQ subspace is approximately ω_{0I}, which is very large compared to the perturbation even at a magnetic field as low as 0.35 T. On the other hand, if the matching condition is fulfilled, states in either the DQ or ZQ subspace are degenerate, resulting in a complete intra-subspace state mixing due to the perturbation, and thus leading to polarization transfer. The perturbation can be truncated to contain only DQ (flip-flip) and ZQ (flip-flop) terms as the following

$$H^{(1)} \approx B\sin\theta I_x S_x \tag{3.2.12}$$

For the positive ω_{eff}, the degeneracy in the DQ subspace leads to the matching condition

$$\omega_{0I} = \omega_{eff} = \sqrt{\Omega_S^2 + \omega_{1S}^2} \tag{3.2.13}$$

If the microwave offset is negligible, the matching condition is simplified to

$$\omega_{1S} \approx \omega_{0I} \tag{3.2.14}$$

which means that the nuclear Larmor frequency equals the Rabi frequency of the electron. In other words, nutation of the nucleus in the laboratory frame matches that of the electron in the rotating frame.

2.3.2.2. Integrated solid effect (ISE)

The ISE was originally developed as an improvement to the SE for cases in which the EPR spectrum is broad, and thus did not exclusively require high microwave power. In this case, the overlap of the positive and the negative SE (differential SE) limits the net DNP enhancement. The idea was to sweep the magnetic field in such a manner so that different electron spin packets constructively contribute to the net DNP enhancement. The first experiment showed a 21-fold improvement compared to the regular SE. In subsequent experiments, ISE was performed while satisfying the Hartman-Hahn matching condition similar to the NOVEL sequence, which led to the name integrated cross polarization (ICP).

The Hamiltonian has the form

$$H = \omega_{0S}(t)S_z - \omega_{0I}(t)I_z + \vec{S}\cdot\vec{\vec{A}}\cdot\vec{I} + 2\omega_{1S}\cos(\omega_{\mu w}t)S_x \qquad (3.2.15)$$

The Zeeman terms are time dependent due to the magnetic field sweep.

In the microwave rotating frame, ignoring the time dependence in the nuclear Zeeman term

$$H = \Omega_S(t)S_z - \omega_{0I}I_z + A_{zx}S_zI_x + A_{zy}S_zI_y + A_{zz}S_zI_z + \omega_{1S}S_x \qquad (3.2.16)$$

$$\Omega_S(t) = \omega_{0S}(t) - \omega_{\mu w} \qquad (3.2.17)$$

And we obtain the following matching condition that is identical to the NOVEL matching condition

$$\omega_{0I}^2 = \Omega_S^2(t) + \omega_{1S}^2 \qquad (3.2.18)$$

Solving for $\Omega_S(t)$

$$\Omega_S(t) = \pm\sqrt{\omega_{0I}^2 - \omega_{1S}^2} \qquad (3.2.19)$$

The $\pm$ sign indicates that two electron spin packets located at $\omega_{0S} \pm \sqrt{\omega_{0I}^2 - \omega_{1S}^2}$ contribute constructively to the DNP enhancement as opposed to the destructive contribution of two spin packets located at $\omega_{0S} \pm \omega_{0I}$ in the original solid effect. Furthermore, sweeping of the magnetic field allows all electron spin packets in a broad EPR line to participate in the DNP process.

2.4. Summary

In summary we have seen that there are now well established methods to perform biomolecular MAS DNP experiments. Perhaps the most successful approach has involved the CE together with nitroxide biradicals. Thus, using AMUPol as a polarizing agent we have achieved enhancement of 400 at 380 MHz/250 GHz and further improvements seem likely. This approach has been used to polarize a variety of biomolecular samples and will likely continue to be important in future experiments. However, in the last few years it has become clear that other mechanisms could be important for high field DNP depending on the availability of suitable polarizing agents and instrumentation. For example, the recently discovered Overhauser effect in insulating solids appears to scale favorably with B_0 and, with polarizing agents that exhibit larger hyperfine couplings, it could become the method of choice for high field CW experiments. In addition, the data in the literature to date appears to indicate that DNP at higher magnetic fields will offer higher resolution due to the dispersion of chemical shifts and truncation of homogeneous couplings that are present in the spectra. Finally, it is possible to perform time domain DNP experiments and these approaches should not exhibit the field dependence displayed by CW methods like the CE or SE. However, implementing pulsed DNP methods will likely require the development of new instrumentation, namely gyroamplifiers, and new methods for time domain polarization transfer. When these become available we anticipate that pulsed DNP will become the method of choice for electron-nuclear polarization transfer.

2.5. Acknowledgement

We would like to thank Drs. Paul Tordo and Olivier Ouari (Aix-Marseille Université) for generously providing AMUPol radial for DNP experiments at 380 MHz/250 GHz. We are grateful to Salima Bahri, Dr. Kevin J. Donovan, Dr. Christy George and Eric G. Keeler for carefully proofreading the manuscript. This research was supported by grants to RGG from the National Institutes of Biomedical Imaging and Bioengineering, (EB-002804, EB-001960, EB-003151, and EB-002026).

2.6. References

[1] A.W. Overhauser, Polarization of Nuclei in Metals, Physical Review, 92 (1953) 411.
[2] T.R. Carver, C.P. Slichter, Polarization of Nuclear Spins in Metals, Physical Review, 92 (1953) 212.
[3] T.R. Carver, C.P. Slichter, Experimental Verification of the Overhauser Nuclear Polarization Effect, Physical Review, 102 (1956) 975.

[4] C.D. Jefferies, Polarization of Nuclei by Resonance Saturation in Paramagnetic Crystals, Physical Review, 106 (1957) 164-165.
[5] C.D. Jefferies, Dynamic Orientation of Nuclei by Forbidden Transitions in Paramagnetic Resonance, Physical Review, 117 (1960) 1056-1069.
[6] A. Abragam, W.G. Proctor, C. R. Acad. Sci., 246 (1958) 2253.
[7] E. Erb, J. Motchane, L., J. Uebersfeld, C. R. Acad. Sci., 246 (1958) 2121.
[8] A. Kessenikh, V., V. Lushchikov, I., A. Manenkov, A., Y. Taran, V., Proton Polarization in Irradiated Polyethylenes, Soviet Physics - Solid State, 5 (1963) 321-329.
[9] A. Kessenikh, V., A. Manenkov, A., G. Pyatnitskii, I., On Explanation of Experimental Data on Dynamic Polarization of Protons in Irradiated Polyethylenes, Soviet Physics - Solid State, 6 (1964) 641-643.
[10] C. Hwang, F., D. Hill, A., Phenomenological Model for the New Effect in Dynamic Polarization, Physical Review Letters, 19 (1967) 1011.
[11] C. Hwang, F., D. Hill, A., New Effect in Dynamic Polarization, Physical Review Letters, 18 (1967) 110.
[12] D. Wollan, S., Dynamic nuclear polarization with an inhomogeneously broadened ESR line. I. Theory, Physical Review B: Condensed Matter, 13 (1976) 3671.
[13] D.S. Wollan, Dynamic nuclear polarization with an inhomogeneously broadened ESR line. II. Experiment, Physical Review B: Condensed Matter, 13 (1976) 3686.
[14] A. Abragam, M. Goldman, Principles of dynamic nuclear polarization, Rep. Prog. Phys., 41 (1978) 395-467.
[15] V.A. Atsarkin, Dynamic Polarization of Nuclei in Solid Dielectrics, Soviet Physics Solid State, 21 (1978) 725-744.
[16] A. Abragam, M. Goldman, Nuclear Magnetism: Order and Disorder, Clarendon Press, Oxford, 1982.
[17] V.A. Atsarkin, A.V. Kessenikh, Dynamic Nuclear Polarization in Solids: The Birth and Development of the Many-Particle Concept, Appl Magn Reson, 43 (2012) 7-19.
[18] R.A. Wind, M.J. Duijvestijn, C. van der Lugt, A. Manenschijn, J. Vriend, Applications of Dynamic Nuclear-Polarization in C-13 NMR in Solids, Progress in Nuclear Magnetic Resonance Spectroscopy, 17 (1985) 33-67.
[19] G.G. Maresch, R.D. Kendrick, C.S. Yannoni, M.E. Galvin, Dynamic Nuclear Polarization via Confined Electrons in Bulk Solids, Jour. Magnetic Resonance, 82 (1989) 41-50.
[20] D.J. Singel, H. Seidel, R.D. Kendrick, C.S. Yannoni, A Spectrometer for EPR, DNP, and Multinuclear High-Resolution NMR, Journal of Magnetic Resonance, 81 (1989) 145-161.
[21] C.S. Yannoni, P.C. Myhre, G.G. Webb, Magic angle spinning nuclear magnetic resonance near liquid-helium temperatures. Variable-temperature CPMAS spectra of the 2-norbornyl cation to 6 K, J. Am. Chem. Soc., 112 (1990) 8991–8992.
[22] M. Afeworki, J. Schaefer, Mechanism of DNP-Enhanced Polarization Transfer across the Interface of Polycarbonate/Polystyrene Heterogeneous Blends, Macromolecules, 25 (1992) 4092-4096.
[23] J.Z. Hu, J. Zhou, B. Yang, L. Li, J. Qiu, C. Ye, M.S. Solum, R.A. Wind, R.J. Pugmire, D.M. Grant, Dynamic nuclear polarization of nitrogen-15 in benzamide, Solid State Nuclear Magnetic Resonance, 8 (1997) 129-137.
[24] L. Becerra, G. Gerfen, R. Temkin, D. Singel, R. Griffin, Dynamic nuclear polarization with a cyclotron resonance maser at 5 T., Physical Review Letters, 71 (1993) 3561-3564.
[25] L.R. Becerra, G.J. Gerfen, B.F. Bellew, J.A. Bryant, D.A. Hall, S.J. Inati, R.T. Weber, S. Un, T.F. Prisner, A.E. McDermott, K.W. Fishbein, K. Kreischer, R.J. Temkin, D.J. Singel, R.G. Griffin, A Spectrometer for Dynamic Nuclear Polarization and Electron Paramagnetic Resonance at High Frequencies, Journal of Magnetic Resonance, A117 (1995) 28-40.

[26] V. Bajaj, C. Farrar, M. Hornstein, I. Mastovsky, J. Vieregg, J. Bryant, B. Elena, K. Kreischer, R. Temkin, R. Griffin, Dynamic nuclear polarization at 9T using a novel 250GHz gyrotron microwave source., J Magn Reson, 160 (2003) 85-90.
[27] M. Rosay, L. Tometich, S. Pawsey, R. Bader, R. Schauwecker, M. Blank, P.M. Borchard, S.R. Cauffman, K.L. Felch, R.T. Weber, R.J. Temkin, R.G. Griffin, W.E. Maas, Solid-state dynamic nuclear polarization at 263 GHz: spectrometer design and experimental results, Physical Chemistry Chemical Physics, 12 (2010) 5850-5860.
[28] A. Barnes, E. Markhasin, E. Daviso, V. Michaelis, E.A. Nanni, S.K. Jawla, E.L. Mena, R. DeRocher, A. Thakkar, P.P. Woskov, J. Herzfeld, R.J. Temkin, R.G. Griffin, Dynamic nuclear polarization at 700 MHz/460 GHz, J Magn Reson, 224 (2012) 1-7.
[29] K.-N. Hu, G.T. Debelouchina, A.A. Smith, R.G. Griffin, Quantum mechanical theory of dynamic nuclear polarization in solid dielectrics, Journal of Chemical Physics, 134 (2011).
[30] F. Mentink-Vigier, U. Akbey, Y. Hovav, S. Vega, H. Oschkinat, A. Feintuch, Fast passage dynamic nuclear polarization on rotating solids, Journal of magnetic resonance (San Diego, Calif. : 1997), 224 (2012) 13-21.
[31] K. Thurber, R. Tycko, Theory for cross effect dynamic nuclear polarization under magic angle spinning in solid state nuclear magnetic resonance: the importance of level crossings, J Chem Phys, 137 (2012) 084508-084501.
[32] Q.Z. Ni, E. Daviso, T.V. Can, E. Markhasin, S.K. Jawla, T.M. Swager, R.J. Temkin, J. Herzfeld, R.G. Griffin, High Frequency Dynamic Nuclear Polarization, Accounts of Chemical Research, 46 (2013) 1933-1941.
[33] A.B. Barnes, G. De Paëpe, P.C.A. van der Wel, K.N. Hu, C.G. Joo, V.S. Bajaj, M.L. Mak-Jurkauskas, J.R. Sirigiri, J. Herzfeld, R.J. Temkin, R.G. Griffin, High-Field Dynamic Nuclear Polarization for Solid and Solution Biological NMR, Applied Magnetic Resonance, 34 (2008) 237-263.
[34] T. Maly, G.T. Debelouchina, V.S. Bajaj, K.-N. Hu, C.-G. Joo, M.L. Mak-Jurkauskas, J.R. Sirigiri, P.C.A. van der Wel, J. Herzfeld, R.J. Temkin, R.G. Griffin, Dynamic nuclear polarization at high magnetic fields, The Journal of Chemical Physics, 128 (2008) 052211-052219.
[35] E.A. Nanni, A.B. Barnes, R.G. Griffin, R.J. Temkin, THz Dynamic Nuclear Polarization NMR, IEEE Trans. Terahertz Sci. Technol., 1 (2011) 145-163.
[36] T.V. Can, M.A. Caporini, F. Mentink-Vigier, B. Corzilius, J.J. Walish, M. Rosay, W.E. Maas, M. Baldus, S. Vega, T.M. Swager, R.G. Griffin, Overhauser effects in insulating solids, Journal of Chemical Physics, 141 (2014).
[37] M. Goldman, Spin Temperature and Nuclear Magnetic Resonance in Solids, Oxford University Press, 1970.
[38] B. Corzilius, A.A. Smith, R.G. Griffin, Solid effect in magic angle spinning dynamic nuclear polarization, J Chem Phys, (2012).
[39] A.A. Smith, B. Corzilius, A.B. Barnes, T. Maly, R.G. Griffin, Solid effect dynamic nuclear polarization and polarization pathways, Journal of Chemical Physics, 136 (2012) 015101-(015101-015116).
[40] B. Corzilius, A.A. Smith, A.B. Barnes, C. Luchinat, I. Bertini, R.G. Griffin, High-Field Dynamic Nuclear Polarization with High-Spin Transition Metal Ions, Journal of the American Chemical Society, 133 (2011) 5648-5651.
[41] K.-N. Hu, C. Song, H.-h. Yu, T.M. Swager, R.G. Griffin, High-frequency dynamic nuclear polarization using biradicals: A multifrequency EPR lineshape analysis, The Journal of Chemical Physics, 128 (2008) 052302-052317.
[42] K. Hu, H. Yu, T. Swager, R. Griffin, Dynamic nuclear polarization with biradicals., Journal of the American Chemical Society, 126 (2004) 10844-10845.

[43] C. Sauvee, M. Rosay, G. Casano, F. Aussenac, R.T. Weber, O. Ouari, P. Tordo, Highly Efficient, Water-Soluble Polarizing Agents for Dynamic Nuclear Polarization at High Frequency, Angewandte Chemie-International Edition, 52 (2013) 10858-10861.
[44] B. Corzilius, L.B. Andreas, A.A. Smith, Q.Z. Ni, R.G. Griffin, Paramagnet induced signal quenching in MAS-DNP experiments in frozen homogeneous solutions, Journal of Magnetic Resonance, 240 (2014) 113-123.
[45] D. Shimon, Y. Hovav, A. Feintuch, D. Goldfarb, S. Vega, DNP in the Solid State: A Transition between the Cross Effect and the Solid Effect., Phys Chem Chem Phys, (2012).
[46] D. Shimon, A. Feintuch, D. Goldfarb, S. Vega, Static H-1 dynamic nuclear polarization with the biradical TOTAPOL: a transition between the solid effect and the cross effect, Physical Chemistry Chemical Physics, 16 (2014) 6687-6699.
[47] Y. Hovav, A. Feintuch, S. Vega, Theoretical aspects of dynamic nuclear polarization in the solid state - spin temperature and thermal mixing, Physical Chemistry Chemical Physics, 15 (2013) 188-203.
[48] T. Maly, A.-F. Miller, R.G. Griffin, In situ High-Field Dynamic Nuclear Polarization- Direct and Indirect Polarization of 13C nuclei, ChemPhysChem, 11 (2010) 999-1001.
[49] T. Maly, L.B. Andreas, A.A. Smith, R.G. Griffin, 2H-DNP-enhanced 2H–13C solid-state NMR correlation spectroscopy, Phys Chem Chem Phys, 12 (2010) 5872-5878.
[50] V.K. Michaelis, B. Corzilius, A.A. Smith, R.G. Griffin, Dynamic Nuclear Polarization of O-17: Direct Polarization, Journal of Physical Chemistry B, 117 (2013) 14894-14906.
[51] A. Zagdoun, G. Casano, O. Ouari, G. Lapadula, A.J. Rossini, M. Lelli, M. Baffert, D. Gajan, L. Veyre, W.E. Maas, M.M. Rosay, R.T. Weber, C. Thieuleux, C. Copéret, A. Lesage, P. Tordo, L. Emsley, A slowly relaxing rigid biradical for efficient DNP surface enhanced NMR spectroscopy: expeditious characterization of functional group manipulation in hybrid materials, J. Am. Chem. Soc., (2012).
[52] A. Zagdoun, G. Casano, O. Ouari, M. Schwarzwalder, A.J. Rossini, F. Aussenac, M. Yulikov, G. Jeschke, C. Copéret, A. Lesage, P. Tordo, L. Emsley, Large Molecular Weight Nitroxide Biradicals Providing Efficient Dynamic Nuclear Polarization at Temperatures up to 200 K, Journal of the American Chemical Society, 135 (2013) 12790-12797.
[53] K.N. Hu, Polarizing Agents for High-Frequency Dynamic Nuclear Polarization – Development and Applications, in: Chemistry, MIT, 2006, pp. 274.
[54] K.-N. Hu, G.T. Debelouchina, A.A. Smith, R.G. Griffin, Quantum mechanical theory of dynamic nuclear polarization in solid dielectrics, J. Chem. Phys., 134 (2011) 125105.
[55] J. Vanhouten, W.T. Wenckebach, N.J. Poulis, Study of Thermal Contact Between Nuclear Zeeman System and Electron Dipole-Dipole Interaction System, Physica B & C, 92 (1977) 210-220.
[56] K.R. Thurber, R. Tycko, Perturbation of nuclear spin polarizations in solid state NMR of nitroxide-doped samples by magic-angle spinning without microwaves, Journal of Chemical Physics, 140 (2014).
[57] N. Bloembergen, P.P. Sorokin, Nuclear Magnetic Resonance in the Cesium Halides, Physical Review, 110 (1958) 865.
[58] R.A. Wind, L. Li, H. Lock, G.E. Maciel, Dynamic nuclear polarization in the nuclear rotating frame, Journal of Magnetic Resonance, 79 (1988) 577-582.
[59] C. Farrar, D. Hall, G. Gerfen, M. Rosay, J. Ardenkjaer-Larsen, R. Griffin, High-frequency dynamic nuclear polarization in the nuclear rotating frame., J Magn Reson, 144 (2000) 134-141.
[60] K. Hu, V. Bajaj, M. Rosay, R. Griffin, High-frequency dynamic nuclear polarization using mixtures of TEMPO and trityl radicals., J Chem Phys, 126 (2007) 044512.

[61] V. Weis, M. Bennati, M. Rosay, R.G. Griffin, Solid effect in the electron spin dressed state: A new approach for dynamic nuclear polarization, J. Chem. Phys., 113 (2000) 6795-6802.
[62] B.R. Mollow, Power Syectrum of Light Scattered by Two-Level Systems, Phys Rev, 188 (1969) 1969-1975.
[63] D.J. van den Heuvel, A. Henstra, T.-S. Lin, J. Schmidt, W.T. Wenckebach, Transient oscillations in pulsed dynamic nuclear polarization, Chemical Physics Letters, 188 (1992) 194-200.
[64] S.R. Hartmann, E.L. Hahn, Nuclear Double Resonance in the Rotating frame, Phys. Rev., 128 (1962) 2042-2053.
[65] A. Henstra, T.-S.Lin, J. Schmidt, W.T. Wenckeback, High Dynamic Nucler Polarization at Room Temperature, Chem. Phys. Letters, 165 (1990) 6-10.
[66] A. Henstra, W. Wenckebach, The theory of nuclear orientation via electron spin locking (NOVEL), Molecular Physics, 106 (2008) 859-871.

Chapter 3: Overhauser Effects in Insulating Solids

Adapted from T.V. Can, M.A. Caporini, F. Mentink-Vigier, B. Corzilius, J.J. Walish, M. Rosay, W.E. Maas, M. Baldus, S. Vega, T.M. Swager, and R.G. Griffin, Journal of Chemical Physics 141 (2014) 064202

We report magic angle spinning (MAS), dynamic nuclear polarization (DNP) experiments at magnetic fields of 9.4 T, 14.1 T and 18.8 T using the narrow line polarizing agents BDPA dispersed in polystyrene, and sulfonated-BDPA and trityl OX063 in glassy glycerol/water matrices. The ^{1}H DNP enhancement field profiles of the BDPA radicals exhibit a significant DNP Overhauser effect (OE) as well as a solid effect (SE) despite the fact that these samples are insulating solids. In contrast, trityl exhibits only a SE enhancement. Data suggest that the appearance of the OE is due to rather strong electron-nuclear hyperfine couplings present in BDPA and SA-BDPA, but which are absent in trityl and d_{21}-BDPA. In addition, and in contrast to other DNP mechanisms such as the solid effect or cross effect, the experimental data suggest that the OE in non-conducting solids scales favorably with magnetic field, increasing in magnitude in going from 5 T, to 9.4 T, to 14.1 T and to 18.8 T. Simulations using a model two spin system consisting of an electron hyperfine coupled to a ^{1}H reproduce the essential features of the field profiles and indicate that the OE in these samples originates from the zero and double quantum cross relaxation induced by fluctuating hyperfine interactions between the intramolecular delocalized unpaired electrons and their neighboring nuclei and that the size of these hyperfine couplings is crucial to the magnitude of the enhancements. Microwave field dependent studies show that the OE saturates at considerably lower power levels than the solid effect in the same samples. Our results provide new insights into the mechanism of the Overhauser effect, and also provide a new approach to perform DNP experiments in chemical, biophysical and physical systems at high magnetic fields.

Introduction

The last decade has witnessed a renaissance in the use of high frequency dynamic nuclear polarization (DNP) to enhance sensitivity in nuclear magnetic resonance (NMR) experiments. In particular, the development of gyrotron and other high frequency microwave sources permits DNP to be performed at magnetic fields used in contemporary NMR experiments (5-20 Tesla) [1-8]. To date these experiments, which have focused mostly on insulating solids formed from glassy, frozen solutions of proteins and other nonconducting materials, have relied primarily on narrow line monoradicals and the solid effect (SE) [1, 9-11] or nitroxide biradicals and the cross effect (CE) [12-18] to mediate the polarization process. These approaches have resulted in large signal enhancements and have enabled many experiments that would otherwise be impossible [19-23]. Nevertheless, with the exception of an early example on a 1D conductor[24], the Overhauser effect (OE), which was the initial DNP mechanism proposed by Overhauser [25] and confirmed by Carver and Slichter [26], has not been identified or utilized during the course of this renaissance. Although the possibility of an OE in insulator was discussed by Abragam [27], the conventional wisdom is that Overhauser DNP is important only in systems with mobile electrons such as conductors (metals and low dimensional conductors) or in liquid solution [28, 29]. Accordingly, it was not expected to be a significant polarization mechanism in non-conducting solids. In contrast to these expectations, we report here the observation of significant Overhauser enhancements using the narrow line radicals SA-BDPA in glycerol/water and BDPA in polystyrene glassy matrices, both insulating solids.

Recently we described the development of a class of narrow line radicals, sulfonated BDPA (SA-BDPA), with the intent of improving SE enhancements in aqueous media [30]. In experiments at 5 T (211 MHz for ^{1}H) these radicals showed the expected SE enhancement at $\omega_{SE} = \omega_{0S} \pm \omega_{0I}$ and in addition a relatively weak, positive enhancement when microwaves were applied at ω_{0S}. We have continued investigations of SA-BDPA and at higher fields, 9.4 and 14.1 T (400 and 600 MHz for ^{1}H), and observed larger enhancements around ω_{0S}. Furthermore, BDPA itself dispersed in polymer matrices also exhibits enhancements at ω_{0S} that are one order of magnitude larger than the SE at 18.8 T. We attributed this central peak to an Overhauser effect even though the samples are nonconducting solids. In particular, the lineshape is characteristic of an OE in which the sign of the DNP enhancement does not depend upon the offset of the microwave frequency.

Interestingly, trityl OX063 radical [31], which was designed to optimize Overhauser effects in solution by eliminating hyperfine couplings[32, 33], shows only SE enhancements at $\omega_{0S} \pm \omega_{0I}$. Thus, the OE effect appears to require the presence of multiple hyperfine or dipolar couplings that permit zero quantum (ZQ) or double quantum (DQ) relaxation, respectively, and Overhauser enhancements. Furthermore, the field dependent studies indicate that the size of the OE enhancements scales at least weakly with ω_{0I}, in contrast to the ω_{0I}^{-1} or ω_{0I}^{-2} dependence observed for the CE or SE [13, 18, 34, 35]. Finally, simulations suggest that a large hyperfine coupling and the dominance of the ZQ or DQ relaxation rate in the polarization process leads to the observed positive or negative Overhauser enhancements, respectively.

Background

Part of our results (*vide infra*) share a characteristic feature with the Overhauser effect in solution where an enhancement is observed around the electron resonance frequencies. In ^{1}H OE-DNP in solutions this enhancement is usually negative and positive enhancements are generally not observed except in the case of scalar relaxation[36]. It is, therefore, convenient to briefly review the concepts leading to the enhancements in liquid-DNP and explain how they can be applied to DNP in rotating solids. In an electron – nuclear system the source of the OE-DNP enhancement is the difference between the zero quantum (ZQ) and the double quantum (DQ) cross-relaxation rates. The rates, $\Gamma_{1,ZQ}$ and $\Gamma_{1,DQ}$, are governed by fluctuating electron – nuclear couplings and are active between the electron-nuclear ZQ and DQ transitions, respectively. The imbalance of the two rates generates a population redistribution during on-resonance microwave (μw) irradiation, resulting in enhanced positive or negative nuclear polarization depending on whether $\Gamma_{1,ZQ} > \Gamma_{1,DQ}$ or $\Gamma_{1,ZQ} < \Gamma_{1,DQ}$. In general, in DNP in liquids $\Gamma_{1,DQ}$ dominates and the OE enhancement are negative for ^{1}H. In addition to observations in liquids, the Overhauser effect is observed earlier in conducting solids [28, 29] and in heavily doped semiconductors [37], where it was treated as a three spin effect. It has been neglected in insulating solids.

We note that the OE mechanism differs from the SE in that the μw radiation is applied to the single quantum (SQ) electron transitions and the enhancement is generated by ZQ and DQ cross relaxation. In contrast in the SE the μw irradiation is applied at the

"forbidden" transitions, either a ZQ or DQ transition, and the enhancement is due to the single quantum relaxation of the electron.

Our experimental results discussed below show that both ZQ and DQ relaxation can dominate the OE process, and data with positive and negative enhancements are observed. When the fluctuating interactions are the hyperfine couplings, the scalar part of the hyperfine coupling leads to ZQ cross relaxation rate $\Gamma_{1,ZQ}$, while the dipolar part lead to DQ cross relaxation rate $\Gamma_{1,DQ}$. All these effects characterizing OE-DNP are relevant in solution and as well in rotating samples, although the origin of the fluctuations of the hyperfine coupling is different.

Experimental

Samples

Polystyrene doped with 2% BDPA or d_{21}-BDPA was prepared by a film casting method [1, 38]. Briefly, 2.4 mg of BDPA in complex with benzene or 2 mg of d_{21}-BDPA and 95 mg of PS-d_8 together with 5 mg of PS-d_5 were dissolved in 2 ml of chloroform. The solution was then spread on a glass surface. A thin film of PS doped with 2% BDPA or d_{21}-BDPA was collected and ground thoroughly upon evaporation of the solvent. Residual solvent was then removed under vacuum for at least 12 hours.

The preparation of DNP samples containing SA-BDPA and trityl OX063 were described elsewhere [30, 34]. For each sample, the corresponding radical was dissolved in a mixture of glycerol-d_8/D_2O/H_2O (60/30/10 volume ratio) supplemented with 100 mM ^{13}C, ^{15}N Proline. The final concentrations of SA-BDPA and trityl OX063 were 40 mM.

DNP Experiments

DNP experiments at 9.4 T and 14.1 T were performed using two NMR/DNP spectrometers (Bruker BioSpin (Billerica, MA)) operating at 600 MHz/395 GHz and 400 MHz/263 GHz of ^1H/electron Larmor frequencies [6]. Experiments at 18.8 T were conducted on a NMR/DNP spectrometer at Utrecht University (Utrecht, The Netherlands) operating at 800 MHz/527 GHz of ^1H/electron Larmor frequencies. The temperature at the sample was ~105 K with μw's on and ~100 K without microwaves as calibrated from the T_1 of ^{79}Br on a KBr sample under the same conditions [39, 40]. The spinning frequency, which does not affect the DNP efficiency in our study, was chosen to be $\omega_r/2\pi$=8 kHz as a compromise between sample heating and signal intensity. The sweep coil supports up to ±20 A

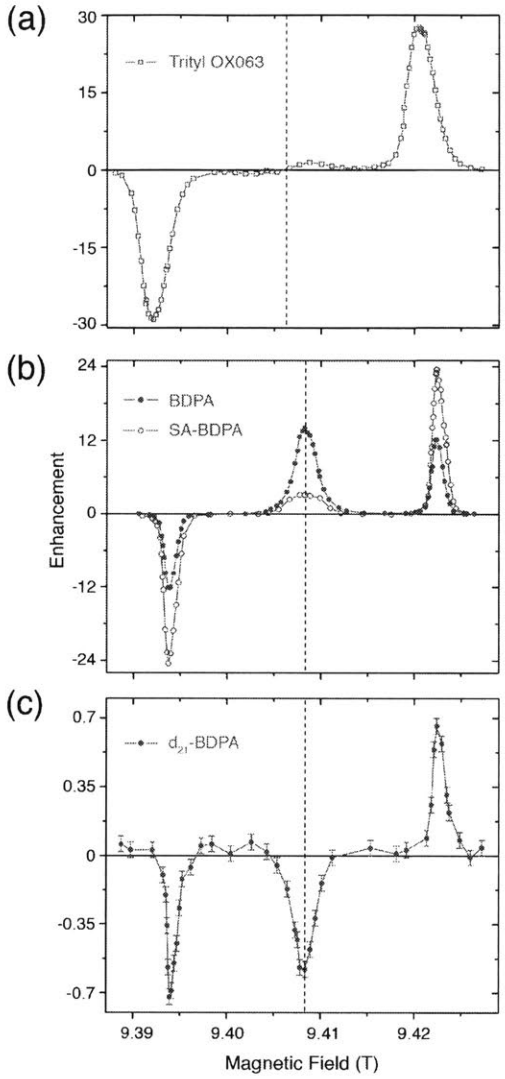

Figure 3.1: ^{1}H DNP enhancement field profiles of (a) trityl OX063, (b) BDPA (red solid circle) and SA-BDPA (blue open circle), and (c) d_{21}-BDPA at 9.4 T. All the field profiles were obtained with about 9 W of microwave power. A well-resolved solid effect is observed for all three radicals. The dashed line indicates the position of the isotropic g-value and the BDPA's are upfield from trityl. In addition, in (b) a significant Overhauser DNP enhancement is also present when irradiating at the EPR transition in BDPA and SA-BDPA. The positive enhancement indicates the DNP process is dominated by a zero-quantum (ZQ) process; (c) The field profile for perdeuterated BDPA show a negative OE indicating it is dominated by a double quantum (DQ) process.

corresponding to ±75 mT at 400 MHz, ± 128 mT at 600 MHz and ±xx mT at 800 MHz. The room temperature shim set provides fine adjustments within the range of 240 ppm at 9.4 T, 150 ppm at 14.1 T and xx ppm at 18.8 T.

The DNP enhancement field profiles were obtained by comparing the intensity of NMR signals with and without microwave at different magnetic fields of the NMR magnet. All

experiments started with a series of saturation pulses followed by recovery period. The magnetically dilute ^{1}H NMR signals present in "DNP Juice" were narrowed by MAS and detected using a rotor-synchronized Hahn echo pulse sequence. The spin-lattice relaxation T_1 and the DNP buildup time constant T_B were measured by varying the recovery time. We found that the T_1 and T_B for each sample at each magnetic field were essentially identical. For the BDPA/PS sample, the T_1 and T_B were 4.6, 6.0 and 7.2 s at 9.4, 14.1 and 18.8 T, respectively. The T_1 and T_B for SA-BDPA in glycerol/water sample were 37 and 45 s at 9.4 and 14.1 T, respectively.

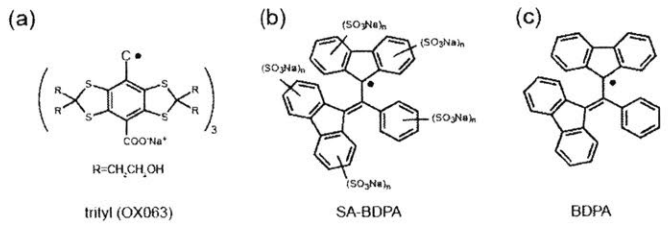

Figure 3.2: Molecular structures of (a) trityl (OX063), (b) sulfonated BDPA (SA-BDPA) and (c) BDPA. Note that the EPR spectrum of trityl exhibits no hyperfine structure due to ^{1}H couplings. BDPA has a total of 21 ^{1}H's coupled to the electron and SA-BDPA has similar couplings but 5 fewer due to the addition of $-SO_3$ groups to the rings.

Results

Figure 3.1a, 3.1b and **3.1c** shows ^{1}H DNP-MAS enhancement field profiles obtained from samples containing the polarizing agents trityl OX063, SA-BDPA, BDPA and perdeuterated BDPA (d_{21}-BDPA) (see **Figure 3.2** and **Figure 3.3** for the molecular structures and EPR spectra, respectively) at 9.4 T using 9 W of microwave power. The data were recorded by observing the intensity of the dilute ^{1}H signals with and without μw irradiation. The enhancement was then calculated according to $\epsilon = (I / I_0) - 1$. The field profiles in **Figure 3.1** clearly show the expected SE enhancements at $\omega_{0S} \pm \omega_{0I}$ for all the radicals. In addition, in the case of SA-BDPA and BDPA there is a strong positive enhancement at the center of the field profile due to the Overhauser effect with ZQ relaxation dominating and yielding a positive enhancement. We also have observed a weak negative OE (ε =-0.6) **Figure 3.1c** when using d_{21}-BDPA, a result that is consistent with DQ relaxation dominating the enhancement.

Similarly, the field profiles of the same samples at 14.1 T were recorded with 13 W of microwave power and are illustrated in **Figure 3.4** and show the same features as in **Figure 3.1**. All the field profiles exhibited well-resolved DNP solid effect (SE) enhancements with

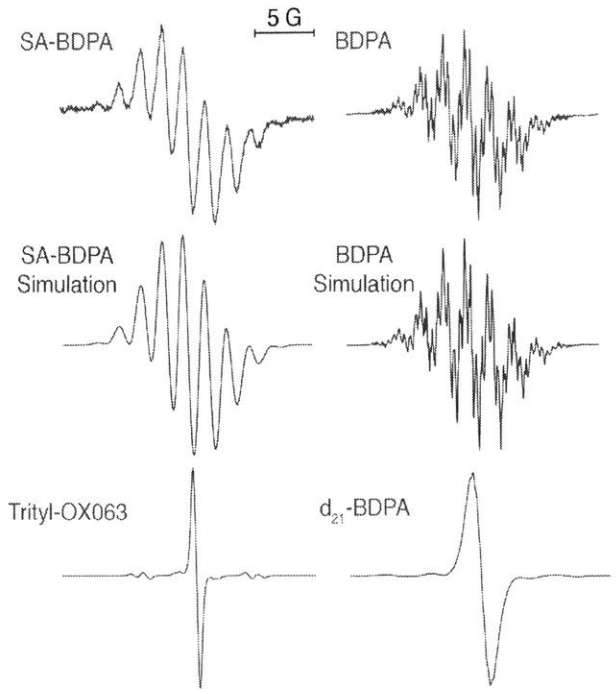

Figure 3.3: Liquid solution EPR spectra of the BDPA's and trityl shown in **Figure 3.2**. BDPA and d_{21}-BDPA were dissolved in toluene whereas SA-BDPA and trityl were dissolved in water. The radical concentration was 50 μM for BDPA's samples and 1 mM for trityl sample. Note that trityl exhibits no hyperfine structure due to ^{1}H couplings. In contrast BDPA has a total of 21 ^{1}H's coupled to the electron [41, 42]. SA-BDPA has 5 fewer ^{1}H's as suggested by Haze *et. al.[30]* due to the addition of –SO3 groups to the rings. The simulation for BPDA uses isotropic hyperfine coupling constants of -0.15 MHz (2), -0.50 MHz (3), 1.09 MHz (4), 1.38 MHz (4), -5.29 MHz (4) and -5.54 MHz (4), where the number in parenthesis indicates the number of ^{1}H's. These are slightly different from the literature values of with coupling constants of -0.29, -0.50, 0.97, 1.37, -5.29 and -5.55 MHz . The simulation for SA-BDPA includes 16 ^{1}H's with isotropic couplings of -0.28 MHz (2), -0.5 MHz (2), 0.98 MHz (4), -5.04 MHz (4) and -5.26 MHz (4). The linebroadening in SA-BDPA is most likely due to the slow tumbling of the radical in water.

the negative and the positive SE corresponding to the zero quantum and double quantum SE transitions, respectively. Note that at 14.1 T the SE enhancement profiles begin to display the presence of a small g-anisotropy from the BDPA's. Furthermore, in contrast to previous SE data where we observed a 10-20% asymmetry in the ZQ and DQ enhancements[12], we find that the maximum positive and negative enhancements are essentially equal. It is important to note that a comparison of **Figures 3.1** and **3.4** shows that at 14.1 T the OE becomes the dominate DNP mechanism in the BDPA/PS sample and increases to ~ 40% of the intensity of the SE transition in SA-BDPA. Thus, the OE exhibits a $\sim \omega_{0I}$ dependence as opposed to the inverse dependences predicted for the SE [1, 9-11] and CE [12-18].

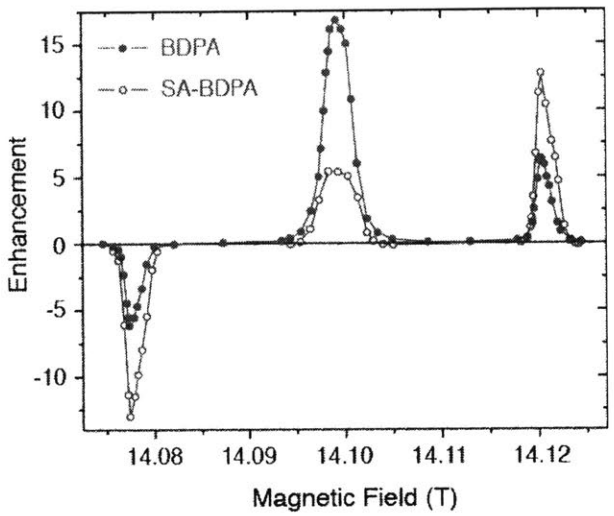

Figure 3.4: ^{1}H DNP enhancement field profile of BDPA (red, solid circle), SA-BDPA (blue, open circle) at 14.1 T. All the field profiles were obtained with 13 W of microwave power. The Overhauser effect in BDPA and SA-BDPA became more efficient at this magnetic field. Note that at this magnetic field the Overhauser effect dominates the SE in the BDPA/PS sample.

We further investigated the field dependence of the OE and SE in the BDPA/PS sample. Shown in **Figure 3.5** is the comparison of the DNP field profiles of this sample at three different magnetic fields. The OE exhibits a $\sim \omega_{0I}$ dependence increasing from 13 at 9.4 T to 17 at 14.1 T and to 20 at 18.8 T. The SE, on the other hand, shows a $\sim \omega_{0I}^{-2}$ dependence decreasing from 12 at 9.4 T to 6 at 14.1 T and to 2 at 18.8 T.

We have also examined the μw power dependence for BDPA sample as shown in **Figure 3.6a**. Note that the DNP enhancement via the OE displays a sharp rise and saturates at very low microwave powers (< 2 W). This indicates that the Overhauser peak relies on irradiation of the allowed EPR transitions at lower microwave power rather than the nominally forbidden SE transitions. In contrast, the enhancement of the DNP solid effect increases monotonically and does not saturate at even at the highest microwave powers.

Discussion

Similar to the published data at 5 T[30], the field profile at 9.4 T of SA-BDPA showed a DNP enhancement symmetrically disposed about ω_{0S} corresponding to μw irradiation on resonance with the EPR transition. We attribute this central peak to an Overhauser effect even though the samples are nonconducting solids. In particular, the lineshape of the center peak is characteristic of OE in which the sign of the DNP enhancement does not depend upon the offset of the microwave frequency.

As mentioned above[27], Abragam predicted that Overhauser effect would dominate in insulating materials given that the isotropic hyperfine interaction is larger than the nuclear Zeeman interaction. The solid effect would otherwise be the dominating DNP mechanism. The prediction is valid for low magnetic fields where the nuclear Zeeman interaction is small and the two DNP mechanisms can overlap. In our study at high fields (> 9 T), the hyperfine coupling is 2 orders of magnitude smaller than the nuclear Zeeman interaction and the two DNP mechanisms are well separated by the nuclear Larmor frequency. Therefore, the central peaks in the field profiles of SA-BDPA and BDPA are purely due to the Overhauser effect.

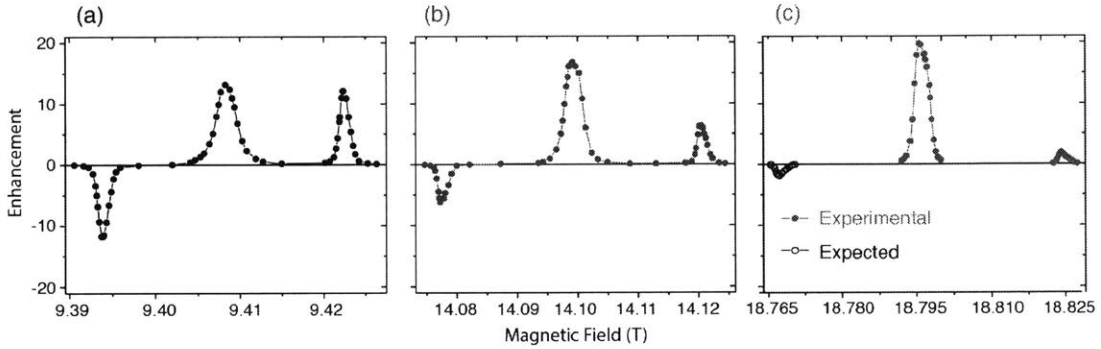

Figure 3.5: ^{1}H DNP enhancement field profile of BDPA at 9.4 T (a), 14.1 T (b) and 18.8 T (c). At 18.8 T, due to the limited experimental time, we only measured the Overhauser effect and the positive solid effect peaks (red, solid circle) using 14 W of microwave power. The peak of the negative solid effect (black, open circle) was then deduced from that of the positive solid effect. Note that the enhancement of the Overhauser effect appears to scale with B_0 whereas that of the solid effect scales very close to B_0^{-2}. At 18.8 T, the maximum enhancement of the Overhauser effect is one order of magnitude larger than that of the solid effect.

Abragam and coworkers also briefly reported observation of an OE enhancement in charcoal and graphite, although the state of the samples was not well characterized [43]. In a more recent study by Dementyev et. al.[37], a negative Overhauser effect was observed at 2.35 T and 1.1 K in a single crystal of doped semiconductors Si:P. Even though the doped semiconductor was in an insulating state, the dopant concentration was sufficiently high to form clusters of electrons. The spin system leading to DNP therefore consists of two electrons, two ^{31}P nuclei and a single ^{29}Si, but the Hamiltonian was simplified to one containing three spins. In this system the strong exchange coupling of up to 100 GHz between the electrons is comparable to the electron Zeeman interaction (66 GHz), and modulates the electron-nuclear coupling, leading to a negative Overhauser effect. Thus, this system is very different from the systems and experiments studied and reported here. In particular, $B_0 \geq 9.4$ T and the electron concentration is ~40 mM, yielding an exchange

coupling that is at least 2-3 orders of magnitude smaller than the electron Zeeman energy. In addition, if this mechanism were present in our experiments, the Overhauser effect would have been observed for all our samples, in particular with a same sign and same intensity of BDPA and d_{21}-BDPA. Thus, the fluctuations leading to the OE enhancements cannot be explained by the exchange coupling.

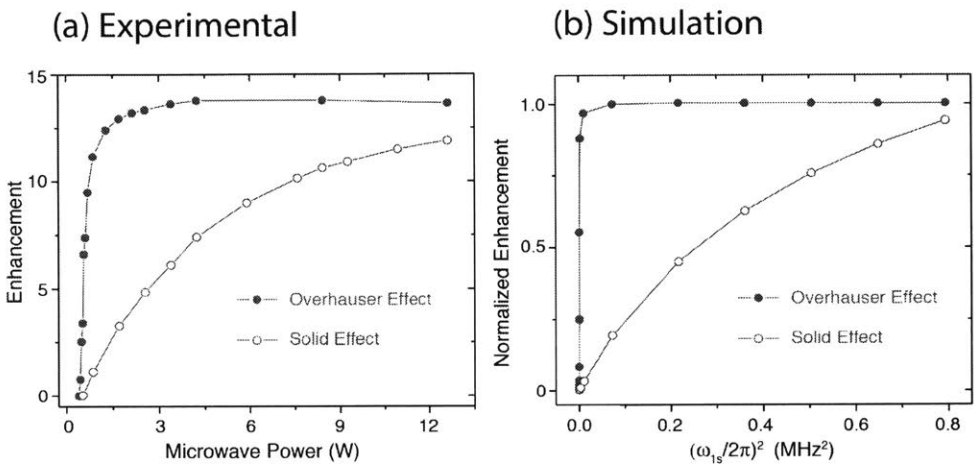

Figure 3.6: (a) Experimental ^{1}H DNP enhancements of BDPA as a function of μw power at 9.4 T. The Overhauser enhancement (red solid circles) showed a sharp rise at low power, whereas the enhancement via the solid effect (blue open circles) gradually increased with μw power. (b) Simulations of the power dependence of the OE and SE using the parameters for BDPA included in the caption of **Figure 3.8** below.

Figure 3.2 shows the molecular structures and **Figure 3.3** shows the solution X-band EPR spectra of all the paramagnetic polarizing agents used in our study, together with simulations of the EPR spectra of SA-BDPA and BDPA performed with EasySpin[44]. As is clear from **Figure 3.3** both BDPA and SA-BDPA exhibit a rich array of hyperfine splittings whereas trityl OX063 and d_{21}-BDPA do not. Specifically, the simulations for BPDA used isotropic hyperfine couplings to 21 ^{1}H's with coupling constants of -0.15 MHz (2), -0.50 MHz (3), 1.09 MHz (4), 1.38 MHz (4), -5.29 MHz (4) and -5.54 MHz (4) similar to the published data[41, 42], where the number in parenthesis indicates the number of ^{1}H's. The sulfonation process removes 5 ^{1}H's [30] and therefore the simulation of the SA-BDPA spectrum shown in **Figure 3.3** includes 16 ^{1}H's with isotropic couplings of -0.28 MHz (2), -0.5 MHz (2), 0.98 MHz (4), -5.04 MHz (4) and -5.26 MHz (4). In contrast, trityl has a maximum proton hyperfine coupling of 0.05 MHz [33]. As we will see below this is the likely source of the Overhauser effect observed in the SA-BDPA and BDPA and absent in trityl OX063. The fact that there is a large enhancement at ω_{0S} could possibly be explained as electron

decoupling and is discussed elsewhere[45]. However, the fact that trityl *does* show paramagnetic quenching in MAS experiments [45] but *does not* exhibit an enhancement at ω_{0S} excludes this possibility.

The relationship between isotropic hyperfine coupling and the Overhauser effect in SA-BDPA and BDPA is also strongly supported by the data on d_{21}-BDPA. Deuteration effectively removes all the hyperfine couplings, which is evident in the EPR spectrum of d_{21}-BDPA in **Figure 3.3**. Thus, any DNP processes in d_{21}-BDPA are mediated by the anisotropic dipolar coupling between the radical and ^{1}H's of polystyrene, which is consistent with the observation of negative Overhauser effect (see **Figure 3.1c**). Moreover, such a coupling is expected to be of smaller amplitude and lead to lower DNP enhancements for both the solid effect and Overhauser effect. This result also implies that in SA-BDPA or BDPA, the main pathway for the polarization transfer starts from the ^{1}H's on the radicals.

It is worth noting that the field profile of trityl (**Figure 3.1a**) exhibits a reproducible asymmetric feature near its center reminiscent of a cross effect field profile. The low field side of this feature is slightly negative and the center field corresponding to the location where OE's are observed is a crossing point and zero intensity. At high field there is a positive lobe to the profile. At the moment we do not have a satisfactory explanation for this feature.

To further explain the experimental data and other observations outlined above, we performed simulations of the SE and the OE field profiles at 8 kHz MAS following the approach described by Mentink-Vigier, et al.[17] with the addition of specific ZQ and DQ cross-relaxation pathways and rates as illustrated in **Figure 3.7**. The evolution superoperator for one rotor period is obtained by step integration and is then applied repetitively to obtain the time evolution of the density matrix and from this the NMR signals. For the SE case the original calculations involved a system composed of an electron coupled to a proton via a dipolar hyperfine interaction. The same system is sufficient to represent the fundamental physics of the Overhauser DNP mechanism during sample rotation when an isotropic hyperfine interaction is added to the system and ZQ and DQ relaxation mechanisms are introduced. Because of the high static magnetic field the hyperfine interactions can be truncated and the laboratory frame spin Hamiltonian during a MAS DNP experiment on the two-spin system can be written as

$$\hat{H} = \hat{H}_0 + \hat{H}_{\mu w}$$

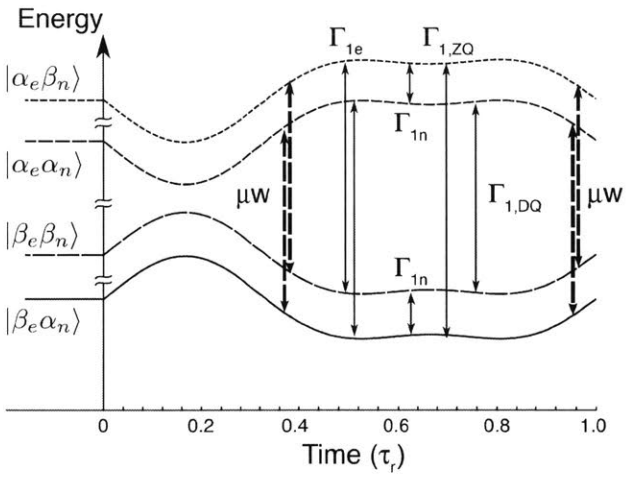

Figure 3.7: Energy level diagram showing the ZQ and DQ, Γ_{ZQ} and Γ_{DQ}, relaxation pathways in the two spins system. Γ_e and Γ_n are the direct electronic and nuclear relaxation rates. The dashed arrows indicate the positions in time where the μw irradiation is on resonance for the SQ transitions.

where

$$\hat{H}_0 = \{g_{iso} + g(\Omega_t)\}\beta_e B_0 \hat{S}_z - g_n \beta_n B_0 \hat{I}_z - \{A_{iso} + A_{dip}(\Omega_t)\}\hat{S}_z \hat{I}_z + A^+_{dip}(\Omega_t)\hat{S}_z \hat{I}^+ + A^-_{dip}(\Omega_t)\hat{S}_z \hat{I}^-$$

and the microwave driving term is $\hat{H}_{\mu w} = 2\omega_{1S}\hat{S}_x \cos(\omega_{0S} t)$

Here $\omega_{0S} = g_{iso}\beta_e B_0$ is the frequency of the isotropic *g* value and Ω_t accounts for the time dependent orientation imparted by the magic angle spinning. This Hamiltonian permits computation of the energy levels via a diagonalization procedure [17]. The relaxation is then introduced in the eigenframe at each angular step and the propagator is computed in Liouville space. During the SE simulations, the relaxation parameters are computed assuming fluctuations of $\hat{S}_{x,y}$ and $\hat{I}_{x,y}$ operators in the eigenframe of the Hamiltonian. In the case of the MAS Overhauser effect we also assumed fluctuations of the hyperfine coupling and added those to the source of relaxation. As illustrated in **Figure 3.7**, the spin operators of the hyperfine coupling supports additional cross relaxation pathways with ZQ $(\Delta m = 0)$ relaxation originating from the $\left(\hat{S}^+\hat{I}^- + \hat{S}^-\hat{I}^+\right)$ operators of its isotropic and anisotropic parts and DQ $(\Delta m = 2)$ relaxation from the $\left(\hat{S}^+\hat{I}^+ + \hat{S}^-\hat{I}^-\right)$ operators of only its anisotropic part. In the presence of strong isotropic contributions the ZQ relaxation time is expected to be shorter than the DQ relaxation time, which leads to a positive Overhauser effect.

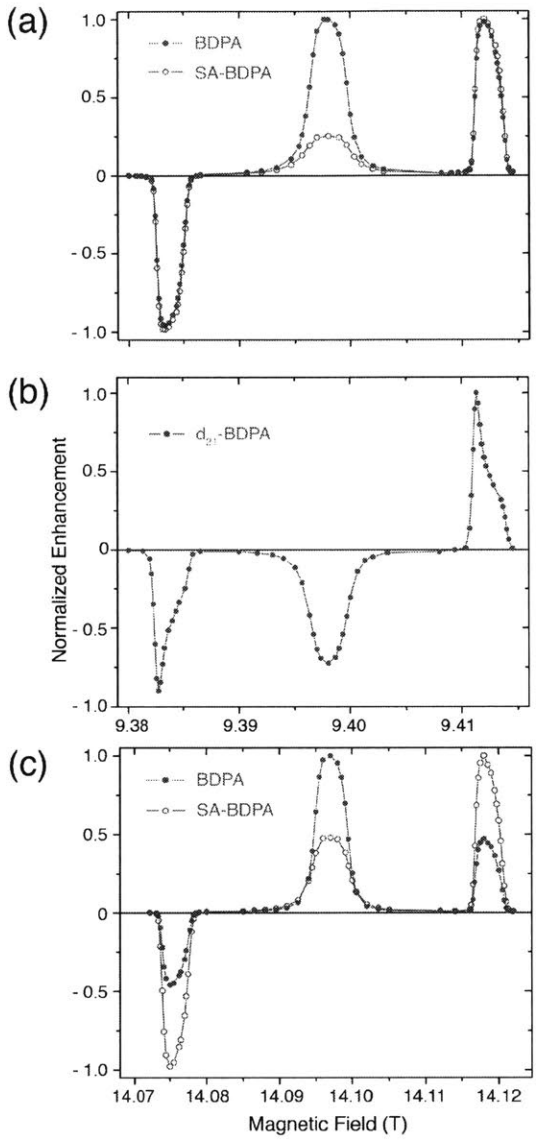

Figure 3.8: DNP field profiles for SA-BDPA and BDPA at (a) 9.4 and (c) 14.1 T and (b) for d_{21}-BDPA at 9.4 T at T=100 K assuming $(\omega_{1S}/2\pi)$ ~0.85 MHz. The following parameters were used in the simulations :

BDPA: A_{iso} =2.5 MHz, A_{dip} =1.5 MHz (in the principal axis frame), is the same order of magnitude as the published data [41, 42]. We employed an average value of the isotropic hyperfine value. $\Gamma_{1,ZQ}=\left(T_1^{ZQ}\right)^{-1}=0.91\ s^{-1}$, $\Gamma_{1,DQ}=\left(T_1^{DQ}\right)^{-1}=0.40\ s^{-1}$, $\Gamma_{1n}=\left(T_{1n}\right)^{-1}=0.16\ s^{-1}$ @ 9 T and 14 T

SA-BDPA: A_{iso} = 2 MHz, A_{dip} = 1.5 MHz (in the principal axis frame), assuming the sulfonation may affect the isotropic values by reducing the number of protons on the rings. $\Gamma_{1,ZQ}=\left(T_1^{ZQ}\right)^{-1}=0.24\ s^{-1}$, $\Gamma_{1,DQ}=\left(T_1^{DQ}\right)^{-1}=0.18\ s^{-1}$, $\Gamma_{1n}=\left(T_{1n}\right)^{-1}=0.03\ s^{-1}$ @ 9 T and $\Gamma_{1n}=\left(T_{1n}\right)^{-1}=0.02\ s^{-1}$ @ 14 T.

d_{21}-BDPA: A purely dipolar coupling of 0.1 MHz which corresponds to e^{-}-^{1}H distance of 0.9 nm, and cross relaxation rates $\Gamma_{1,ZQ}=\left(T_1^{ZQ}\right)^{-1}=0.001\ s^{-1}$, $\Gamma_{1,DQ}=\left(T_1^{DQ}\right)^{-1}=0.003\ s^{-1}$ were used.

In our calculations, we defined two cross-relaxation rates $\Gamma_{1,ZQ} = T_{1,ZQ}^{-1}$ and $\Gamma_{1,DQ} = T_{1,DQ}^{-1}$ that are different and that are the coefficients of the relaxation rates derived from the ZQ and DQ operators, respectively. Realizing that in our case the hyperfine coefficients satisfy $|A_{iso}| > |A_{dip}^{\pm}|$ we can expect the cross relaxation rates to satisfy $\Gamma_{ZQ} > \Gamma_{DQ}$. The introduction of the two relaxation pathways seems necessary to achieve a buildup time of the order of T_{1n}.

Based on this model we performed a series of simulations for the case of BDPA's where the external magnetic field, B_0, and the μw power were swept. The simulations employed the parameters compiled in the figure captions below which were chosen to approximate the experimental values.

Figure 3.8 illustrates the intensity of the predicted field profile for SA-BDPA and BDPA at two different fields (a) 9.4 T and (c) 14.1 T. **Figure 3.8b** presents the simulated field profile of d_{21}-BDPA. At this point there are significant uncertainties in the values of experimental parameters, so the simulations cannot predict the absolute enhancement values, but only rather their relative intensities and accordingly are presented as normalized plots in **Figure 3.8**. Nevertheless, we observe the expected SE signal at $\omega_{0S} \pm \omega_{0I}$ as well as a positive enhancement at ω_{0S} Experimentally, the Overhauser enhancement is larger in BDPA than in SA-BDPA, presumably because of the stronger coupling to 21 ^{1}H's, and we have increased A_{iso} in the BDPA simulations to account for this fact. We also note that for the results presented here the ratio $\epsilon_{OE}/\epsilon_{SE}$ increases with B_0. For SA-BDPA it increases from 0.13 to 0.46 and for BDPA from 1.25 to 2.9 at 9.4 and 14.1 T, respectively. These results are in good agreement with the experimental data. It is worth noting the shapes of the simulated field profiles do not depend strongly on either $\Gamma_{1e} = T_{1e}^{-1}$ or $\Gamma_{1n} = T_{1n}^{-1}$ but are primarily determined by the ratio $\Gamma_{1,ZQ}/\Gamma_{1,DQ}$.

The origin of the observation that the Overhauser effect enhancement appears to scale with B_0 (**Figure 3.5**) is not well established, again, due to the lack of experimental parameters especially electronic relaxations at high fields. We suggest that the cross relaxation rates increase with B_0 as calculated by Pines *et. al.*[46]. Note that the cross relaxation rates Γ_{ZQ} and Γ_{DQ} are proportional to the spectral density $J(\omega_{0S} \pm \omega_{0I})$,

respectively, both of which can be approximated as $J(\omega_{0S})$ since $\omega_{0S} \gg \omega_{0I}$. Thus, faster cross relaxation rates would be evident in shorter electron T_{1e} at high fields in the case of SA-BDPA and BDPA. A similar result was reported for trityl OX063 in glycerol/water glassy matrix [47].

In addition, as illustrated in **Figure 3.1c** we have observed a weak negative OE when using d_{21}-BDPA as the polarizing agent. In this case dipolar mediated DQ relaxation rather than ZQ processes dominate the Overhauser effect enhancement profile. Simulations shown in **Figure 3.8b** reproduce the essential features of the negative OE.

Finally, as shown in **Figure 3.6b** we are able to correctly predict the DNP enhancement as a function of the μw field strength ω_{1S} for both the SE and Overhauser case. The Overhauser enhancement increases steeply with ω_{1S} and saturates, while the SE increases more slowly. Again the simulations reproduce the essential features of the experimental power dependence of the Overhauser and solid effect.

Conclusions

In summary we present here the initial experimental observation of microwave driven OE DNP around ω_{0S} in an insulating solid at high field using the narrow line radicals SA-BDPA and BDPA. It is present along with the expected solid effect occurring at $\omega_{0S} \pm \omega_{0I}$. The experimental and simulated enhancement field profiles demonstrate a field dependence $\sim \omega_{0I}$, in contrast to the inverse dependence predicted for the SE and CE. The relative intensity of the two contributions depends strongly on the ratio Γ_{ZQ}/Γ_{DQ} and the sizes and/or numbers of the nuclear hyperfine couplings. These observations suggests that OE's could be seen in other systems and should stimulate the development of additional narrow line radicals that possess the features. They should be useful for MAS DNP at higher magnetic fields.

Acknowledgements

This research was supported by grants to RGG from the National Institutes of Biomedical Imaging and Bioengineering, EB-002804 and EB002026 and to TMS from the National Institutes of Health of General Medical Sciences, GM095843. SV acknowledges the support of a grant from the German-Israeli Project Cooperation of the DFG through a special allotment by the Ministry of Education and Research (BMBF) of the Federal republic of

Germany. B.C. was supported by the Deutsche Forschungsgemeinschaft (DFG research fellowship CO 802/1-1). We thank Leo Tometich (Bruker BioSpin) for extensive technical assistance.

References

[1] L.R. Becerra, G.J. Gerfen, R.J. Temkin, D.J. Singel, R.G. Griffin, Dynamic nuclear-polarization with a cyclotron-resonance maser at 5-T, Physical Review Letters, 71 (1993) 3561-3564.

[2] G.J. Gerfen, L.R. Becerra, D.A. Hall, R.G. Griffin, R.J. Temkin, D.J. Singel, High frequency (140 GHz) dynamic nuclear polarization: polarization transfer to a solute in frozen aqueous solution, J. Chem. Phys., 102 (1995) 9494-9497.

[3] L.R. Becerra, G.J. Gerfen, B.F. Bellew, J.A. Bryant, D.A. Hall, S.J. Inati, R.T. Weber, S. Un, T.F. Prisner, A.E. McDermott, K.W. Fishbein, K.E. Kreischer, R.J. Temkin, D.J. Singel, R.G. Griffin, A spectrometer for dynamic nuclear-polarization and electron-paramagnetic-resonance at high-frequencies, J. Magn. Reson. Ser. A, 117 (1995) 28-40.

[4] M.K. Hornstein, V.S. Bajaj, R.G. Griffin, K.E. Kreischer, I. Mastovsky, M.A. Shapiro, J.R. Sirigiri, R.J. Temkin, Second harmonic operation at 460 GHz and broadband continuous frequency tuning of a gyrotron oscillator, IEEE Transactions on Electron Devices, 52 (2005) 798-807.

[5] V.S. Bajaj, M.K. Hornstein, K.E. Kreischer, J.R. Sirigiri, P.P. Woskov, M.L. Mak-Jurkauskas, J. Herzfeld, R.J. Temkin, R.G. Griffin, 250 GHz CW gyrotron oscillator for dynamic nuclear polarization in biological solid state NMR, Journal of Magnetic Resonance, 189 (2007) 251-279.

[6] M. Rosay, L. Tometich, S. Pawsey, R. Bader, R. Schauwecker, M. Blank, P.M. Borchard, S.R. Cauffman, K.L. Felch, R.T. Weber, R.J. Temkin, R.G. Griffin, W.E. Maas, Solid-state dynamic nuclear polarization at 263 GHz: spectrometer design and experimental results, Physical Chemistry Chemical Physics, 12 (2010) 5850-5860.

[7] M. Rosay, A.-C. Zeri, N.S. Astrof, S.J. Opella, J. Herzfeld, R.G. Griffin, Sensitivity-Enhanced NMR of Biological Solids: Dynamic Nuclear Polarization of Y21M fd Bacteriophage and Purple Membrane, Journal of the American Chemical Society, 123 (2001) 1010-1011.

[8] K.R. Thurber, W.-M. Yau, R. Tycko, Low-temperature dynamic nuclear polarization at 9.4 T with a 30 mW microwave source, Journal of Magnetic Resonance, 204 (2010) 303-313.

[9] A.A. Smith, B. Corzilius, A.B. Barnes, T. Maly, R.G. Griffin, Solid Effect Dynamic Nuclear Polarization and Polarization Pathways, Journal of Chemical Physics, 136 (2012) 015101.

[10] W.T. Wenckebach, The Solid Effect, Appl. Magn. Reson., 34 (2008) 227-235.

[11] Y. Hovav, A. Feintuch, S. Vega, Theoretical aspects of dynamic nuclear polarization in the solid state – The solid effect, J. Magn. Reson., 207 (2010) 176-189.

[12] K.N. Hu, V.S. Bajaj, M. Rosay, R.G. Griffin, High-frequency dynamic nuclear polarization using mixtures of TEMPO and trityl radicals, Journal of Chemical Physics, 126 (2007) 7.

[13] K.N. Hu, G.T. Debelouchina, A.A. Smith, R.G. Griffin, Quantum mechanical theory of dynamic nuclear polarization in solid dielectrics, Journal of Chemical Physics, 134 (2011) 19.

[14] K.N. Hu, C. Song, H.H. Yu, T.M. Swager, R.G. Griffin, High-frequency dynamic nuclear polarization using biradicals: A multifrequency EPR lineshape analysis, Journal of Chemical Physics, 128 (2008) 17.

[15] K.N. Hu, H.H. Yu, T.M. Swager, R.G. Griffin, Dynamic nuclear polarization with biradicals, Journal of the American Chemical Society, 126 (2004) 10844-10845.
[16] Y. Matsuki, T. Maly, O. Ouari, H. Karoui, F. Le Moigne, E. Rizzato, S. Lyubenova, J. Herzfeld, T. Prisner, P. Tordo, R.G. Griffin, Dynamic Nuclear Polarization with a Rigid Biradical, Angewandte Chemie-International Edition, 48 (2009) 4996-5000.
[17] F. Mentink-Vigier, U. Akbey, Y. Hovav, S. Vega, H. Oschkinat, A. Feintuch, Fast passage dynamic nuclear polarization on rotating solids, J, Magn. Reson., 224 (2012) 13-21.
[18] K. Thurber, R. Tycko, Theory for cross effect dynamic nuclear polarization under magic angle spinning in solid state nuclear magnetic resonance: the importance of level crossings, J Chem Phys, 137 (2012) 084508-084501.
[19] T. Maly, G.T. Debelouchina, V.S. Bajaj, K.N. Hu, C.G. Joo, M.L. Mak-Jurkauskas, J.R. Sirigiri, P.C.A. van der Wel, J. Herzfeld, R.J. Temkin, R.G. Griffin, Dynamic nuclear polarization at high magnetic fields, Journal of Chemical Physics, 128 (2008) 19.
[20] A.B. Barnes, G. De Paëpe, P.C.A. van der Wel, K.N. Hu, C.G. Joo, V.S. Bajaj, M.L. Mak-Jurkauskas, J.R. Sirigiri, J. Herzfeld, R.J. Temkin, R.G. Griffin, High-Field Dynamic Nuclear Polarization for Solid and Solution Biological NMR, Applied Magnetic Resonance, 34 (2008) 237-263.
[21] Q.Z. Ni, E. Daviso, T.V. Can, E. Markhasin, S.K. Jawla, R.J. Temkin, J. Herzfeld, R.G. Griffin, High Frequency Dynamic Nuclear Polarization Accounts of Chem Research, 46 (2013) 1933-1941.
[22] U. Akbey, W.T. Franks, A. Linden, S. Lange, R.G. Griffin, B.J. van Rossum, H. Oschkinat, Dynamic nuclear polarization of deuterated proteins, Angewandte Chemie-International Edition, 49 (2010) 7803-7806.
[23] A.J. Rossini, A. Zagdoun, M. Lelli, J. Canivet, S. Aguado, O. Ouari, P. Tordo, M. Rosay, W.E. Maas, C. Copéret, D. Farrusseng, L. Emsley, A. Lesage, Dynamic Nuclear Polarization Enhanced Solid-State NMR Spectroscopy of Functionalized Metal–Organic Frameworks, Angewandte Chemie International Edition, 51 (2012) 123-127.
[24] S. Un, T. Prisner, R.T. Weber, M.J. Seaman, K.W. Fishbein, A.E. McDermott, D.J. Singe1, R.G. Griffin, Pulsed dynamic nuclear polarization at 5 T, Chem. Phys. Letters, 189 (1992) 54-59.
[25] A.W. Overhauser, Polarization of Nuclei in Metals, Physical Review, 92 (1953) 411-415.
[26] T.R. Carver, C.P. Slichter, Polarization of Nuclear Spins in Metals, Physical Review, 92 (1953) 212.
[27] A. Abragam, Overhauser Effect in Nonmetals., Phys. Rev., 98 (1955) 1729–1735.
[28] C. Griesinger, M. Bennati, H. Vieth, C. Luchinat, G. Parigi, P. Hofer, F. Engelke, S. Glaser, V. Denysenkov, T. Prisner, Dynamic nuclear polarization at high magnetic fields in liquids, 64 (2012) 4-28.
[29] C. Cheng, S. Han, Dynamic Nuclear Polarization Methods in Solids and Solutions to Explore Membrane Proteins and Membrane Systems, Annual Review of Physical Chemistry, 64 (2013) 507-532.
[30] O. Haze, B. Corzilius, A.A. Smith, R.G. Griffin, T.M. Swager, Water-Soluble Narrow-Line Radicals for Dynamic Nuclear Polarization, Journal of the American Chemical Society, 134 (2012) 14287-14290.
[31] J.H. Ardenkjær-Larsen, B. Fridlund, A. Gram, G. Hansson, L. Hansson, M.H. Lerche, R. Servin, M. Thaning, K. Golman, Increase in signal-to-noise ratio of > 10,000 times in liquid-state NMR, Proceedings of the National Academy of Sciences, 100 (2003) 10158-10163.
[32] T.J. Reddy, T. Iwama, H.J. Halpern, V.H. Rawal, General Synthesis of Persistent Trityl Radicals for EPR Imaging of Biological Systems, J. Org. Chem., 67 (2002) 4635-4639.

[33] S.N. Trukhan, V.F. Yudanov, V.M. Tormyshev, O.Y. Rogozhnikova, D.V. Trukhin, M.K. Bowman, M. D. Krzyaniak, H. Chen, O.N. Martyanov, Hyperfine interactions of narrow-line trityl radical with solvent molecules, J, Magnetic Resonance, 223 (2013) 29-36.
[34] B. Corzilius, A.A. Smith, R.G. Griffin, Highly Efficient Solid Effect in Magic Angle Spinning Dynamic Nuclear Polarization at High Field, Journal of Chemical Physics, 137 (2012) 054201.
[35] Y. Hovav, A. Feintuch, S. Vega, Dynamic nuclear polarization assisted spin diffusion for the solid effect case, Journal of Chemical Physics, 134 (2011).
[36] N.M. Loening, M. Rosay, V. Weis, R.G. Griffin, Solution-state dynamic nuclear polarization at high magnetic field, J Am Chem Soc, 124 (2002) 8808-8809.
[37] A.E. Dementyev, D.G. Cory, C. Ramanathan, High-field Overhauser dynamic nuclear polarization in silicon below the metal-insulator transition, Journal of Chemical Physics, 134 (2011).
[38] M. Afeworki, R.A. Mckay, J. Schaefer, Dynamic Nuclear-Polarization Enhanced Nuclear-Magnetic-Resonance of Polymer-Blend Interfaces, Materials Science and Engineering a-Structural Materials Properties Microstructure and Processing, 162 (1993) 221-228.
[39] R. Sarkar, M. Concistre, O.G. Johannessen, P. Beckett, M. Denning, M. Carravetta, M. al-Mosawi, C. Beduz, Y. Yang, M.H. Levitt, An NMR thermometer for cryogenic magic-angle spinning NMR: The spin-lattice relaxation of I-127 in cesium iodide, Journal of Magnetic Resonance, 212 (2011) 460-463.
[40] K.R. Thurber, R. Tycko, Measurement of sample temperatures under magic-angle spinning from the chemical shift and spin-lattice relaxation rate of Br-79 in KBr powder, Jour Magn Resonance, 196 (2009) 84-87.
[41] N.S. Dalal, D.E. Kennedy, C.A. McDowell, EPR and ENDOR studies of hyperfine interactions in solutions of stable organic free radicals, J. Chem. Phys., 61 (1974).
[42] V. Weis, M. Bennati, M. Rosay, J.A. Bryant, R.G. Griffin, High-field DNP and ENDOR with a novel multiple-frequency resonance structure, J Magn Reson, 140 (1999) 293-299.
[43] A. Abragam, A. Landesman, J.M. Winter, Effet Overhauser dan les charbons et graphites, C.R._Rendus, 247 (1958) 1852-1853.
[44] S. Stoll, A. Schweiger, EasySpin, a Comprehensive Software Package for Spectral Simulation and Analysis in EPR, J. Magn. Reson., 178 (2006) 42-55.
[45] B. Corzilius, L.B. Andreas, A.A. Smith, Q.Z. Ni, R.G. Griffin, Paramagnet induced signal quenching in MAS–DNP experiments in frozen homogeneous solutions, J. Magn. Reson., (2013).
[46] D. Pines, J. Bardeen, C.P. Slichter, Nuclear Polarization and Impurity-State Spin Relaxation Processes in Silicon, Physical Review, 106 (1957) 489-498.
[47] L. Lumata, Z. Kovacs, A.D. Sherry, C. Malloy, S. Hill, J.v. Tol, L. Yu, L. Song, M.E. Merritt, Electron spin resonance studies of trityl OX063 at a concentration optimal for DNP, Phys. Chem. Chem. Phys. , 15 (2013) 9800-9807.

Chapter 4: Time Domain DNP with the NOVEL Sequence

Adapted from T.V. Can, J.J. Walish, T.M. Swager, and R.G. Griffin, Journal of Chemical Physics 143 (2015) 054201

We present results of a pulsed dynamic nuclear polarization (DNP) study at 0.35 T (9.7 GHz /14.7 MHz for electron/^{1}H Larmor frequency) using a lab frame-rotating frame cross polarization experiment that employs electron spin locking fields that match the ^{1}H nuclear Larmor frequency, the so called NOVEL (nuclear orientation via electron spin locking) condition. We apply the method to a series of DNP samples including a single crystal of diphenyl nitroxide (DPNO) doped into benzophenone (BzP), 1,3-bisdiphenylene-2-phenylallyl (BDPA) doped into polystyrene (PS) and sulfonated-BDPA (SA-BDPA) doped into glycerol/water glassy matrices. The optimal Hartman-Hahn matching condition is achieved when the nutation frequency of the electron matches the Larmor frequency of the proton, $\omega_{1S} = \omega_{0I}$, together with possible higher order matching conditions at lower efficiencies. The magnetization transfer from electron to protons occurs on time scale of ~ 100 ns, consistent with the electron-proton couplings on the order of 1-10 MHz in these samples. In a fully protonated single crystal DPNO/BzP, at 270 K, we obtained a maximum signal enhancement of $\varepsilon = 165$ and the corresponding gain in sensitivity of $\varepsilon\left(T_1/T_B\right)^{1/2} = 230$ due to the reduction in the buildup time under DNP. In a sample of partially deuterated PS doped with BDPA, we obtained an enhancement of 323 which is a factor of ~ 3.2 higher compared to the protonated version of the same sample, and accounts for 49% of the theoretical limit. For SA-BDPA doped in glycerol/water glassy matrix at 80 K, the sample condition used in most applications of DNP in nuclear magnetic resonance (NMR), we also observed a significant enhancement. Our findings demonstrate that pulsed DNP via the NOVEL sequence is highly efficient, and can potentially surpass continuous wave DNP mechanisms such as the solid effect and cross effect which scale unfavorably with increasing magnetic field.

Introduction

Dynamic nuclear polarization (DNP) transfers polarization from electrons to nuclei, thereby enhancing the nuclear polarization. The initial DNP mechanism, the Overhauser effect (OE), was proposed in 1953 [1] and confirmed experimentally soon thereafter [2, 3] in samples with conductive metals. Recently, we reported the existence of OE in insulating solids[4]. Furthermore, in insulating solids such as biological samples, DNP can also be performed via the solid effect [5, 6], the cross effect [7-11] and thermal mixing [12]. Initially, the primary application of DNP was to prepare polarized targets for neutron scattering experiments [13], however over the past decade, DNP has been used extensively to enhance the inherently low sensitivity of nuclear magnetic resonance (NMR) signals [14-19]. Enhancements on the order of 10^2-10^3 were made possible via the solid effect using narrow-line radicals [20-23] and cross effect using biradicals [24-27] as polarizing agents and high frequency gyrotrons as microwave sources [28-30]. The latter operate in the 140-560 GHz regime and enable DNP to be performed at magnet field strengths used in contemporary NMR experiments (5-20 T).

All of the DNP mechanisms mentioned above employ continuous wave (CW) microwave irradiation. In addition, all of them, except for the OE in insulating solids, scale unfavorably with the magnetic field, displaying a B_0^{-n} field dependence where n~1-2 or larger. Thus, for DNP to be successful at high magnetic fields and broadly applicable, a strategy to overcome this deficiency is required. An analogous situation existed in the early 1970's in solution NMR where ^{1}H-^{13}C nuclear Overhauser enhancements were shown to vanish above 60-100 MHz ^{1}H frequencies, and therefore it was predicted that high fields would not be useful for ^{13}C protein NMR [31]. The development of J-mediated transfers, in particular the INEPT pulsed experiment, circumvented this problem because it is field-independent [32]. Similarly, time domain DNP experiments are in principle field-independent, and, when the instrumentation becomes available, they can be performed efficiently at high Zeeman fields.

To date, there are a handful of sequences for pulsed DNP including nuclear orientation via electron spin locking (NOVEL) [33], the integrated solid effect (ISE) [34], DNP in the nuclear rotating frame (NRF) DNP [35] and dressed state solid effect (DSSE) [36]. Neither NRF DNP nor DSSE requires a strong microwave field. NRF DNP is essentially solid effect in the NRF instead of the nuclear lab frame. The mixing of state is inversely proportional to the radio frequency (RF) field instead of the B_0 field. The sensitivity gain in

NRF DNP is the result of the ability to recycle the NMR experiment at the rate of the nuclear $T_{1\rho}$ instead of the nuclear T_1. DSSE utilizes an off-resonance RF field to drive the polarization transfer. The matching condition requires that the RF field is applied off-resonance and the resonance offset is governed by the isotropic hyperfine coupling as well as the microwave field strength.

Both NOVEL and ISE, on the other hand, rely on the Hartman-Hahn matching condition between the electron rotating frame and the nuclear lab frame, thus, require strong microwave field strengths. Similar to cross polarization in NMR, the polarization transfer is driven by the dipolar coupling, which is typically on the order of MHz, resulting in a short sub-microsecond contact time. Both sequences were originally developed for neutron spin polarizer experiments using short-lived photoexcited triplet states. In these experiments, NOVEL showed very modest efficiency. An enhancement of ~ 10 was obtained for ^{29}Si in uniaxially stressed silicon doped with boron acceptors [33], and ε~200 was observed for ^{1}H using a photoexcited triplet state of pentacene doped into naphthalene [37]. In both cases, the efficiency is less than 1%. NOVEL was soon replaced by ISE which gives a much higher efficiency due to the adiabatic sweep of the magnetic field [34, 38-40]. Note that both of these samples were especially chosen to demonstrate the NOVEL or ISE effect. Thus, one of our goals in the results reported here was to investigate the potential of the NOVEL sequence in samples used in current applications of DNP in NMR, *i.e.* samples doped with a few tens of mM of stable free radicals such as the narrow-line species 1,3-bisdiphenylene-2-phenylallyl (BDPA) or nitroxides, both of which are used in contemporary CW DNP experiments. We found that enhancements on the order of 10^2 can be obtained on these samples. For example, we obtained an enhancement of 323 corresponding to 49% efficiency in a sample of partially deuterated polystyrene (PS) doped with 2% BDPA. Our results suggest that pulsed DNP NOVEL is an excellent candidate for high field DNP.

Background

In this section we derive the matching condition that will be used in our discussion (*vide infra*). To this end, it is sufficient to consider a 2-spin system consisting of nuclear spin *I* and electron spin *S*. For an extensive theoretical discussion of the NOVEL sequence, readers are directed to the papers by Wenckebach *et al.* [41, 42]. In the lab frame, the Hamiltonian for the NOVEL experiment has the form

$$H = \omega_{0S} S_z - \omega_{0I} I_z + \vec{S} \cdot \vec{\vec{A}} \cdot \vec{I} + 2\omega_{1S} \cos(\omega_{\mu w} t) S_x \qquad (1)$$

wherein the first two terms are the Zeeman interactions; the third is the electron-nuclear interaction; and the fourth is the microwave spin lock field. Upon transforming to the microwave rotating frame using the following operator

$$U_1 = \exp\left(iS_z\omega_{\mu w}t\right) \tag{2}$$

the Hamiltonian is truncated to

$$H = \Omega_S S_z - \omega_{0I} I_z + A_{zx} S_z I_x + A_{zy} S_z I_y + A_{zz} S_z I_z + \omega_{1S} S_x \tag{3}$$

where Ω_S is the microwave offset

$$\Omega_S = \omega_{0S} - \omega_{\mu w} \tag{4}$$

Transformation to the tilted frame is achieved with the operator

$$U_2 = \exp\left(iS_y\theta\right) \tag{5}$$

where the angle θ is defined as

$$\tan\theta = \frac{\omega_{1S}}{\Omega_S} \tag{6}$$

The Hamiltonian is transformed to

$$H = \omega_{eff} S_z - \omega_{0I} I_z + \left(A_{zx} I_x + A_{zy} I_y + A_{zz} I_z\right)\left(S_z\cos\theta - S_x\sin\theta\right) \tag{7}$$

where

$$\omega_{eff} = \pm\sqrt{\Omega_S^2 + \omega_{1S}^2} \tag{8}$$

The sign of ω_{eff} depends on the phase as well as the offset of the microwave.

Next, we redefine the transverse axes of the nuclear spin by the following transformation

$$U_3 = \exp\left(iI_z\phi\right) \tag{9}$$

where the angle ϕ is defined as

$$\tan\phi = \frac{A_{zy}}{A_{zx}} \tag{10}$$

Leading to the Hamiltonian

$$H = \omega_{eff} S_z - \omega_{0I} I_z + \left(AI_z + BI_x\right)\left(S_z \cos\theta - S_x \sin\theta\right) \quad (11)$$

where A and B are secular and pseudo-secular hyperfine coupling constants, respectively.

$$A = A_{zz} \quad (12)$$

$$B = \sqrt{A_{zx}^2 + A_{zy}^2} \quad (13)$$

Using perturbation theory, we can separate the Hamiltonian

$$H = H_0 + H_1 \quad (14)$$

wherein the unperturbed Hamiltonian H_0 and the perturbation H_1 are given as

$$H_0 = \omega_{eff} S_z - \omega_{0I} I_z + A\cos\theta I_z S_z \quad (15)$$

$$H_1 = BI_x\left(S_z \cos\theta - S_x \sin\theta\right) - A\sin\theta I_z S_x \quad (16)$$

Using the direct product $|IS\rangle$ basis set

$$|1\rangle = \left|\frac{1}{2}\ \frac{1}{2}\right\rangle;\quad |2\rangle = \left|\frac{1}{2}\ \frac{-1}{2}\right\rangle;\quad |3\rangle = \left|\frac{-1}{2}\ \frac{1}{2}\right\rangle;\quad |4\rangle = \left|\frac{-1}{2}\ \frac{-1}{2}\right\rangle \quad (17)$$

As usual we define the subspace spanned by $|1\rangle$ and $|4\rangle$ as the double quantum (DQ) subspace and that spanned by $|2\rangle$ and $|3\rangle$ as the zero quantum (ZQ) subspace. In the NOVEL experiment, the inter-subspace splitting is approximately ω_{0I}, which is very large compared to the perturbation even at a magnetic field as low as 0.35 T. On the other hand, if the matching condition is fulfilled, states in the either DQ or ZQ subspace are degenerate, resulting in a complete intra-subspace state mixing as a result of the perturbation and, thus, the polarization transfer. The perturbation can be truncated to contain only DQ (flip-flip) and ZQ (flip-flop) terms as the following

$$H_1^{truncated} = B\sin\theta I_x S_x \quad (18)$$

For the positive ω_{eff}, the degeneracy in the DQ subspace leads to the matching condition

$$\omega_{0I} = \omega_{eff} = \sqrt{\Omega_S^2 + \omega_{1S}^2} \quad (19)$$

If the microwave offset is negligible, the matching condition is simplified to

$$\omega_{1S} \approx \omega_{0I} \quad (20)$$

and the nuclear Larmor frequency equals the Rabi frequency of the electron. In other words, the nutation of the nucleus in the laboratory frame matches that of the electron in the rotating frame. We note that Hartmann and Hahn also mentioned the possibility of this type of rotating frame-laboratory frame cross polarization [43].

Experimental

Samples

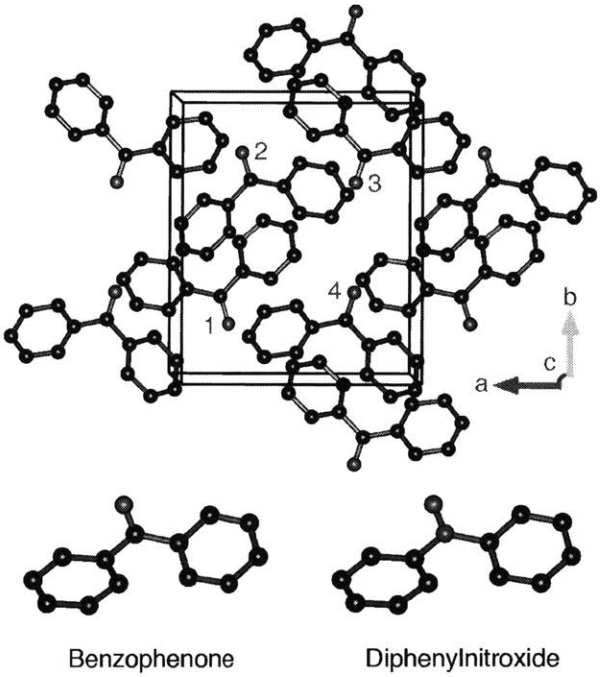

Figure 4.1: (Top) Crystal structure of benzophenone. The crystal has space group symmetry $P2_12_12_1$ with four molecules per unit cell. Molecules 1 to 4 are of the same unit cell represented by the rectangular parallelepiped. Molecules 2, 3 and 4 are 180° rotated about the crystallographic *a*, *b* and *c* axis, respectively, with respect to molecule 1. (Bottom) Molecular structures of benzophenone (left) and diphenylnitroxide (right) with oxygen atoms in red, nitrogen in blue and carbon atoms in black. The figure was rendered in VESTA software [44].

Preparation of samples containing 2% BDPA (weight ratio) doped in polystyrene (PS) and 40 mM SA-BDPA doped in glycerol/water glassy matrices are described elsewhere[4]. Single crystals of benzophenone (BzP) doped with diphenylnitroxide (DPNO) were grown from ethanol upon slow evaporation. 12 mg of 10% DPNO stock (courtesy of Dr. Tien-Sung Lin, Washington University, St. Louis) and 188 mg of BzP (Sigma Alrdrich) were dissolved in 1 g of ethanol. The final sample contained 0.6% or 40 mM of the DPNO radical which is similar to the concentrations normally used in DNP applications[14] [17-19]. Single

crystals were harvested and polished to fit into a quartz capillary of 0.4 mm inner diameter for experiments at 5 T. For experiments at 0.35 T, a larger sample that fit into a 4 mm EPR sample tube was used. In order to suppress the ^{1}H NMR signal from trapped solvent, we used perdeuterated ethanol (Cambridge Isotope). **Figure 4.1** shows the crystal structure of BzP according to Fleischer *et al.*[45]. BzP has an orthorhombic structure with the $P2_12_12_1$ space group and therefore four molecules per unit cell. The similarity in the molecular structures of BzP and DPNO (**Figure 4.1**) allows DPNO to substitute into the host crystal of BzP with negligible perturbation [46, 47]. **Figure 4.1** was generated using VESTA software [44].

Experiments

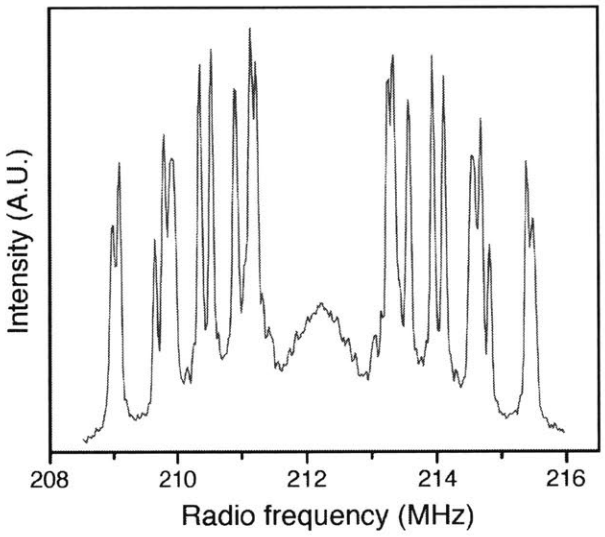

Figure 4.2: Davies ENDOR spectrum of a single crystal of 90% deuterated BzP doped with 0.6% DPNO at 5 T. The magnetic field lies in the *ab* crystallographic plane. Ten pairs of sharp peaks correspond to ten ^{1}H's on DPNO molecule.

Experiments at 5 T were carried out on a homebuilt pulsed DNP/EPR/NMR spectrometer operating at 5 T or 140 GHz/ 211 MHz of electron/ ^{1}H Larmor frequency [22]. Experiments at 0.35 T were performed on a Bruker ElexSys E580 X-band EPR spectrometer using an EN 4118X-MD4 pulsed ENDOR resonator. The RF coil of the probe also serves as the NMR sample coil upon the integration of a module of tuning and matching capacitors. The RF excitation and detection of NMR signals were done with an iSpin-NMR spectrometer purchased from Spincore Technologies, Inc. (Gainesville, FL, US). The ^{1}H NMR signals were acquired via a solid echo sequence with 8-step phase cycling. The signals were processed using a custom-built MATLAB program [48].

Results

The quality of the single crystals is best assessed using high frequency EPR techniques as it allows observation of any inhomogeneity in the *g* value due to imperfections in the single crystal. **Figure 4.2** shows the Davies ENDOR spectrum obtained from a single crystal grown with 90% BzP-d_{10}/10% BzP-h_{10} at 5 T. Even though the exact orientation of the crystal was not determined, it is certain that the magnetic field lies in the crystallographic *ab*-plane. The deuteration of the sample suppresses the contribution from matrix protons, which permits the observation of all ten pairs of sharp resonances from ten protons of each DPNO molecule. **Figure 4.3a** presents the EPR spectrum and the ^{1}H DNP field profile from a sample with 94% ^{13}C carbonyl labeled BzP-h_{10}. In this case, the crystal was orientated such that B_0 is aligned with the crystallographic *b*-axis. Thus, the EPR spectrum displays one sharp peak corresponding to g_{xx} = 2.0091 with four-fold degeneracy, a result that is consistent with a previous study [46]. The DNP field profile is indicative of a well-resolved solid effect.

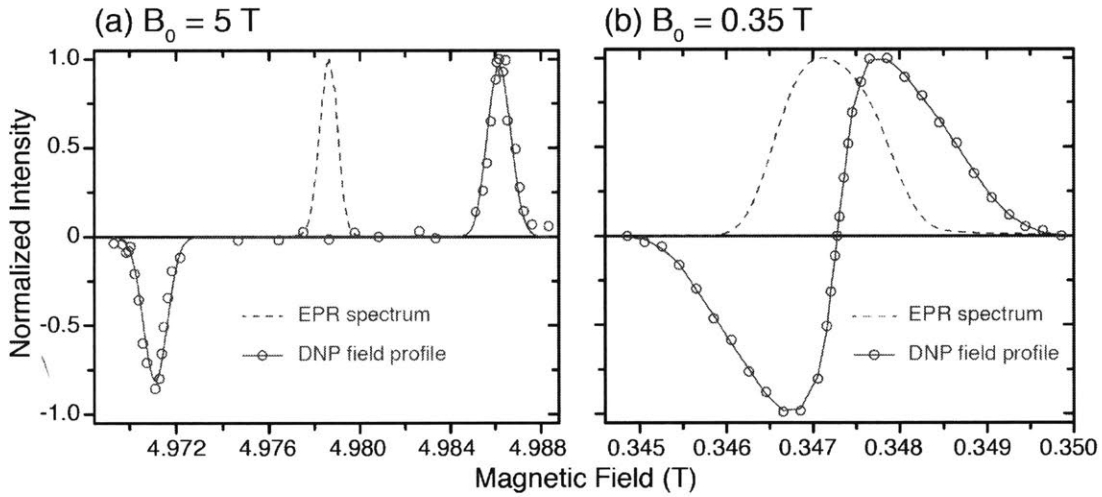

Figure 4.3: EPR spectrum (dashed blue) and DNP field profile (red) of single crystal DPNO/BzP at 5 T (a) and 0.35 T (b). The magnetic field B_0 is along the crystallographic *b*-axis of the crystal, thus the EPR spectra contain only one peak with four-fold degeneracy. The DNP field profile at 5 T shows a well-resolved solid effect as opposed to an unresolved solid effect at 0.35 T. The maximum enhancement is 330 at 0.35 T and remains unknown at 5 T.

Figure 4.3b shows the echo detected EPR spectrum and the ^{1}H DNP field profile of a single crystal DPNO/BzP at 0.35 T. Again, the crystallographic *b*-axis of the crystal was aligned with B_0. The spectrum exhibits a linewidth of 8.6 G due to unresolved hyperfine

couplings, consistent with previous studies on similar samples [46, 47]. The *b*-axis was chosen because of the narrow EPR linewidth, allowing more efficient microwave excitation.

The ^{1}H DNP field profile in **Figure 4.3b** was obtained at the microwave field strength of $\omega_{1S} = 2.4 MHz$ and microwave frequency of $\omega_{0S} = 9.7224 GHz$. The DNP enhanced ^{1}H NMR signal was measured as a function of the B_0 field. The enhancement is defined as $\varepsilon = \left(I_{\mu w\, on} / I_{\mu w\, off}\right)$. The DNP field profile resembles an unresolved solid effect in which the EPR linewidth (24 MHz) is greater than the Larmor frequency of ^{1}H (14.7 MHz), but smaller than twice that frequency. Despite the overlap between the positive and negative solid effect, the maximum enhancement was as high as 330 due to the extensive state mixing present at low magnetic field. For subsequent pulsed DNP experiments, the magnetic field was carefully adjusted to the exact center of the field profile to avoid contribution of the SE in the DNP enhancement.

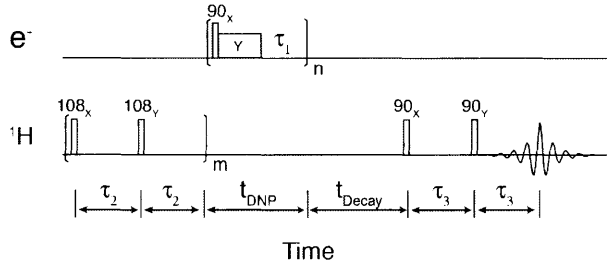

Figure 4.4: Timing scheme for NOVEL pulsed DNP. After a period of presaturation, the magnetization of ^{1}H buildups for a period of t_{DNP}. The decay period can be used to measure the T_1 of protons. The DNP enhanced ^{1}H signal is then read out by a solid echo sequence. The fixed parameters include $\tau_2 = 5ms$, $m = 8$ and $\tau_3 = 20\mu s$. Other parameters such as the mixing time (t_{mix} or the length of the microwave Y pulse) and the repetition time (essentially τ_1) were optimized as described in **Figure 4.5**.

Figure 4.4 shows the pulse sequence for NOVEL experiment. After a period of ^{1}H presaturation, the magnetization of ^{1}H builds up with (on signal) or without (off signal) microwave pulses. For the solid effect DNP, the microwave pulses are simply a continuous wave irradiation. On the other hand, for NOVEL experiment, a sequence consisting of a 90° flip pulse, a spin lock pulse (mixing time) and a delay is applied repeatedly. The buildup time constant T_B of the DNP enhanced NMR signal is measured by varying the length of the buildup period. The T_1 relaxation of ^{1}H is obtained by varying the decay period that follows buildup.

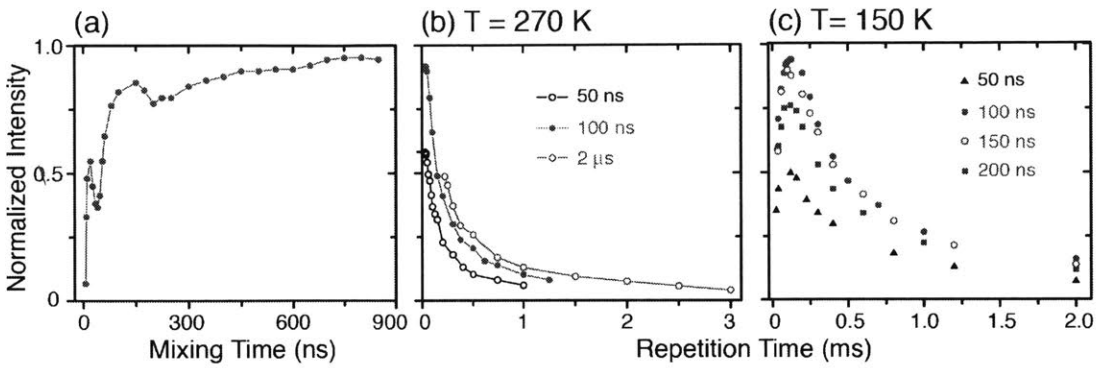

Figure 4.5: Optimization of NOVEL pulse sequence in DPNO/BzP. (a) The signal intensity increases quickly after τ_{mix}~100 ns and exhibits a transient oscillation. Both features are consistent with the electron-^{1}H dipolar coupling in the order of 1-10 MHz. Optimization in term of the repetition time (essentially τ_1) at 270 K (b) and 150 K (c) with different mixing times. At 270 K, we observed mostly the decay of the signal with respect to the repetition time. At 150 K, the signal intensity reached the maxima at ~ 130 μs of repetition time.

For the pulsed DNP NOVEL sequence, the microwave field strength, the mixing time (the length of the microwave Y pulse in **Figure 4.4**), and the repetition time (essentially τ_1 in **Figure 4.4**) require optimization. The microwave field strength was calibrated by measuring the nutation frequencies at different microwave power levels. Data illustrating the optimization of the mixing time and the repetition time are given in **Figure 4.5** for a DPNO/BzP sample with the microwave field strength set to ~ 14.7 MHz. In **Figure 4.5a**, we varied the mixing time, which reveals the signal intensity to increase rapidly after ~100 ns, followed by a slower progression. We then measured the signal as a function of the repetition time at different mixing times ranging from 50 ns to 2 μs at 270 K (**Figure 4.5b**). At this temperature, we were only able to observe the decay of the signal with respect to the repetition time. As we lowered the temperature to 150 K (**Figure 4.5c)**, we could clearly see the maxima at ~ 130 μs of repetition time. At 270 K, the optimum conditions were τ_{mix}~ 100 ns and τ_1=40 μs of repetition time. Longer locking pulses required a longer repetition time subject to the 1% duty cycle available with the TWT amplifier, leading to lower DNP efficiency. Overall, we obtained a higher enhancement at 270 K. The same optimizations were performed on BDPA/PS sample at 300 K (data not shown), yielding a τ_{mix}~150 ns and τ_1= 36 μs.

Figure 4.6a reveals the enhancement obtained via the NOVEL sequence as a function of ω_{1S} in a fully protonated BzP single crystal doped with 0.6% DPNO at 270 K. The

matching condition clearly occurs at $\omega_{1S} = \omega_{0I} \approx 14.7 MHz$ and an enhancement of up to 165 is observed (**Figure 4.6b**). The T_B and T_1 time constants are given in **Figure 4.6c**. **Figure 4.7** and 4.**8** show the enhancement obtained in BDPA/PS at 300 K and SA-BDPA in glycerol-d_8/D_2O/H_2O at 80 K.

Discussion

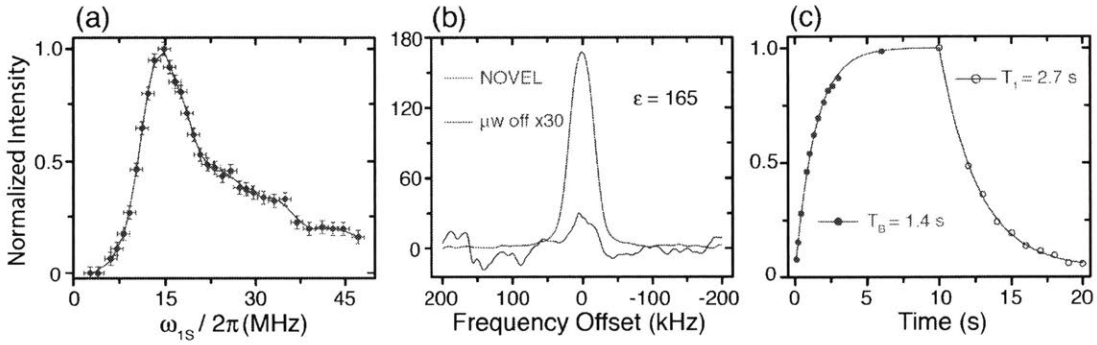

Figure 4.6: (a) Matching condition of NOVEL pulse sequence in DPNO/BzP sample. The enhancement was measured as a function of the microwave field strength. The spin lock pulse is fixed to 100 ns, whereas the length of the flip pulse is adjusted to give 90° tip angle. The matching occurs at $\omega_{1S} = \omega_{0I}$.
(b) ^1H spectra with (red) and without (blue) DNP. For the DNP enhanced spectrum, the sample was polarized for 10 s with 16 ns flip pulse followed by 100 ns spin lock pulse. The repetition time was 40 μs. The off spectrum was obtained with 10 s of recovery time. The enhancement in signal intensity was $\varepsilon = 165$. The intensities were normalized to the μw off signal.
(c) DNP buildup time constant T_B using NOVEL pulse sequence and the spin-lattice relaxation time constant T_1. Reduction in the buildup time constant results in a sensitivity gain of 230.

In DNP experiments using a free radical dopant, the theoretical limit for the enhancement is given by the ratio γ_e / γ_n which is ~ 658 for ^1H. The enhancement of 165 (**Figure 4.6b**) that we obtained in a protonated sample of DPNO/BzP corresponds to 25% of the theoretical efficiency. We attribute the improvement in the efficiency over previous studies to the increase in the radical concentration as well as the narrow EPR linewidth. In the original study by Henstra [33] on uniaxially stressed boron-doped silicon, the acceptor concentration was 10^{17} cm^{-3} or 0.16 mM which is about two orders of magnitude more dilute than that used in contemporary DNP experiments [14]. Moreover, the EPR linewidth was 60 MHz compared to 24 MHz in our case, resulting in lower excitation efficiency. In another example of naphthalene doped with pentacene [37], electrons in triplet states are created by laser irradiation. In such a case, the concentration of electron is limited by both the dopant concentration (< 5 mM) and the efficiency of the optical excitation (< 5%).

The enhancement that we obtained is, to some degree, limited by the 1% duty cycle of the TWT microwave amplifier. **Figure 4.5c** shows the dependence of the enhancement on the repetition time in DPNO/BzP sample at 150 K. The enhancement increases quickly and then decays. We attribute this observation to two competing factors including the electron spin-lattice relaxation and the number of times that electrons transfer magnetization to protons. At 270 K (**Figure 4.5b**), we only observed the decay of the signal as a result of the short electron T_1 and the limitation in the duty cycle of the TWT amplifier. Nevertheless, we obtained a higher enhancement at 270 K. The NOVEL sequence was originally developed for short-lived photo excited triplet states, which requires fast polarization transfer and allows fast repetition. It partially explains why the sequence works well at high temperature where the short T_{1e} gives rise to a larger number of polarization transfer events per unit time or, in other words, a faster recycling of the electron polarization. Furthermore, a short T_{1e} reduces the saturation of the electron polarization. A similar effect was reported [20, 21] for the solid effect even though the microwaves were off-resonance. For the NOVEL sequence, such an effect might be more detrimental because the microwaves are on-resonance with the EPR transitions.

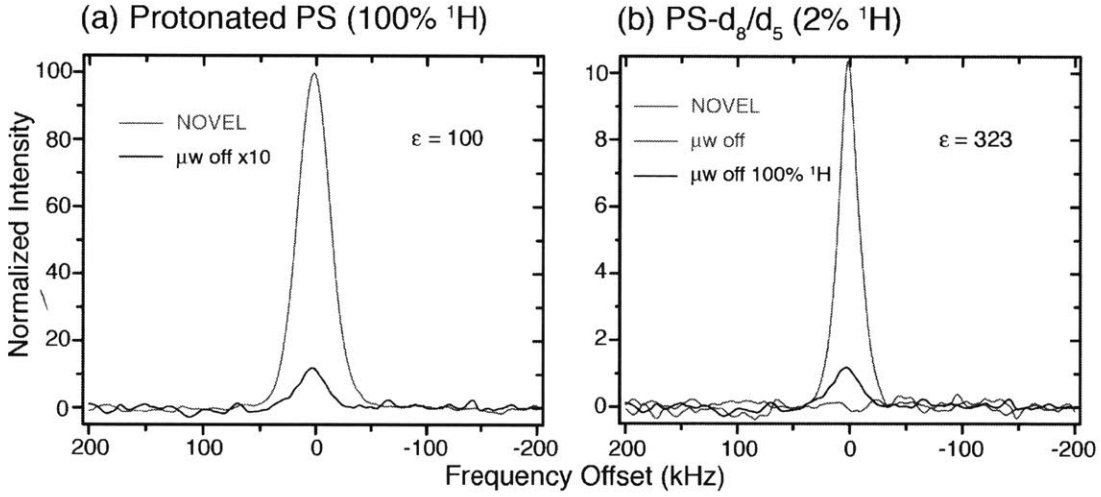

Figure 4.7: NOVEL experiments in BDPA/PS samples at 300 K using 150 ns mixing and 36 μs repetition time. (a) In fully protonated sample, we obtained an enhancement of 100. (b) In sample with mixed PS-d_8/d_5 (95:5), the ^{1}H concentration is diluted by a factor of 50, making it impossible to acquire the off signal in a reasonable amount of time. We, therefore, estimate the enhancement in the sample using the off signal of the fully protonated sample as the reference. Taking into account the dilution factor and the amount of sample, we obtained an enhancement of 323. The intensities were normalized to the μw off signal from protonated PS sample.

Despite the limitation in the duty cycle of the TWT amplifier, we have obtained an unprecedented high DNP efficiency in fully protonated samples: 165 in DPNO/BzP at 270 K (**Figure 4.6b**) and 100 in BDPA/PS at 300 K (**Figure 4.7a**). Furthermore, partial deuteration of the BDPA/PS sample, leaving 2% proton, results in an enhancement of 323, which is a ~ 3.2-fold improvement and corresponds to 49% efficiency (**Figure 4.7b**). It is worth noting that in quasi-equilibrium (infinite mixing time) the efficiency of a non-adiabatic cross polarization from ^{1}H to other nuclei in a static sample is 50% and the maximum of the transient oscillation is less than 75% [49]. We expect a similar upper bound for the efficiency of the NOVEL sequence. The efficiency of 49% is, therefore, very close to the optimum value and, to the best of our knowledge, is the highest efficiency reported for NOVEL sequence.

The mixing time dependence curve of both the DPNO/BzP (**Figure 4.5b**) and BDPA/PS (not shown) displays the characteristics of a dipolar driven cross polarization process. In DPNO/BzP, the intensity increases rapidly after ~100 ns, in good agreement with the electron-^{1}H couplings up to ~10 MHz [46, 47, 50]. Similarly, for BDPA/PS, the corresponding mixing time is ~150 ns, consistent with a somewhat weaker coupling of ~ 5.5 MHz in BDPA [51, 52]. After the quick rise, the curve exhibits a transient oscillation due to the dipolar coupling which is another characteristic of a cross polarization experiment, a result that has also been observed previously in NOVEL experiments [37].

The matching conditions in both DPNO/BzP (**Figure 4.6a**) and BDPA/PS (not shown) show a maximum at ~14.7 MHz and a long tail extending well beyond $3\omega_{0I}$. The feature at high microwave field strength was first observed in naphthalene doped with pentacene-h_{14} [37], and recently in naphthalene doped with pentacene-d_{14} [39]. However, in both cases, the tail ended well below $2\omega_{0I}$. We think that our observation is likely the result of high order processes involving one electron and multiple protons as suggested by Eichhorn *et al.* [39]. Another possibility is that at $\omega_{1S} > \omega_{0I}$, not only the EPR transitions, but also the double quantum and zero quantum transitions, are excited by the microwaves. The details of the DNP process in this regime is then dependent on relaxation. In both scenarios, the feature at high microwave power is a first order perturbation effect which should vanish at higher magnetic fields.

We notice the reduction of the buildup time constant of the ^{1}H polarization during DNP compared to the nuclear spin-lattice relaxation (**Figure 4.6c**). This behavior was

observed for the solid effect (SE) at 5 T [20-22]. The short T_B enables a faster recycle of NMR experiment, resulting in a net gain in sensitivity of $\varepsilon(T_1/T_B)^{1/2} = 230$ for the DPNO/BzP sample. We explain this by the fact that both SE and NOVEL are 2-spin processes; the same semi-classical rate equation treatment used for the SE can, therefore, be applied to the NOVEL experiment. In this treatment, the DNP effect is encoded in a DNP rate constant that acts to increase the buildup rate of the NMR signal, thus, shorten the buildup time constant. This effect has only been observed in the case of large enhancement corresponding to large differentiation between T_1 and T_B.

At 0.35 T, the solid effect outperforms NOVEL DNP by a factor of ~2 (330 vs. 165 for DPNO/BzP and 200 vs. 100 for BDPA/PS). As the magnetic field increases, the efficiency of the SE decreases rapidly as predicted by theory and also observed in experiments [4, 17, 19, 53]. Pulsed DNP in general and the NOVEL experiment in particular, does not depend on the B_0. An analogy is that cross polarization is operating at all magnetic fields in solid state NMR. We predict that at magnetic fields of 0.5 T and above, NOVEL DNP would surpass the SE. With the recent advances in the gyroamplifier technology [54-56], we anticipate that pulsed DNP will become available at high magnetic fields in the near future.

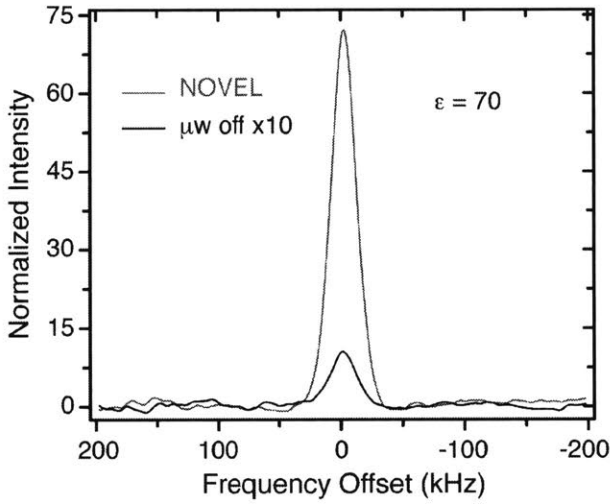

Figure 4.8: NOVEL experiments in glycerol-d_8/D_2O/H_2O glassy matrix doped with 40 mM SA-BDPA at 80 K. The DNP enhanced signal was obtained using 150 ns mixing time, 8 ms of repetition time, 24 s of DNP buildup time. The enhancement is 70.

Finally, we implemented the NOVEL pulse sequence on a sample containing 40 mM SA-BDPA dispersed in glycerol-d_8/D_2O/H_2O (60/30/10 volume ratio) glassy matrix at 80 K, sample conditions frequently used in current applications of DNP in NMR. **Figure 4.8** shows

the NMR signal obtained with and without NOVEL. The mixing time was set to 150 ns same as what we used for BDPA/PS because the sulfonation process retains all the protons that are strongly coupled to the electron in BDPA [57]. The repetition time was optimized at 8 ms due to longer T_{1e} at 80K. We obtained an enhancement of 70. The long repetition time allows longer mixing time. However, as seen in **Figure 4.5a**, the enhancement almost reaches maximum at 150 ns of mixing time. Using mixing time up to 8 μs results in a slight increase (~10%) in the enhancement.

Conclusions

In summary, we demonstrate that pulsed DNP via the NOVEL sequence is highly efficient under sample conditions that are currently used for contemporary DNP/NMR applications despite the limitation in the duty cycle of the TWT microwave amplifier. Except for the repetition time that is subject to the duty cycle of the TWT, all other parameters including the matching condition, the mixing time and the polarizing time are fully optimized. The mixing time and the transient oscillation in the mixing time dependence curve are consistent with a dipolar driven cross polarization process. In a fully protonated single crystal DPNO/BzP, at 270 K, we obtain an enhancement of 165 which is 25% of the theoretical limit. Reduction in the buildup time constant of the NMR signal under DNP gives rise to a net gain in sensitivity of 230. By partially deuterating the BDPA/PS sample, we obtained an enhancement of 323 at 300 K, corresponding to 49% efficiency. We also observed a significant enhancement in a sample containing 40 mM SA-BDPA dispersed in glycerol/water glassy matrix at 80 K. We believe that the NOVEL pulse sequence is a strong candidate for pulsed DNP NMR at high fields. Finally, since this method does not have field dependence, time domain DNP at high field could lead to larger enhancements than the CW counterparts such as the solid effect and cross effect.

Acknowledgements

This research was supported by grants to RGG from the National Institutes of Biomedical Imaging and Bioengineering, Grant Nos. EB-002804 and EB-002026 and to T.M.S from the National Institutes of Health of General Medical Sciences, Grant No. GM095843. We thank Dr. Ralph Weber (Bruker BioSpin, Billerica, MA), Dr. Thomas Pratum (Western Washington University, Bellingham, WA), Ajay Tharkar and Jeff Bryant for technical assistances. We are grateful to Dr. Albert A. Smith for helping with the ENDOR experiment at 5 T.

References

[1] A.W. Overhauser, Polarization of Nuclei in Metals, Physical Review, 92 (1953) 411.
[2] T.R. Carver, C.P. Slichter, Polarization of Nuclear Spins in Metals, Physical Review, 92 (1953) 212.
[3] T.R. Carver, C.P. Slichter, Experimental Verification of the Overhauser Nuclear Polarization Effect, Physical Review, 102 (1956) 975.
[4] T.V. Can, M.A. Caporini, F. Mentink-Vigier, B. Corzilius, J.J. Walish, M. Rosay, W.E. Maas, M. Baldus, S. Vega, T.M. Swager, R.G. Griffin, Overhauser effects in insulating solids, Journal of Chemical Physics, 141 (2014).
[5] A. Abragam, W.G. Proctor, C. R. Acad. Sci., 246 (1958) 2253.
[6] E. Erb, J. Motchane, L., J. Uebersfeld, C. R. Acad. Sci., 246 (1958) 2121.
[7] A.V. Kessenikh, V.I. Lushchikov, A.A. Manenkov, Y.V. Taran, Proton polarization in irradiated polyethylenes, Soviet Physics-Solid State, 5 (1963) 321-329.
[8] A.V. Kessenikh, A.A. Manenkov, G.I. Pyatnitskii, On explanation of experimental data on dynamic polarization of protons in irradiated polyethylenes, Soviet Physics-Solid State, 6 (1964) 641-643.
[9] C. Hwang, F., D. Hill, A., New Effect in Dynamic Polarization, Physical Review Letters, 18 (1967) 110.
[10] C. Hwang, F., D. Hill, A., Phenomenological Model for the New Effect in Dynamic Polarization, Physical Review Letters, 19 (1967) 1011.
[11] D. Wollan, S., Dynamic nuclear polarization with an inhomogeneously broadened ESR line. I. Theory, Physical Review B: Condensed Matter, 13 (1976) 3671.
[12] R.A. Wind, M.J. Duijvestijn, C. van der Lugt, A. Manenschijn, J. Vriend, Applications of Dynamic Nuclear-Polarization in C-13 NMR in Solids, Progress in Nuclear Magnetic Resonance Spectroscopy, 17 (1985) 33-67.
[13] A. Abragam, M. Goldman, Nuclear magnetism : order and disorder, Clarendon Press Oxford University Press, Oxford New York, 1982.
[14] Q.Z. Ni, E. Daviso, T.V. Can, E. Markhasin, S.K. Jawla, T.M. Swager, R.J. Temkin, J. Herzfeld, R.G. Griffin, High frequency dynamic nuclear polarization, Accounts of Chemical Research, 46 (2013) 1933-1941.
[15] A.J. Rossini, A. Zagdoun, M. Lelli, A. Lesage, C. Coperet, L. Emsley, Dynamic nuclear polarization surface enhanced NMR spectroscopy, Accounts of Chemical Research, 46 (2013) 1942-1951.
[16] R. Tycko, NMR at low and ultra low temperatures, Accounts of Chemical Research, 46 (2013) 1923-1932.
[17] T. Maly, G.T. Debelouchina, V.S. Bajaj, K.-N. Hu, C.-G. Joo, M.L. Mak-Jurkauskas, J.R. Sirigiri, P.C.A. van der Wel, J. Herzfeld, R.J. Temkin, R.G. Griffin, Dynamic nuclear polarization at high magnetic fields, The Journal of Chemical Physics, 128 (2008) 052211-052219.
[18] A.B. Barnes, G. De Paëpe, P.C.A. van der Wel, K.N. Hu, C.G. Joo, V.S. Bajaj, M.L. Mak-Jurkauskas, J.R. Sirigiri, J. Herzfeld, R.J. Temkin, R.G. Griffin, High-Field Dynamic Nuclear Polarization for Solid and Solution Biological NMR, Applied Magnetic Resonance, 34 (2008) 237-263.
[19] T.V. Can, Q.Z. Ni, R.G. Griffin, Mechanisms of dynamic nuclear polarization in insulating solids, Journal of magnetic resonance (San Diego, Calif. : 1997), 253 (2015) 23-35.
[20] B. Corzilius, A.A. Smith, R.G. Griffin, Solid effect in magic angle spinning dynamic nuclear polarization, Journal of Chemical Physics, 137 (2012) 054201.
[21] A.A. Smith, B. Corzilius, A.B. Barnes, T. Maly, R.G. Griffin, Solid effect dynamic nuclear polarization and polarization pathways, Journal of Chemical Physics, 136 (2012) 015101.

[22] A.A. Smith, B. Corzilius, J.A. Bryant, R. DeRocher, P.P. Woskov, R.J. Temkin, \R.G. Griffin, A 140 GHz pulsed EPR/212 MHz NMR spectrometer for DNP studies, Journal of Magnetic Resonance, 223 (2012) 170-179.
[23] Y. Hovav, A. Feintuch, S. Vega, Theoretical aspects of dynamic nuclear polarization in the solid state - The solid effect, Journal of Magnetic Resonance, 207 (2010) 176-189.
[24] K. Hu, H. Yu, T. Swager, R. Griffin, Dynamic nuclear polarization with biradicals., Journal of the American Chemical Society, 126 (2004) 10844-10845.
[25] C. Song, K.-N. Hu, C.-G. Joo, T.M. Swager, R.G. Griffin, TOTAPOL: A biradical polarizing agent for dynamic nuclear polarization experiments in aqueous media, Journal of the American Chemical Society, 128 (2006) 11385-11390.
[26] C. Sauvee, M. Rosay, G. Casano, F. Aussenac, R.T. Weber, O. Ouari, P. Tordo, Highly Efficient, Water-Soluble Polarizing Agents for Dynamic Nuclear Polarization at High Frequency, Angewandte Chemie-International Edition, 52 (2013) 10858-10861.
[27] A. Zagdoun, G. Casano, O. Ouari, M. Schwarzwalder, A.J. Rossini, F. Aussenac, M. Yulikov, G. Jeschke, C. Coperet, A. Lesage, P. Tordo, L. Emsley, Large Molecular Weight Nitroxide Biradicals Providing Efficient Dynamic Nuclear Polarization at Temperatures up to 200 K, Journal of the American Chemical Society, 135 (2013) 12790-12797.
[28] L. Becerra, G. Gerfen, R. Temkin, D. Singel, R. Griffin, Dynamic nuclear polarization with a cyclotron resonance maser at 5 T., Physical Review Letters, 71 (1993) 3561-3564.
[29] A.B. Barnes, E. Markhasin, E. Daviso, V.K. Michaelis, E.A. Nanni, S.K. Jawla, E.L. Mena, R. DeRocher, A. Thakkar, P.P. Woskov, J. Herzfeld, R.J. Temkin, R.G. Griffin, Dynamic nuclear polarization at 700 MHz/460 GHz, Journal of Magnetic Resonance, 224 (2012) 1-7.
[30] A.B. Barnes, E.A. Nanni, J. Herzfeld, R.G. Griffin, R.J. Temkin, A 250 GHz gyrotron with a 3 GHz tuning bandwidth for dynamic nuclear polarization, Journal of Magnetic Resonance, 221 (2012) 147-153.
[31] E. Oldfield, R.S. Norton, A. Allerhand, Studies of individual carbon sites of proteins in solution by natural abundance carbon 13 nuclear magnetic-resonance spectroscopy - relaxation behavior, Journal of Biological Chemistry, 250 (1975) 6368-6380.
[32] G.A. Morris, R. Freeman, Enhancement of nuclear magnetic-resonance signals by polarization transfer, Journal of the American Chemical Society, 101 (1979) 760-762.
[33] A. Henstra, P. Dirksen, J. Schmidt, W.T. Wenckebach, Nuclear-spin orientation via electron-spin locking (NOVEL), Journal of Magnetic Resonance, 77 (1988) 389-393.
[34] A. Henstra, P. Dirksen, W.T. Wenckebach, Enhanced dynamic nuclear-polarization by the integrated solid effect, Physics Letters A, 134 (1988) 134-136.
[35] C.T. Farrar, D.A. Hall, G.J. Gerfen, M. Rosay, J.H. Ardenkjaer-Larsen, R.G. Griffin, High-frequency dynamic nuclear polarization in the nuclear rotating frame, Journal of Magnetic Resonance, 144 (2000) 134-141.
[36] V. Weis, M. Bennati, M. Rosay, R.G. Griffin, Solid effect in the electron spin dressed state: A new approach for dynamic nuclear polarization, Journal of Chemical Physics, 113 (2000) 6795-6802.
[37] D.J. van den Heuvel, A. Henstra, T.-S. Lin, J. Schmidt, W.T. Wenckebach, Transient oscillations in pulsed dynamic nuclear polarization, Chemical Physics Letters, 188 (1992) 194-200.
[38] A. Kagawa, Y. Murokawa, K. Takeda, M. Kitagawa, Optimization of 1H spin density for dynamic nuclear polarization using photo-excited triplet electron spins, Journal of Magnetic Resonance, 197 (2009) 9-13.
[39] T.R. Eichhorn, B. van den Brandt, P. Hautle, A. Henstra, W.T. Wenckebach, Dynamic nuclear polarisation via the integrated solid effect II: experiments on naphthalene-h(8) doped with pentacene-d(14), Molecular Physics, 112 (2014) 1773-1782.

[40] K. Tateishi, M. Negoro, S. Nishida, A. Kagawa, Y. Morita, M. Kitagawa, Room temperature hyperpolarization of nuclear spins in bulk, Proceedings of the National Academy of Sciences of the United States of America, 111 (2014) 7527-7530.
[41] A. Henstra, W.T. Wenckebach, The theory of nuclear orientation via electron spin locking (NOVEL), Molecular Physics, 106 (2008) 859-871.
[42] A. Henstra, W.T. Wenckebach, Dynamic nuclear polarisation via the integrated solid effect I: theory, Molecular Physics, 112 (2014) 1761-1772.
[43] S.R. Hartmann, E.L. Hahn, Nuclear double resonance in rotating frame, Physical Review, 128 (1962) 2042-&.
[44] K. Momma, F. Izumi, VESTA 3 for three-dimensional visualization of crystal, volumetric and morphology data, Journal of Applied Crystallography, 44 (2011) 1272-1276.
[45] E.B. Fleischer, N. Sung, S. Hawkinson, Crystal structure of benzophenone, Journal of Physical Chemistry, 72 (1968) 4311-&.
[46] T.S. Lin, Epr study of diphenylnitroxide in benzophenone, Journal of Chemical Physics, 57 (1972) 2260-&.
[47] C. Cheng, T.S. Lin, D.J. Sloop, Electron spin-echo experiments of diphenylnitroxide in benzophenone crystals, Journal of Magnetic Resonance, 33 (1979) 71-81.
[48] MathWorks, MatLab, in, MathWorks, Natick, 2010.
[49] L. Muller, A. Kumar, T. Baumann, R.R. Ernst, Transient oscillations in NMR cross-polarization experiments in solids, Physical Review Letters, 32 (1974) 1402-1406.
[50] A.L. Maniero, M. Brustolon, Electron-spin resonance and electron nuclear double-resonance study of mixed-crystals of benzophenone and diphenylnitroxide, Journal of the Chemical Society-Faraday Transactions I, 84 (1988) 2875-2884.
[51] N.S. Dalal, D.E. Kennedy, C.A. McDowell, EPR and ENDOR studies of hyperfine interactions in solutions of stable organic free radicals, The Journal of Chemical Physics, 61 (1974) 1689-1697.
[52] V. Weis, M. Bennati, M. Rosay, J.A. Bryant, R.G. Griffin, High-field DNP and ENDOR with a novel multiple-frequency resonance structure, Journal of Magnetic Resonance, 140 (1999) 293-299.
[53] K.-N. Hu, G.T. Debelouchina, A.A. Smith, R.G. Griffin, Quantum mechanical theory of dynamic nuclear polarization in solid dielectrics, Journal of Chemical Physics, 134 (2011) 125105.
[54] C.D. Joye, M.A. Shapiro, J.R. Sirigiri, R.J. Temkin, Demonstration of a 140-GHz 1-kW confocal gyro-traveling-wave amplifier, Ieee Transactions on Electron Devices, 56 (2009) 818-827.
[55] H.J. Kim, E.A. Nanni, M.A. Shapiro, J.R. Sirigiri, P.P. Woskov, R.J. Temkin, Amplification of picosecond pulses in a 140-GHz gyrotron-traveling wave tube, Physical Review Letters, 105 (2010) 135101.
[56] E.A. Nanni, S.M. Lewis, M.A. Shapiro, R.G. Griffin, R.J. Temkin, Photonic-Band-Gap Traveling-Wave Gyrotron Amplifier, Physical Review Letters, 111 (2013).
[57] O. Haze, B. Corzilius, A.A. Smith, R.G. Griffin, T.M. Swager, Water-Soluble Narrow-Line Radicals for Dynamic Nuclear Polarization, Journal of the American Chemical Society, 134 (2012) 14287-14290.

Chapter 5: Ramped-Amplitude NOVEL

Adapted from T.V. Can, R.T. Weber, J.J. Walish, T.M. Swager, and R.G. Griffin, Journal of Chemical Physics 146 (2017) 154204

We present a pulsed DNP study using a ramped-amplitude NOVEL (RA-NOVEL) sequence that utilizes a fast arbitrary waveform generator (AWG) to modulate the microwave pulses together with samples doped with narrow-line radicals such as 1,3-bisdiphenylene-2-phenylallyl (BDPA), sulfonated-BDPA (SA-BDPA) and trityl-OX063. Similar to ramped-amplitude cross polarization (RA-CP) in solid-state NMR, RA-NOVEL improves the DNP efficiency by a factor of up to 1.6 compared to constant-amplitude NOVEL (CA-NOVEL) but requires a longer mixing time. For example, at τ_{mix}=8 μs, the DNP efficiency reaches a plateau at a ramp amplitude of ~20 MHz for both SA-BDPA and trityl-OX063, regardless of the ramp profile (linear vs. tangent). At shorter mixing times (τ_{mix}=0.8 μs), we found that the tangent ramp is superior to its linear counterpart and in both cases there exists an optimum ramp size and therefore ramp rate. Our results suggest that RA-NOVEL should be used instead of CA-NOVEL as long as the electronic spin lattice relaxation T_{1e} is sufficiently long and/or the duty cycle of the microwave amplifier is not exceeded. To the best of our knowledge, this is the first demonstration of a time domain DNP experiment that utilizes modulated microwave pulses. Our results also suggest that precise modulation of microwave pulses can play an essential role in optimizing the efficiency of pulsed DNP experiments and an AWG is an elegant instrumental solution for this purpose.

Introduction

Dynamic nuclear polarization (DNP) is widely accepted as a powerful technique for improving the sensitivity of nuclear magnetic resonance (NMR) signals [1], but instrumental considerations to date have dictated that only continuous wave (CW) microwave irradiation be utilized in the experiments [2-8]. These CW experiments, namely the cross effect and solid effect, enhance signal intensities by one to two orders of magnitude and enable otherwise impossible experiments [9-16], but they nevertheless exhibit an inverse dependence on the B_0 field [3; 8; 17-21]. Furthermore, to adjust the relaxation times so that the experiments function with optimal efficiency, it is often necessary to perform them at cryogenic temperatures and/or high microwave power [22-29]. As a consequence, these requirements limit the applicability of DNP in NMR. There are ongoing efforts that address these limitations, for example by utilizing the Overhauser effect in insulating solids that scales linearly with the Zeeman field, B_0, and requires much less microwave power [30; 31]. However, a more general approach to address the inverse field dependence is pulsed or time domain DNP. Specifically, what is needed is a repertoire of pulse sequences that allow efficient transfer of polarization from electrons to nuclei regardless of B_0. Although pulsed DNP often requires intense peak microwave power, the average power is low due to the low duty cycle. Thus, in combination with rapid polarization transfers, pulsed DNP is potentially the method of choice for experiments at ambient temperature.

The development of time domain DNP dates from the late 1980's and was stimulated by the need for methods to prepare polarized targets for neutron diffraction experiments using short lifetime photo-excited triplet states [32; 33]. Pulse sequences including nuclear orientation via electron spin locking (NOVEL) and the integrated solid effect (ISE) were introduced and employed for these applications [34-37]. In contrast, contemporary applications in magic angle spinning (MAS) NMR rely heavily on CW DNP, in particular the cross effect using biradical polarizing agents [38-40; 41]. It is worth noting that attempts to apply pulsed DNP were initiated about the same time as the first gyrotron based MAS DNP/NMR experiments, a technique that has been widely used over the last decade [42]. The slow progress of pulsed DNP is the result of a paucity of pulse microwave amplifiers operating at high output powers (kW) and high frequencies (above 100 GHz). Nevertheless, the potential of time domain experiments has stimulated the development of new DNP sequences such as DNP in the nuclear rotating frame (NRF), the dressed state solid effect (DSSE), polarization of nuclear spin enhanced by ENDOR (PONSEE), and a sequence

based on optimum control theory [43-46]. Furthermore, recent advancements in microwave amplifier technology, establish pulsed DNP as a promising technique on the horizon [47; 48].

Among these sequences listed above, NOVEL, a rotating frame-lab frame analogue of Hartmann-Hahn cross polarization (CP), can potentially play the same role for DNP as does CP in solid state NMR [49; 50]. CP belongs to a family of "*sudden*" experiments in which the density operator nutates around the Hamiltonian, giving rise to the transfer of polarization. In powder samples, the interference of different dipolar coupling strengths leads to 50% polarization transfer efficiency at quasi-equilibrium (long contact time). Even though ramped amplitude (RA)-CP appears to be very similar to CP, it differs fundamentally in that it is an "*adiabatic*" process whereby the Hamiltonian changes slowly allowing the density operator to follow, and the polarization transfer occurs virtually at the center of the ramp. This happens approximately simultaneously for all orientations and distances, thereby suppressing transient oscillations and generating 100% polarization transfer efficiency that is a factor of 2 improvement compared to constant amplitude (CA)-CP [51-53].

Recently, we demonstrated high DNP efficiency using the NOVEL pulse sequence under the sample conditions used in DNP/NMR experiments [54; 55]. Inspired by the advantage of RA-CP (*vide supra*), we report herein the performance of the ramped amplitude (RA)-NOVEL sequence utilizing the newly available arbitrary waveform generator (AWG) function on a X-band EPR spectrometer. The AWG allows precise and convenient manipulations of microwave pulses, and was used to ramp the amplitude of the spin locking pulse. With this innovation we obtained a factor of up to 1.6 improvement in the DNP enhancement. The improvement factor appears to be versatile with respect to the polarizing agent as well as the shape of the ramp (linear vs. tangent) as long as the ramp is sufficiently long.

Background

In this section, we briefly provide relevant theoretical description to the experiments that follow. The description is in part similar to what we presented previously. The difference or extension comes into play in the discussion of linear RA-NOVEL. With the microwave applied on resonant with the EPR transition, the Hamiltonian in the microwave rotating frame can be written as

$$H = \omega_{1S} S_x - \omega_{0I} I_z + \left(A I_z + B I_x \right) S_z$$

where the first term originates from the microwave spinlock field; the second term corresponds to the Zeeman interaction of proton; A and B are the isotropic and anisotropic hyperfine coupling, respectively. In the tilted frame defined such that

$$S_x \to S_z;\ S_y \to S_y;\ S_z \to -S_x$$

the Hamiltonian is transformed to

$$H = \omega_{1S} S_z - \omega_{0I} I_z - \left(A I_z + B I_x\right) S_x$$

Using perturbation theory, we separate the Hamiltonian into the unperturbed H_0 and the perturbation H_1 which are given as follows

$$H_0 = \omega_{1S} S_z - \omega_{0I} I_z$$

$$H_1 = -A I_z S_x - B I_x S_x$$

At the NOVEL condition ($\omega_{1S} = \omega_{0I}$), the contribution from the A term of H_1 is proportional to $\frac{A}{2\omega_{0I}}$. Even in the case of BDPA or SA-BDPA radicals ($A \sim 5$ MHz), and at low field ($\omega_{0I} \approx 15$ MHz), the ratio is quite small ($1/6$). Moreover, our experimental data (*vide infra*) on RA-NOVEL show strong similarity between SA-BDPA and trityl-OX063 which has negligible isotropic coupling. Thus, to simplify the subsequent treatment of the Hamiltonian, let's assume that the isotropic hyperfine coupling term can be ignored. This will become more relevant at higher B_0 fields. Under such assumption, the H_1 is truncated to

$$H_1 \approx -B I_x S_x$$

The Hamiltonian becomes block diagonal

$$H = H_0 + H_1 \approx \omega_{1S} S_z - \omega_{0I} I_z - B I_x S_x = H_{ZQ} \oplus H_{DQ}$$

where ZQ and DQ correspond to zero quantum and double quantum, respectively. At the NOVEL condition, the matrix form of the Hamiltonian in each subspace is given as

$$H_{ZQ} = \frac{1}{2}\begin{pmatrix} -\left(\omega_{1S} + \omega_{0I}\right) & \frac{B}{2} \\ \frac{B}{2} & \left(\omega_{1S} + \omega_{0I}\right) \end{pmatrix} = \begin{pmatrix} -\omega_{0I} & \frac{B}{4} \\ \frac{B}{4} & \omega_{0I} \end{pmatrix}$$

$$H_{DQ} = \frac{1}{2}\begin{pmatrix} -(\omega_{1S} - \omega_{0I}) & \frac{B}{2} \\ \frac{B}{2} & (\omega_{1S} - \omega_{0I}) \end{pmatrix} = \begin{pmatrix} 0 & \frac{B}{4} \\ \frac{B}{4} & 0 \end{pmatrix}$$

While the perturbation effect in the ZQ subspace can be ignored ($\frac{B}{2\omega_{0I}}$ is small), its contribution in the DQ subspace drives the polarization transfer of which the rate depends on the strength of the anisotropic interaction. In a powder sample, interference of different distances and orientations leads to 50% efficiency at quasi-equilibrium (long mixing time).

In the case of a linear ramp centering at $\omega_{1S} = \omega_{0I}$, let's assume that the mixing time τ_{mix} is much longer than the period of the microwave, in which case the matrix form of the H_{DQ} has the form

$$H_{DQ}(t) = \begin{pmatrix} -\frac{1}{2}\dot{\omega}_{1S}t & \frac{B}{4} \\ \frac{B}{4} & \frac{1}{2}\dot{\omega}_{1S}t \end{pmatrix}$$

where $\dot{\omega}_{1S}$ is the ramp rate and $-\frac{\tau_{mix}}{2} \le t \le \frac{\tau_{mix}}{2}$. Thus we arrive at the situation discussed in Landau-Zener theory (C. Zener, Proc. R. Soc. London 137 (1932), 696-702). If the ramp in the microwave amplitude is adiabatically slow in the sense that

$$\frac{B^2}{16\dot{\omega}_{1S}} \gg 1$$

for all possible values of B, then the polarization transfer occurs at the center of the ramp for all orientations and distances, leading to 100% efficiency which is a factor of 2 improvement compared to CA-NOVEL. The adiabatic condition also suggests that a stronger coupling enables a faster ramp rate.

Experimental

EPR and pulsed DNP/NMR experiments were performed on a Bruker ElexSys E580 X-band EPR spectrometer using an EN 4118X-MD4 ENDOR probe. The probe consists of a dielectric resonator wrapped with a saddle coil for RF excitation. In normal operation, the

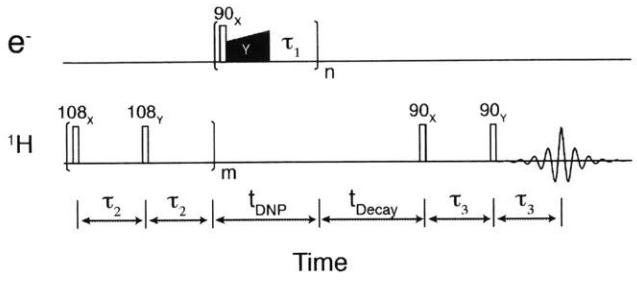

Figure 5.1: Ramped-amplitude NOVEL pulsed DNP sequence. The pulse sequence is identical to the constant-amplitude NOVEL sequence except for the amplitude modulation of the microwave locking pulse (Y pulse). The amplitude is ramped from $\omega_{1S} - \frac{\Delta\omega_{1S}}{2}$ to $\omega_{1S} + \frac{\Delta\omega_{1S}}{2}$, corresponding to the ramp size of $\Delta\omega_{1S}$, with linear or tangent shape profiles.

coil is untuned to permit ENDOR experiments across a broad range of RF frequencies. However, for our DNP/NMR experiments, the RF coil was locally tuned to the desired frequency (~15 MHz) by a module of tuning and matching capacitors to improve the RF excitation efficiency and detection sensitivity. An iSpin-NMR spectrometer purchased from Spincore Technologies, Inc. (Gainesville, FL, US) was used for the RF excitation and detection of the NMR signals. The ^{1}H NMR signals were acquired via a solid echo sequence with 8-step phase cycling. The signals were processed using a home-written MATLAB program [56].

The microwave bridge of the EPR spectrometer is equipped with a SpinJet AWG commercially available from Bruker BioSpin. The desired waveform is achieved by sideband suppression mixing of the main carrier frequency with the waveform generated by the SpinJet. The AWG has 8 output channels each of which has 192 kSa of memory, 14 bits of amplitude resolution and 0.625 ns time resolution corresponding to a bandwidth of ±400 MHz about the carrier. The SpinJet AWG allows the amplitude modulation (amplitude ramp) during the locking pulse (microwave pulse Y in **Fig. 5.1**). In this paper, the locking pulse is used interchangeably with the mixing time or contact time.

Samples for the experimental data shown in **Figure 5.2** and **5.3** consisted of 40 mM SA-BDPA dissolved in glycerol-d8/D_2O/H_2O (60/30/10 volume ratio) at 80 K. The data in **Figure 5.4** was obtained from a polystyrene doped with 2% BDPA at 300 K.

Results

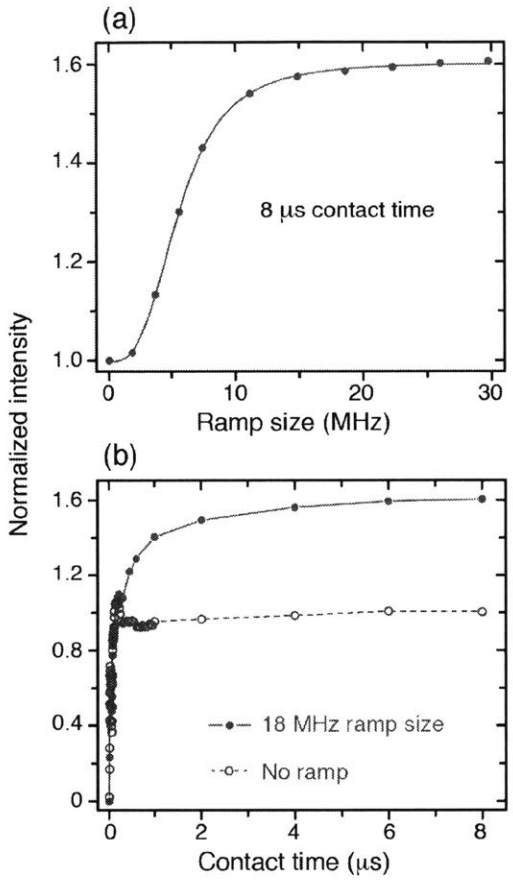

Figure 5.2: Performance of the RA-NOVEL sequence on a sample containing 40 mM SA-BDPA in glycerol-d8/D_2O/H_2O (60/30/10 volume ratio) at 80 K. (a) Optimization of the ramp size. The length of the locking pulse was fixed at 8 μs whereas the ramp size was varied from 0 to ~30 MHz. The resulting DNP-enhanced NMR signals were normalized to that obtained with CA-NOVEL sequence (ramp size of 0 MHz). The intensity reaches a plateau at ~ 18 MHz of ramp size (ramp from 6 MHz to 24 MHz). (b) Contact time dependent curves for CA-NOVEL (no ramp) and RA- NOVEL with 18 MHz ramp size. In comparison, RA-NOVEL builds up more slowly (3 μs compared to 150 ns) and reaches higher efficiency in a quasi-equilibrium state (long mixing time). The DNP efficiency is improved by a factor of 1.6 using RA-NOVEL.

We implemented the pulse sequence shown in **Figure 5.1,** which is identical to the NOVEL sequence except for the amplitude modulation of the microwave locking pulse (the Y pulse). The optimization of all the experimental parameters was accomplished using the procedure described in our previous study [54]. For the pre-saturation on ^1H, we used a chain of 16 pulses ($m = 8$) with the inter-pulse delay of $\tau_2 = 5$ ms. For NMR signal detection, the solid echo sequence was used with $\tau_3 = 20\,\mu s$. The recovery delay for the electron (τ_1) was typically 10 ms and 1.5 ms for SA-BDPA and trityl-OX063, respectively, at 80 K. The microwave pulses were repeated n times for the ^1H polarization to buildup. For a

full saturation, we used $n = 3T_b / \tau_1$ in which T_b is the buildup time constant of ^{1}H. Typically, n can be as large as ~10,000. Additionally, the size, rate and shape of the ramp required optimization. **Figure 5.2a** illustrates the effect of the ramp size on the DNP efficiency while the mixing time was fixed at 8 μs on a sample containing 40 mM SA-BDPA. The DNP-enhanced NMR signals were normalized to those obtained with the CA-NOVEL sequence (ramp size = 0 MHz). The intensity increases with the ramp size and plateaus at ~18 MHz, which corresponds to a ramp from 6 MHz to 24 MHz. We obtained an enhancement of ~85 with CA-NOVEL, consistent with our previous study, and ~135 with RA-NOVEL which corresponds to a factor of up to 1.6 improvement. The improvement in the DNP enhancement is further confirmed in **Figure 5.2b** wherein we incremented the mixing time up to 8 μs with and without the amplitude ramp. In comparison to CA-NOVEL, the polarization in the RA-NOVEL builds more slowly, but results in higher efficiency.

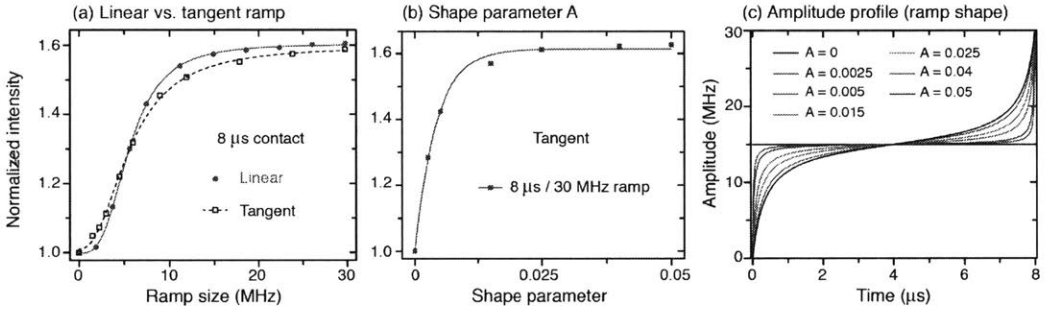

Figure 5.3: Comparison between different ramp profiles at 8 μs contact time and 30 MHz ramp size. (a) Negligible difference between linear and tangent ramp at 8 μs contact time. (b) Performance of difference tangent ramp schemes characterized by a single shape parameter A. The corresponding amplitude profiles are given in (c). The data were taken on the same samples and temperatures described in **Fig. 5.2**.

We investigated the performance of a tangential ramp at τ_{mix}=8 μs (**Figure 5.3**). As revealed in **Figure 5.3a**, we found negligible differences between linear and tangent ramp, with both saturating at a ~ 20 MHz ramp size with 1.6 improvement. In **Figure 5.3b** and **5.3c**, we varied the ramp shape, characterized by a single shape parameter A, with the following ramp profile:

$$\omega_{1S}(t) = \omega_{0I} - A \cdot \tan\left\{\arctan\left[\frac{\omega_{0I}}{A}\left(1 - 2\frac{t}{\tau_{mix}}\right)\right]\right\}$$

A = 0 corresponds to constant-NOVEL sequence (no ramp). For A > 0 we obtain different tangent profiles having an initial slope decreasing with increasing A (**Figure 5.3c)**, but the ramp size is fixed to $2\omega_{01}$ (~30 MHz).

In **Figure 5.4**, we compare the performance of linear and tangent ramp at a short mixing time of 0.8 μs as opposed to 8 μs used on a sample of polystyrene doped with 2% BDPA. These data were acquired at room temperature (300 K). We found that there exists an optimum ramp size and thus ramp rate, which is indicative of the adiabaticity of the pulse sequence.

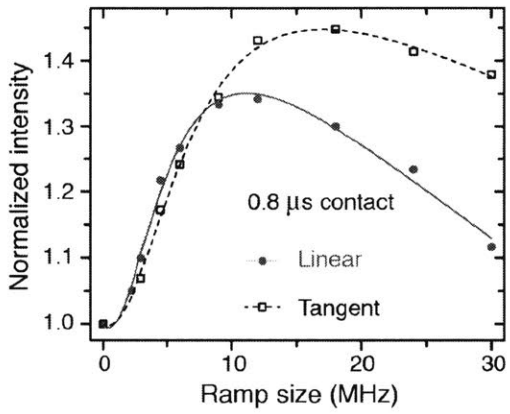

Figure 5.4: Linear vs. tangent ramp at short contact time (0.8 μs). The difference becomes apparent at large ramp size. In this case, tangent ramp appears to be more efficient. In both cases, the optimum ramp rate is indicative of the adiabaticity of the ramped-NOVEL sequence. Experiments were performed at room temperature on a sample of polystyrene doped with 2% BDPA.

Discussion

The improvement (ramped-amplitude vs. constant-amplitude) obtained with RA-NOVEL is similar to that achieved experimentally with RA-CP. A detailed study by Metz *et al.* in CP MAS NMR experiments showed an improvement factor of up to 1.6, and the possibility of extending this effect to a 1.8 enhancement with an sufficiently long mixing time [51]. In our experiments, the longest mixing times allowed by the TWT were ~10 μs, and larger improvements might be possible with extended microwave pulses. The theoretical limit (a factor of 2 improvement) was only observed with RA-CP in a model system of diluted spin pairs such as ^{1}H-^{13}C in a sample of 2-^{13}C-$^{2}H_3$-alanine diluted in perdeuterated alanine [57]. Our results approach the theoretical value and optimization of the sample conditions may lead to further improvement.

In practice, when applied on multi-spin systems, the improved performance of RA-CP is often attributed to the compensation for the chemical shift anisotropy (CSA) by a broader excitation bandwidth and for the Hartmann-Hahn mismatch due to the inhomogeneity of radio frequency irradiations. Our experiments were performed at low field at which the g-anisotropy, an analog of the CSA, is negligible. If the broader bandwidth were responsible, one would expect the efficiency to monotonically increase with the size of the ramp. However, as seen in **Figure 5.4**, this was not the case. At short mixing time (τ_{mix}=0.8 μs), we observed an optimum ramp size above which the efficiency decreases. Furthermore, the inhomogeneity of the Larmor frequency is negligible and the microwave field strength ω_{1S} measured by nutation experiments (data not shown) show ~10% inhomogeneity (~ 1.5 MHz at the NOVEL condition) which is one order of magnitude smaller than the optimum ramp size, thus the mismatch is less of an issue in NOVEL than it is in CP. Therefore, it is likely that the improvement in the DNP enhancement of RA-NOVEL is due to the adiabaticity of the pulse sequence. This also explains the difference between linear and tangent ramps. At long mixing times, the difference is negligible because the sweep rate is slow regardless of the modulation scheme. At short mixing times, the difference is apparent and the superior performance of a tangent ramp compared to its linear counterpart is also well-known for RA-CP [52].

It is worth noting that RA-NOVEL requires a longer mixing time. In particular, the mixing time employed in a CA-NOVEL is ~10^2 ns as compared to the μs (~10^3 ns) time for RA-NOVEL. This has a practical implication on the design of pulsed DNP experiments. Given the same experimental conditions, a ramped-amplitude experiment would impose a higher duty cycle on the microwave amplifier. Furthermore, the repetition time is on the order of the electronic relaxation time, and when T_{1e} is short, RA-NOVEL might exceed the duty cycle limit of the microwave amplifier. For example, in our previous study we obtained a high enhancement at room temperature on a BDPA/PS sample when running the microwave amplifier near its designed 1% duty cycle[54]. Making the contact time ~10 times longer is not possible in such cases. However, as long as the duty cycle permits, RA-NOVEL always provided larger enhancements compared to CA-NOVEL.

Furthermore, the long mixing time in RA-NOVEL makes it more suitable for radicals with long electronic relaxation T_{1e}'s such as BDPA or SA-BDPA, the latter being a water-soluble derivative of BDPA. SA-BDPA has a long T_{1e} ~50 ms at 1 mM concentration in frozen solution at 80 K and 5 T [58]. Our experiment utilized a concentrated sample of 40

mM, with a T_{1e} of ~10 ms. At the longest contact time (~10 μs) allowed by the TWT the duty cycle is 0.1%, which is still significantly below the 1% limit for the TWT. We note that RA-NOVEL might not be the method of choice for DNP using photo-excited triplet states wherein the short lifetime (μs or less) of the triplet states does not favor long mixing time.

Another prominent feature of BDPA-type radicals is the strong hyperfine coupling, which can be as large as 5.3 MHz [54; 59; 60]. The trityl-OX063 radical, on the other hand, was designed to remove all the ^{1}H's that couple to the unpaired electron to facilitate solution Overhauser effect DNP mediated by electron-nuclear dipolar coupling [61-63]. Our experimental data on both SA-BDPA and trityl-OX063 radicals show consistent results. Specifically, both require a ramp size of ~20 MHz and contact time of ~3 μs. Furthermore, the improvement factors are also similar: 1.6 for SA-BDPA and 1.45 for trityl-OX063 (enhancement of 175 for CA-NOVEL and 250 for RA-NOVEL on sample containing 40 mM radical, data not shown). This suggests that the improvement of RA-NOVEL is generic, regardless of the radicals used. At higher fields where the difference in *g* anisotropy becomes significant, the difference between the two types of radicals might be more pronounced.

Finally, we emphasize the benefit of modulating the microwave amplitude to improve the DNP enhancement. Various groups have demonstrated this in the context of CW DNP [64-69]. Our results show that it is also important to modulate the microwave power in pulsed DNP experiments. To this end, an AWG is an elegant solution to conveniently manipulate the properties of the microwave pulses in a precise manner. In particular, using an AWG allows control of the amplitude, frequency, and phase of the microwave pulses. In a forthcoming paper, we will discuss another pulsed DNP sequence based on modulation of the frequency rather than the amplitude of the microwave pulses. Our study parallels the trend in recent years of integrating an AWG into EPR spectrometers [70]. The implementation of this approach has been performed at both low and high frequencies [68; 70]. With the availability of fast (a few GSa/s) and cost-effective AWG, we anticipate that AWG will evolve into a standard component for the next generation of DNP/NMR instrumentation.

Conclusions

In summary, by modulating the amplitude of the microwave pulses using an arbitrary waveform generator (AWG), we have demonstrated that ramped-amplitude NOVEL gives

rise to a significant improvement in the DNP enhancement when compared to constant amplitude-NOVEL. In particular, RA-NOVEL lengthens the contact time by about an order of magnitude and improves the DNP efficiency by a factor of up to 1.6 which is 80% of the theoretical value. The fact that it requires longer mixing times suggests that RA-NOVEL should be used instead of constant-NOVEL as long as the T_{1e} is long and/or the duty cycle of the microwave amplifier is not exceeded. Thus, at the moment RA-NOVEL is suitable for narrow-line radicals with long T_{1e}'s such as BDPA and its derivative SA-BDPA. Our study emphasizes the importance of the ability to modulate the microwave pulses in order to optimize the DNP efficiency.

Acknowledgements

This research was supported by grants EB-002804 and EB-002026 to RGG from the National Institutes of Biomedical Imaging and Bioengineering and to grant GM095843 to TMS from the National Institutes of Health of General Medical Sciences, Grant No. We thank Ajay Thakkar and Jeff Bryant for their extensive technical assistance.

References

[1] R.G. Griffin, and T.F. Prisner, "High Field Dynamic Nuclear Polarization – The Renaissance", Phys. Chem. Chem. Phys. 112 (2010) 5737-5740

[2] A.N. Smith, and J.R. Long, "Dynamic Nuclear Polarization as an Enabling Technology for Solid State Nuclear Magnetic Resonance Spectroscopy", Analytical Chemistry 88 (2016) 122-132.

[3] T.V. Can, Q.Z. Ni, and R.G. Griffin, "Mechanisms of Dynamic Nuclear Polarization in Insulating Solids", Journal of magnetic resonance (San Diego, Calif. : 1997) 253 (2015) 23-35.

[4] Q.Z. Ni, E. Daviso, T.V. Can, E. Markhasin, S.K. Jawla, T.M. Swager, R.J. Temkin, J. Herzfeld, and R.G. Griffin, "High Frequency Dynamic Nuclear Polarization", Accounts of Chemical Research 46 (2013) 1933-1941.

[5] A.J. Rossini, A. Zagdoun, M. Lelli, A. Lesage, C. Coperet, and L. Emsley, "Dynamic Nuclear Polarization Surface Enhanced NMR Spectroscopy", Accounts of Chemical Research 46 (2013) 1942-1951.

[6] R. Tycko, "NMR at Low and Ultralow Temperatures", Accounts of Chemical Research 46 (2013) 1923-1932.

[7] A.B. Barnes, G. De Paëpe, P.C.A. van der Wel, K.N. Hu, C.G. Joo, V.S. Bajaj, M.L. Mak-Jurkauskas, J.R. Sirigiri, J. Herzfeld, R.J. Temkin, and R.G. Griffin, "High-Field Dynamic Nuclear Polarization for Solid and Solution Biological NMR", Applied Magnetic Resonance 34 (2008) 237-263.

[8] T. Maly, G.T. Debelouchina, V.S. Bajaj, K.-N. Hu, C.-G. Joo, M.L. Mak-Jurkauskas, J.R. Sirigiri, P.C.A. van der Wel, J. Herzfeld, R.J. Temkin, and R.G. Griffin, "Dynamic nuclear polarization at high magnetic fields", The Journal of Chemical Physics 128 (2008) 052211.

[9] M.L. Mak-Jurkauskas, V.S. Bajaj, M.K. Hornstein, M. Belenky, R.G. Griffin, and J. Herzfeld, "Energy transformations early in the bacteriorhodopsin photocycle revealed by

DNP-enhanced solid-state NMR", Proceedings of the National Academy of Sciences 105 (2008) 883-888.
[10] V.S. Bajaj, M.L. Mak-Jurkauskas, M. Belenky, J. Herzfeld, and R.G. Griffin, "Functional and shunt states of bacteriorhodopsin resolved by 250 GHz dynamic nuclear polarization-enhanced solid-state NMR", Proceedings of the National Academy of Sciences 106 (2009) 9244-9249.
[11] G.T. Debelouchina, M.J. Bayro, P.C.A. van der Wel, M.A. Caporini, A.B. Barnes, M. Rosay, W.E. Maas, and R.G. Griffin, "Dynamic nuclear polarization-enhanced solid-state NMR spectroscopy of GNNQQNY nanocrystals and amyloid fibrils", Physical Chemistry Chemical Physics 12 (2010) 5911-5919.
[12] Ü. Akbey, W.T. Franks, A. Linden, S. Lange, R.G. Griffin, B.-J.v. Rossum, and H. Oschkinat, "Dynamic Nuclear Polarization of Deuterated Proteins", Angewandte Chemie International Edition 49 (2010) 7803-7806.
[13] A. Lesage, M. Lelli, D. Gajan, M.A. Caporini, V. Vitzthum, P. Mieville, J. Alauzun, A. Roussey, C. Thieuleux, A. Mehdi, G. Bodenhausen, C. Coperet, and L. Emsley, "Surface Enhanced NMR Spectroscopy by Dynamic Nuclear Polarization", Journal of the American Chemical Society 132 (2010) 15459-15461.
[14] M.J. Bayro, G.T. Debelouchina, M.T. Eddy, N.R. Birkett, C.E. MacPhee, M. Rosay, W.E. Maas, C.M. Dobson, and R.G. Griffin, "Intermolecular Structure Determination of Amyloid Fibrils with Magic-Angle Spinning and Dynamic Nuclear Polarization NMR", Journal of the American Chemical Society 133 (2011) 13967-13974.
[15] H. Takahashi, D. Lee, L. Dubois, M. Bardet, S. Hediger, and G. De Paepe, "Rapid Natural-Abundance 2D C-13-C-13 Correlation Spectroscopy Using Dynamic Nuclear Polarization Enhanced Solid-State NMR and Matrix-Free Sample Preparation", Angewandte Chemie-International Edition 51 (2012) 11766-11769.
[16] M. Kaplan, A. Cukkemane, G.C.P. van Zundert, S. Narasimhan, M. Daniels, D. Mance, G. Waksman, A.M.J.J. Bonvin, R. Fronzes, G.E. Folkers, and M. Baldus, "Probing a cell-embedded megadalton protein complex by DNP-supported solid-state NMR", Nature Methods 12 (2015) 649-+.
[17] D. Mance, P. Gast, M. Huber, M. Baldus, and K.L. Ivanov, "The magnetic field dependence of cross-effect dynamic nuclear polarization under magic angle spinning", Journal of Chemical Physics 142 (2015).
[18] K. Thurber, and R. Tycko, "Theory for cross effect dynamic nuclear polarization under magic angle spinning in solid state nuclear magnetic resonance: the importance of level crossings", J Chem Phys 137 (2012) 084508-1.
[19] F. Mentink-Vigier, U. Akbey, Y. Hovav, S. Vega, H. Oschkinat, and A. Feintuch, "Fast passage dynamic nuclear polarization on rotating solids", Journal of magnetic resonance (San Diego, Calif. : 1997) 224 (2012) 13-21.
[20] K.-N. Hu, G.T. Debelouchina, A.A. Smith, and R.G. Griffin, "Quantum mechanical theory of dynamic nuclear polarization in solid dielectrics", Journal of Chemical Physics 134 (2011) 125105.
[21] Y. Hovav, A. Feintuch, and S. Vega, "Theoretical aspects of dynamic nuclear polarization in the solid state- The solid effect", Journal of Magnetic Resonance 207 (2010) 176-189.
[22] L. Becerra, G. Gerfen, R. Temkin, D. Singel, and R. Griffin, "Dynamic nuclear polarization with a cyclotron resonance maser at 5 T.", Physical Review Letters 71 (1993) 3561-3564.
[23] L.R. Becerra, G.J. Gerfen, B.F. Bellew, J.A. Bryant, D.A. Hall, S.J. Inati, R.T. Weber, S. Un, T.F. Prisner, A.E. McDermott, K.W. Fishbein, K. Kreischer, R.J. Temkin, D.J. Singel, and R.G. Griffin, "A Spectrometer for Dynamic Nuclear Polarization and Electron

Paramagnetic Resonance at High Frequencies", Journal of Magnetic Resonance A117 (1995) 28-40.
[24] V. Bajaj, C. Farrar, M. Hornstein, I. Mastovsky, J. Vieregg, J. Bryant, B. Elena, K. Kreischer, R. Temkin, and R. Griffin, "Dynamic nuclear polarization at 9T using a novel 250GHz gyrotron microwave source.", J Magn Reson 160 (2003) 85-90.
[25] M. Rosay, L. Tometich, S. Pawsey, R. Bader, R. Schauwecker, M. Blank, P.M. Borchard, S.R. Cauffman, K.L. Felch, R.T. Weber, R.J. Temkin, R.G. Griffin, and W.E. Maas, "Solid-state dynamic nuclear polarization at 263 GHz: spectrometer design and experimental results", Physical Chemistry Chemical Physics 12 (2010) 5850-5860.
[26] A. Barnes, E. Markhasin, E. Daviso, V. Michaelis, E.A. Nanni, S.K. Jawla, E.L. Mena, R. DeRocher, A. Thakkar, P.P. Woskov, J. Herzfeld, R.J. Temkin, and R.G. Griffin, "Dynamic nuclear polarization at 700 MHz/460 GHz", J Magn Reson 224 (2012) 1-7.
[27] Y. Matsuki, S. Nakamura, S. Fukui, H. Suematsu, and T. Fujiwara, "Closed-cycle cold helium magic-angle spinning for sensitivity-enhanced multi-dimensional solid-state NMR", Journal of Magnetic Resonance 259 (2015) 76-81.
[28] E. Bouleau, P. Saint-Bonnet, F. Mentink-Vigier, H. Takahashi, J.F. Jacquot, M. Bardet, F. Aussenac, A. Purea, F. Engelke, S. Hediger, D. Lee, and G. De Paepe, "Pushing NMR sensitivity limits using dynamic nuclear polarization with closed-loop cryogenic helium sample spinning", Chemical Science 6 (2015) 6806-6812.
[29] M. Rosay, M. Blank, and F. Engelke, "Instrumentation for solid-state dynamic nuclear polarization with magic angle spinning NMR", Journal of Magnetic Resonance 264 (2016) 88-98.
[30] T.V. Can, M.A. Caporini, F. Mentink-Vigier, B. Corzilius, J.J. Walish, M. Rosay, W.E. Maas, M. Baldus, S. Vega, T.M. Swager, and R.G. Griffin, "Overhauser effects in insulating solids", Journal of Chemical Physics 141 (2014) 064202.
[31] M. Lelli, S.R. Chaudhari, D. Gajan, G. Casano, A.J. Rossini, O. Ouari, P. Tordo, A. Lesage, and L. Emsley, "Solid-State Dynamic Nuclear Polarization at 9.4 and 18.8 T from 100 K to Room Temperature", Journal of the American Chemical Society 137 (2015) 14558-14561.
[32] A. Henstra, P. Dirksen, and W.T. Wenckebach, "Enhanced dynamic nuclear polarization by the integrated solid effect", Physics Letters A 134 (1988) 134-136.
[33] A. Henstra, P. Dirksen, J. Schmidt, and W.T. Wenckebach, "Nuclear Spin Orientation via Electron Spin Locking (NOVEL)", J. Magn. Reson. 77 (1988) 389-393.
[34] A. Henstra, T.-S. Lin, J. Schmidt, and W.T. Wenckebach, "High dynamic nuclear polarization at room temperature", Chemical Physics Letters 165 (1990) 6-10.
[35] D.J. van den Heuvel, A. Henstra, T.-S. Lin, J. Schmidt, and W.T. Wenckebach, "Transient oscillations in pulsed dynamic nuclear polarization", Chemical Physics Letters 188 (1992) 194-200.
[36] T.R. Eichhorn, N. Niketic, B. van den Brandt, U. Filges, T. Panzner, E. Rantsiou, W.T. Wenckebach, and P. Hautle, "Proton polarization above 70% by DNP using photo-excited triplet states, a first step towards a broadband neutron spin filter", Nuclear Instruments & Methods in Physics Research Section a-Accelerators Spectrometers Detectors and Associated Equipment 754 (2014) 10-14.
[37] K. Tateishi, M. Negoro, S. Nishida, A. Kagawa, Y. Morita, and M. Kitagawa, "Room temperature hyperpolarization of nuclear spins in bulk", Proceedings of the National Academy of Sciences of the United States of America 111 (2014) 7527-7530.
[38] K. Hu, H. Yu, T. Swager, and R. Griffin, "Dynamic nuclear polarization with biradicals.", Journal of the American Chemical Society 126 (2004) 10844-5.
[39] C. Song, K.-N. Hu, C.-G. Joo, T.M. Swager, and R.G. Griffin, "TOTAPOL – A Biradical Polarizing Agent for Dynamic Nuclear Polarization Experiments in Aqueous Media", J. Am Chem. Soc 128 (2006) 11385-90.

[40] C. Sauvee, M. Rosay, G. Casano, F. Aussenac, R.T. Weber, O. Ouari, and P. Tordo, "Highly Efficient, Water-Soluble Polarizing Agents for Dynamic Nuclear Polarization at High Frequency", Angewandte Chemie-International Edition 52 (2013) 10858-10861.
[41] K.-N. Hu, C. Song, H.-h. Yu, T.M. Swager, and R.G. Griffin, "High-Frequency Dynamic Nuclear Polarization Using Biradicals: A Multifrequency EPR Lineshape Analysis", J. Chem. Phys. 128 (2008) 052321.
[42] S. Un, T. Prisner, R.T. Weber, M.J. Seaman, K.W. Fishbein, A.E. McDermott, D.J. Singel, and R.G. Griffin, "Pulsed dynamic nuclear polarization at 5 T", Chemical Physics Letters 189 (1992) 54-59.
[43] C. Farrar, D. Hall, G. Gerfen, M. Rosay, J. Ardenkjaer-Larsen, and R. Griffin, "High-frequency dynamic nuclear polarization in the nuclear rotating frame.", J Magn Reson 144 (2000) 134-41.
[44] V. Weis, M. Bennati, M. Rosay, and R.G. Griffin, "Solid effect in the electron spin dressed state: A new approach for dynamic nuclear polarization", J. Chem. Phys. 113 (2000) 6795-6802.
[45] G.W. Morley, J. van Tol, A. Ardavan, K. Porfyrakis, J.Y. Zhang, and G.A.D. Briggs, "Efficient dynamic nuclear polarization at high magnetic fields", Physical Review Letters 98 (2007).
[46] N. Khaneja, "Switched control of electron nuclear systems", Physical Review A 76 (2007) 032326.
[47] H.J. Kim, E.A. Nanni, M.A. Shapiro, J.R. Sirigiri, P.P. Woskov, and R.J. Temkin, "Amplification of Picosecond Pulses in a 140-GHz Gyrotron-Traveling Wave Tube", Physical Review Letters 105 (2010) 135101 (1-4).
[48] E.A. Nanni, S.M. Lewis, M.A. Shapiro, R.G. Griffin, and R.J. Temkin, "Photonic-Band-Gap Traveling-Wave Gyrotron Amplifier", Physical Review Letters 111 (2013).
[49] S.R. Hartmann, and E.L. Hahn, "Nuclear Double Resonance in the Rotating Frame", Phys. Rev. 128 (1962) 2042-2053.
[50] A. Pines, M.G. Gibby, and J.S. Waugh, "Proton Enhanced Nuclear Induction Spectroscopy. A Method for High Resolution NMR of Dilute Spins in Solids", J. Chem. Phys. 56 (1972) 1776-1777.
[51] G. Metz, X.L. Wu, and S.O. Smith, "Ramped-Amplitude Cross-Polarization In Magic-Angle-Spinning NMR", Journal of Magnetic Resonance Series A 110 (1994) 219-227.
[52] S. Hediger, B.H. Meier, N.D. Kurur, G. Bodenhausen, and R.R. Ernst, "NMR Cross-Polarization by Adiabatic Passage Through the Hartmann-Hahn Condition (APHH)", Chemical Physics Letters 223 (1994) 283-288.
[53] G.C. Chingas, A.N. Garroway, W.B. Moniz, and R.D. Bertrand, "Adiabatic-J Cross-Polarization in Liquids for Signal Enhancement in NMR", Journal of the American Chemical Society 102 (1980) 2526-2528.
[54] T.V. Can, J.J. Walish, T.M. Swager, and R.G. Griffin, "Time domain DNP with the NOVEL sequence", The Journal of Chemical Physics 143 (2015) 054201-054201.
[55] G. Mathies, S. Jain, M. Reese, and R.G. Griffin, "Pulsed Dynamic Nuclear Polarization with Trityl Radicals", Journal of Physical Chemistry Letters 7 (2016) 111-116.
[56] MathWorks, MatLab, MathWorks, Natick, 2010.
[57] M. Ernst, and B.H. Meier, "Adiabatic Polarization-Transfer Methods in MAS Spectroscopy", eMagRes (2010).
[58] O. Haze, B. Corzilius, A.A. Smith, R.G. Griffin, and T.M. Swager, "Water-Soluble Narrow-Line Radicals for Dynamic Nuclear Polarization", Journal of the American Chemical Society 134 (2012) 14287-14290.
[59] N.S. Dalal, D.E. Kennedy, and C.A. McDowell, "EPR and ENDOR studies of hyperfine interactions in solutions of stable organic free radicals", The Journal of Chemical Physics 61 (1974) 1689-1697.

[60] V. Weis, M. Bennati, M. Rosay, J.A. Bryant, and R.G. Griffin, "High-Field DNP and ENDOR with a Novel Multiple-Frequency Resonance Structure", Journal of Magnetic Resonance 140 (1999) 293-299.
[61] S. Anderson, K. Golman, F. Rise, H. Wikstrom, and L.-G. Wistrand, 5,530,140, 1996.
[62] J. Ardenkjær-Larsen, B. Fridlund, A. Gram, G. Hansson, L. Hansson, M. Lerche, R. Servin, M. Thaning, and K. Golman, "Increase in signal-to-noise ratio of > 10,000 times in liquid-state NMR.", Proc Natl Acad Sci U S A 100 (2003) 10158-63.
[63] S.N. Trukhan, V.F. Yudanov, V.M. Tormyshev, O.Y. Rogozhnikova, D.V. Trukhin, M.K. Bowman, M.D. Krzyaniak, H. Chen, and O.N. Martyanov, "Hyperfine interactions of narrow-line trityl radical with solvent molecules", Journal of Magnetic Resonance 233 (2013) 29-36.
[64] Y. Hovav, A. Feintuch, S. Vega, and D. Goldfarb, "Dynamic nuclear polarization using frequency modulation at 3.34 T", Journal of Magnetic Resonance 238 (2014) 94-105.
[65] A. Bornet, J. Milani, B. Vuichoud, A.J.P. Linde, G. Bodenhausen, and S. Jannin, "Microwave frequency modulation to enhance Dissolution Dynamic Nuclear Polarization", Chemical Physics Letters 602 (2014) 63-67.
[66] T. Idehara, E.M. Khutoryan, Y. Tatematsu, Y. Yamaguchi, A.N. Kuleshov, O. Dumbrajs, Y. Matsuki, and T. Fujiwara, "High-Speed Frequency Modulation of a 460-GHz Gyrotron for Enhancement of 700-MHz DNP-NMR Spectroscopy", Journal of Infrared Millimeter and Terahertz Waves 36 (2015) 819-829.
[67] D.E.M. Hoff, B.J. Albert, E.P. Saliba, F.J. Scott, E.J. Choi, M. Mardini, and A.B. Barnes, "Frequency swept microwaves for hyperfine decoupling and time domain dynamic nuclear polarization", Solid State Nuclear Magnetic Resonance 72 (2015) 79-89.
[68] M.L. Guy, L. Zhu, and C. Ramanathan, "Design and characterization of a W-band system for modulated DNP experiments", Journal of Magnetic Resonance 261 (2015) 11-18.
[69] D. Yoon, M. Soundararajan, P. Cuanillon, F. Braunmueller, S. Alberti, and J.P. Ansermet, "Dynamic nuclear polarization by frequency modulation of a tunable gyrotron of 260 GHz", Journal of Magnetic Resonance 262 (2016) 62-67.
[70] T. Kaufmann, T.J. Keller, J.M. Franck, R.P. Barnes, S.J. Glaser, J.M. Martinis, and S. Han, "DAC-board based X-band EPR spectrometer with arbitrary waveform control", Journal of Magnetic Resonance 235 (2013) 95-108.

Chapter 6: Frequency-Swept Integrated Solid Effect

Adapted from T.V. Can, R.T. Weber, J.J. Walish, T.M. Swager, and R.G. Griffin Angewandte Chemie International Edition (accepted)

The efficiency of continuous wave dynamic nuclear polarization (DNP) experiments decreases at the high magnetic fields used in contemporary high-resolution NMR applications. To recover the expected signal enhancements from DNP, we explored time domain experiments such as NOVEL which matches the electron Rabi and nuclear Larmor frequencies to mediate polarization transfer. However, satisfying this matching condition at high frequencies is technically demanding. As an alternative we report here frequency-swept integrated solid effect (FS-ISE) experiments that utilize low power sweeps of the exciting microwave frequencies to constructively integrate the negative and positive polarizations of the solid effect, thereby producing a polarization efficiency comparable to (±10% difference) NOVEL. Finally, the microwave frequency modulation results in field profiles that exhibit new features which resemble a "stretched" solid effect.

Introduction

The history of the development of both nuclear magnetic resonance (NMR) and electron paramagnetic resonance (EPR) techniques provides clear examples of the evolution from continuous wave (CW) to pulsed methods that enable researchers to achieve a variety of new experimental goals. For instance, Fourier transform methods revolutionized the sensitivity of NMR and multidimensional experiments dramatically increased the resolution. Similarly, pulsed EPR methods have enabled a variety of new structural studies and dramatically increased resolution allowing observation of new couplings and multiple paramagnetic species. As a hybrid of the two techniques, it would not be surprising if DNP evolved along a similar path. Specifically, after more than half a century since its birth[1] and following two decades of development of high frequency DNP instrumentation for CW experiments[2-8], DNP is transitioning from CW to pulsed techniques. The initial efforts to develop time domain DNP resulted in a handful of experiments[9-14] demonstrating time domain polarization transfer methods and applications preparing polarized targets for neutron diffraction experiments. In the case of the former, at low field (0.35 T) and room temperature[15, 16], polarization was transferred from the photo-excited triplet state of pentacene to the protons of the host crystal of naphthalene. Since the lifetime of the triplet state is short, the time domain DNP mechanisms were preferred over CW DNP.

The motivation for developing pulsed DNP in NMR applications is somewhat different. In this case, the polarization enhancements available from CW DNP mechanisms (the solid effect and cross effect) scale at least as ω_0^{-1}, and therefore decrease dramatically in high field experiments[17-23]. This decrease motivates the quest for DNP mechanisms that are independent of B_0, and pulsed DNP is an untapped resource with high potential. However, time domain experiments using high frequency microwaves are technically challenging due to the limited availability of high power, pulse microwave amplifiers and microwave switches operating in the 150-600 GHz regime. Nevertheless, recent advances in this area[24, 25] stimulated us to initiate investigations of different pulse schemes for DNP. In particular, we have demonstrated that high DNP efficiencies are possible using the NOVEL pulse sequence, which is a lab frame-rotating frame analogy of cross polarization[26]. Furthermore, we showed that by adiabatically ramping the amplitude of the microwave locking pulse (ramped-NOVEL)[27] it is possible to improve the efficiency of constant amplitude NOVEL by a factor of 1.6.

Here, we present a study of pulsed DNP that utilizes the frequency swept integrated solid effect (FS-ISE), which is closely related to NOVEL. Originally, the ISE was performed by sweeping the Zeeman field B_0, with both the amplitude and frequency of the microwaves held constant[10]. For triplet-DNP, the ISE performs optimally at the NOVEL condition since it facilitates fast polarization transfers[28]. However, since our goal is to use this pulse sequence to enhance signal intensities in high-resolution magic angle spinning (MAS) NMR experiments, which require time stable, homogeneous B_0 fields, it is technically clear that sweeping the B_0 field is not an option. Results reported here demonstrate that the ISE can be implemented efficiently by sweeping the microwave frequency rather than the B_0, an approach that takes advantage of the state-of-the-art fast arbitrary waveform generator (AWG) to modulate the frequency of the microwave pulses. We found that for free radical polarizing agents, the FS-ISE yields enhancements comparable to NOVEL. Furthermore, for radicals, FS-ISE can be performed with Rabi frequencies that are an order of magnitude lower than for the NOVEL condition. In this case, the polarization transfer is slower, but achieves a similar efficiency because the lifetime of the radical is not an issue as in triplet-DNP. Thus, the FS-ISE can be performed with the microwave field strengths used in current MAS DNP spectrometers and therefore could be much more widely applicable than NOVEL or its ramped version.

Results and Discussion

The pulse sequence for the frequency-swept ISE is illustrated in **Figure 6.1a**. The waveforms (real and imaginary parts) of the chirp pulses were calculated based on the following equation.

$$s(t) = \exp\left\{ i \int_0^t dt' \left[\left(\frac{t'}{\tau_p} - \frac{1}{2} \right) \Delta\omega \right] \right\}$$

where τ_p is the pulse length and $\Delta\omega/2\pi$ is the width of the frequency sweep. The frequency modulation is performed with single sideband mixing of the carrier frequency with the desired waveform from the AWG. This scheme is achieved by essentially operating a quadrature phase detector backwards, taking the real and imaginary channels as the input instead of output. FS-ISE involves three events including the inversion of electron spin at the center of the sweep (point O) sandwiched by double quantum (DQ) and zero quantum (ZQ) transitions at points A and B, respectively (**Fig. 6.1b**)[28]. Note that the enhancements at A and B would cancel if it were not for the fact that the electron spin is inverted at O. The fact

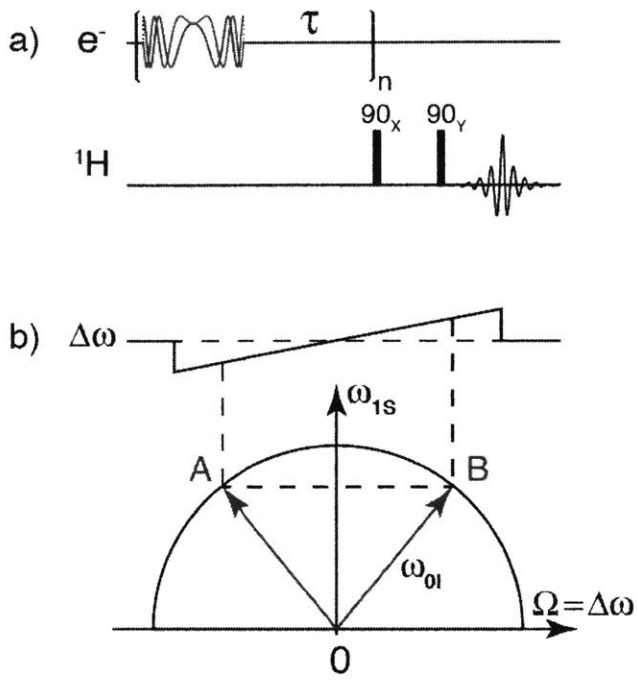

Figure 6.1: (a) Pulse sequence for the frequency-swept integrated solid effect. ^{1}H signals are detected with a solid echo. (b) During the sweep, the spin system undergoes three adiabatic events including DQ and ZQ at A and B, respectively, as well as electron spin inversion at O. The semicircle represents the relationship $\omega_{0I}^2 = \Omega^2 + \omega_{1S}^2$, which is satisfied at A and B where Ω is the microwave frequency offset. The inversion leads to the constructive addition of DNP enhancement at A and B, thus the name integrated solid effect.

that those enhancements interfere constructively gives rise to the name "integrated solid effect" to distinguish it from the unresolved solid effect in which the DQ and ZQ enhancements partially overlap and cancel.

Figure 6.2 shows the DNP enhancements as a function of the sweep width $\Delta\omega / 2\pi$ and the length of the contact time τ_p. The Zeeman field value, B_0, was set on resonance with the EPR line and the microwave field strength was adjusted to match the NOVEL condition $\omega_{1S} / 2\pi = \omega_{0I} / 2\pi \approx 15\ MHz$. At each $\Delta\omega/2\pi$ ranging from 5 MHz to 180 MHz, we obtained an optimum contact time (**Figure 6.2a**). The optimum enhancement with respect to the sweep width is given in **Figure 6.2b**, suggesting that a sweep width of 50 MHz is sufficient. Furthermore, we extracted the optimum sweep rate from **Figure 6.2a** and compared the results from two different radicals including trityl-OX063 and sulfonated-BDPA (SA-BDPA) [29] (**Figure 6.2c**). We found that SA-BDPA was capable of a faster sweep rate when compared to trityl-OX063 (50 MHz/μs vs. 32 MHz/μs).

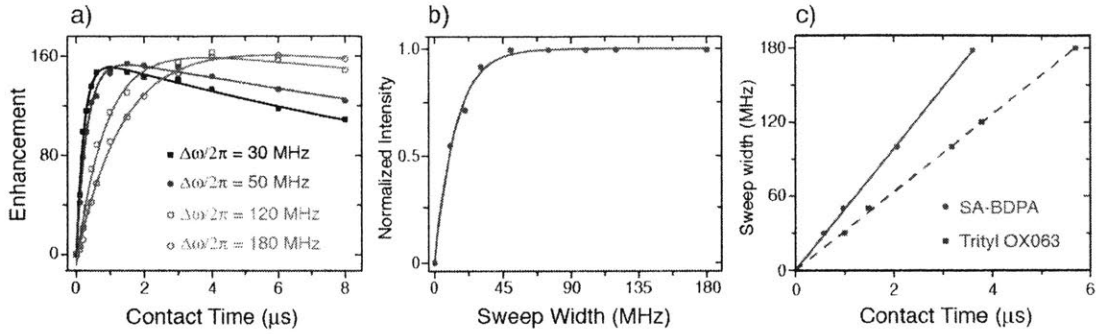

Figure 6.2: (a) DNP enhancement as a function of the contact time and the sweep width on a sample of 40 mM trityl-OX063 in glycerol-d_8/D_2O/H_2O (60/30/10 volume ratio) at 80 K and ~0.35 T with microwave irradiation being on resonant. The microwave Rabi frequency was set to match the NOVEL condition corresponding to $\omega_{1S}/2\pi = 15$ MHz. At each sweep width, there exists an optimum contact time. The corresponding maximum enhancement is normalized and plotted in (b) suggesting that a sweep width of ~50 MHz is sufficient. Similar results were obtained for sulfonated-BDPA (SA-BDPA) [29] (**Fig. 6.4**). The correlation between the sweep width and the optimum contact time in (c) indicates a faster optimum sweep rate for SA-BDPA (50 MHz/μs) compared to trityl-OX063 (32 MHz/μs) due to stronger coupling in SA-BDPA.

The optimum sweep rate found in FS-ISE is governed by the adiabatic nature of the pulse sequence when operating at the NOVEL condition[28]. All three aforementioned events at A, B, and O are adiabatic processes resulting from the interplay between the sweep rate and the e^--^{1}H pseudo secular hyperfine coupling (for A and B) or between that rate and the microwave field strength (for O). In general, the stronger hyperfine coupling and microwave field strength enable a faster sweep rate[28]. This explains the more rapid sweep rate in SA-BDPA compared to trityl-OX063. In SA-BDPA, the free electron has strong proton hyperfine couplings of up to 5.3 MHz[29-32], whereas in trityl-OX063 the coupling is mainly from the electron to the protons of the solvent, which is less than 1 MHz[33, 34].

The DNP Zeeman field profiles of the ISE sequence are shown in **Figure 6.3**, where again the sequence is operating at the NOVEL condition. The contact time of 3 μs was used throughout as it was near optimal regardless of $\Delta\omega/2\pi$ (**Figure 6.2a**). The magnetic field B_0 was incremented and the RF tuning/matching was adjusted at each of the data points. At $\Delta\omega/2\pi = 0$ (constant frequency) the DNP field profile resembles that of unresolved solid effect with no enhancement at the center. This is partially due to line broadening of the EPR spectrum by the strong hyperfine coupling in SA-BDPA as well as the e^--e^- interaction at high concentration. However, the primary reason is that at the NOVEL condition the microwave field can no longer be treated as a small perturbation as in the CW solid effect. Thus, even a sample with a low concentration of trityl-OX063 (5 mM) with a very narrow

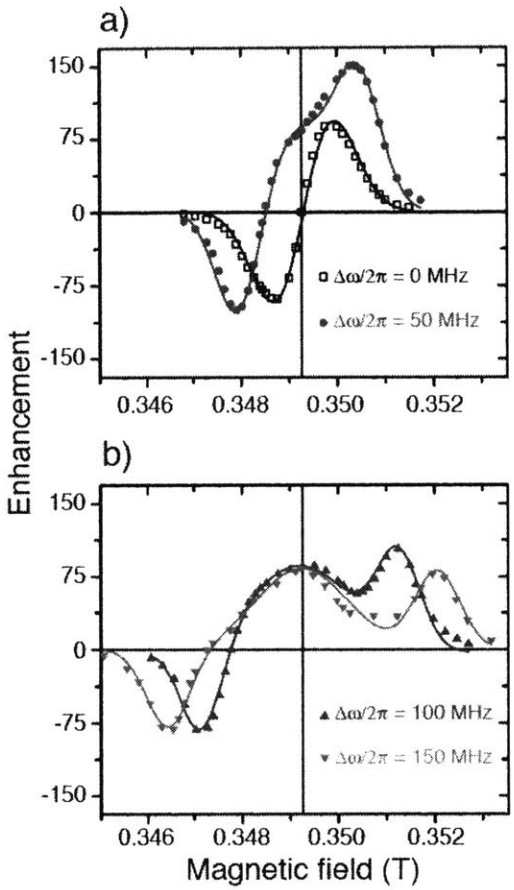

Figure 6.3: (a) DNP field profiles obtained with constant microwave frequency (black) and with microwave chirp pulses of different sweep width including 50 MHz (red), and (b) 100 MHz (blue) and 150 MHz (green). With microwave frequency kept constant, the DNP is characteristic of unresolved solid effect or differential solid effect without enhancement at the center. The enhancement at this position is non-zero when chirp pulses were used which is indicative of FS-ISE. Furthermore, the normal solid effect peaks were displaced linearly with increasing the sweep width. The data were obtained at 80 K on a sample of 40 mM SA-BDPA in glycerol-d_8/D_2O/H_2O (60/30/10 volume ratio).

EPR linewidth exhibits an unresolved solid effect field profile at $\Delta\omega/2\pi = 0$ and $\omega_{1S}/2\pi = \omega_{0I}/2\pi$ (data not shown).

At $\Delta\omega/2\pi > 0$, the enhancement at the center (on resonance with the EPR line) becomes nonzero which is characteristic of the FS-ISE sequence. The efficiency of the ISE then decreases going away from the center of the EPR line. In fact, the FS-ISE field profile is expected to follow the EPR lineshape[10]. In addition, we observed positive and negative peak enhancements, which resemble those expected from the SE but these are displaced from the position of the original solid effect peaks. The displacement is found to be half of $\Delta\omega/2\pi$, similar to the observation by Hovav *et al.* in frequency-modulated CW DNP[35].

Therefore, the full field profile of the frequency-swept ISE is a convolution of the intrinsic FS-ISE and the "displaced" or "stretched" SE field profiles.

It is worth noting that the "stretched" SE shows not only resemblances but also differences in comparison to the previous study on frequency-modulated CW DNP. The underlying reason is that both our study and the work by Hovav *et al.* utilized frequency modulation but with fundamentally different focuses (ISE vs. SE) and experimental settings (strong power pulse vs. low power CW). In particular, Hovav *et al.* showed that, under the optimal condition, frequency modulation improved the DNP enhancement by a factor of 2-3. This required modulation amplitudes smaller than the ^{1}H Larmor frequency and repetition rates faster than the spin-lattice relaxation rate of electron ($1/T_{1e}$). In comparison, we also found that the "stretched" SE can be very efficient (**Fig. 6.3a**). However, FS-ISE requires sweeping through both DQ and ZQ transitions, thus necessitating modulation amplitudes larger than twice the ^{1}H Larmor frequency. Furthermore, when operating at the NOVEL condition, FS-ISE leads to a fast polarization transfer, thus the repetition rate is slower than $1/T_{1e}$ to allow electron polarization to recover upon being depleted. Nevertheless, further investigation is required to determine if the "stretched" SE remains efficient at high fields and under MAS conditions.

In **Figure 6.4**, we present a comparison of the FS-ISE with $\omega_{1S} \ll \omega_{0I}$ that demonstrates the feasibility of using this pulse sequence far below the NOVEL condition. In particular, we set $\omega_{1S}/2\pi$ =1.5 MHz instead of 15 MHz which corresponds to ~1% of the microwave power. **Figure 6.4a** and **6.4b** show that FS-ISE operates differently under the two conditions. In comparison, the pulse length in **Figure 6.4b** is about 2 orders of magnitude longer. Nevertheless, the DNP field profiles are very similar (**Fig. 6.4c**) and the enhancements at the center and at the stretched solid effect are almost identical. Note that the adiabaticity of the inversion of electron spin is proportional to $\omega_{1S}^2/\dot{\omega}_{\mu w}$ or $P_{\mu w}/\dot{\omega}_{\mu w}$, in which $P_{\mu w}$ and $\dot{\omega}_{\mu w}$ is the microwave power and sweep rate, respectively[28]. Thus, at 1% power, the sweep rate needs to be 100 times slower or the pulse length needs to be 100 times longer.

In contemporary MAS DNP spectrometers, even though the microwave power available is ~10 W, the field strength is $\leq$1 MHz due to the absence of a microwave resonant structure[36, 37]. Thus, ω_{1S} is 2-3 orders of magnitude below the NOVEL condition. In order to satisfy the NOVEL matching condition, one would need to not only increase the

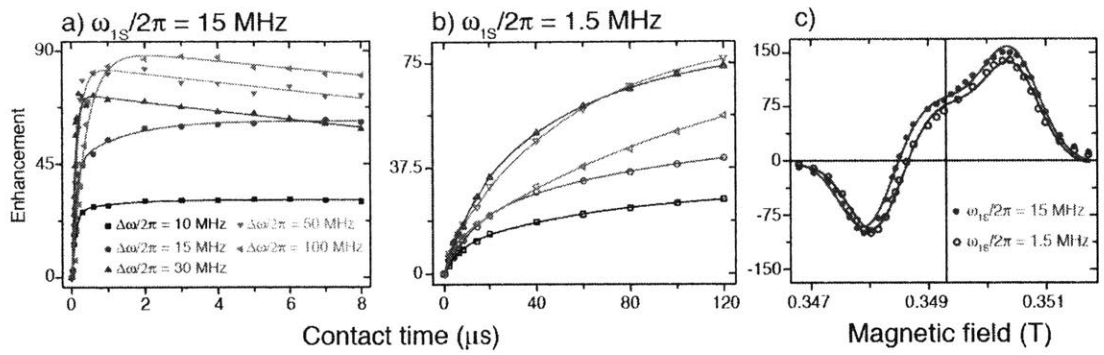

Figure 6.4: Comparison of ISE at the NOVEL condition and far below the NOVEL condition. DNP enhancements were measured at different contact times and sweep widths at microwave field strength of 15 MHz (a) and 1.5 MHz (b) in the SA-BDPA sample at 80 K. In (a) the behavior is similar to what is observed with trityl-OX063 (**Fig. 6.2a**), whereas, the enhancement in (b) monotonically increases. The pulse length was limited to 120 μs due to the memory of the AWG. In (c) are the DNP field profiles obtained with 15 MHz (red, solid circle) and 1.5 MHz (blue, open circle). The contact time was 2 μs and 120 μs, respectively. In both cases, the sweep width was 50 MHz as suggested by the data in (a) and (b). The two field profiles are similar.

microwave power, but also and more importantly to increase the Q factor by using a microwave cavity. Roughly speaking, a combination of 10^2-10^3 W of power and a Q factor of ~10^2-10^3 is needed to match the NOVEL condition at high field (> 5 T), making NOVEL a technically demanding sequence. Furthermore, the high Q factor would significantly restrict the filling factor, reducing the absolute sensitivity of the experiment. The fact that ISE can operate far below the NOVEL condition alleviates the field strength requirement as well as the restriction in the filling factor.

Note that even though our data show highly efficient FS-ISE at $\omega_{1S}/2\pi$ =1.5 MHz, it does not mean that the sequence can be straightforwardly applied to contemporary DNP/NMR spectrometers operating in the range of 400-800 MHz. The reason is that the transition moment of the ZQ and DQ scales with B_0^{-1}. In going to high fields one would need to maintain the ratio ω_{1S}/ω_{0I} which equals to 10% in our case. Such a ratio would still translate into strong microwave fields (tens of MHz). Moreover, the sweep width scales roughly with B_0 and thus so does the optimum pulse length. The pulse length might get very long even for slow relaxing radicals such as SA-BDPA. Thus, it is very likely that for FS-ISE to work at high fields $\omega_{1S}/2\pi$ will need to account for a significant fraction of $\omega_{0I}/2\pi$. Nevertheless, the flexibility to operate below the NOVEL condition makes FS-ISE a very promising sequence for high field pulsed DNP.

In comparison, we found that ISE and NOVEL give similar enhancements (±10% difference). This was not the case for triplet-DNP where ISE showed superior performance. This is probably because of the broad EPR line of the triplet state. The ISE makes use of all the spin packets by sweeping either the B_0 or microwave frequency, whereas the efficiency of NOVEL might be compromised if the excitation bandwidth is small compared to the EPR linewidth. Furthermore, NOVEL requires homogenous field strength for optimum efficiency whereas ISE appears to be more robust.

Conclusions

In summary, we have presented experimental data that indicates that FS-ISE is a new strategy for time domain DNP. In contrast to the original implementation of the ISE that employs sweeps of B_0, our strategy is suitable for high-resolution NMR applications. The frequency modulation is conveniently achieved with high precision by using an arbitrary waveform generator. FS-ISE can be performed under various microwave power settings. When operated at the NOVEL matching condition, ISE exhibits fast polarization transfer. At lower microwave field strength similar to that being used in MAS DNP spectrometers, the buildup time for the polarization is increased when utilizing ISE, but it achieves the same efficiency. Our findings expand the repertoire of pulse sequences for DNP and emphasize the advantages of using an AWG to manipulate microwave pulses.

Experimental Section

Samples used in our study include glycerol-d_8/D_2O/H_2O (60/30/10 volume ratio) glassy matrix doped with 40 mM of SA-BDPA or 40 mM of trityl-OX063. Experiments were performed at 80 K on a X-band EPR spectrometer equipped with a MD-4 ENDOR resonator as described previously.[27] We emphasize on the use of an arbitrary waveform generator (AWG) to modulate the microwave frequency. The AWG functionality is available from Bruker BioSpin as an upgrade to the existing spectrometer. The waveform of the chirp pulses with linear frequency sweep comes as part of a standard library included in the Xepr software, making it convenient to program the ISE sequence. The program takes the center frequency, the sweep width and the pulse length as inputs, which can be varied independently.

The chirp pulse was applied repeatedly with suitable repetition rate for the nuclear polarization to build up. The recovery delay τ (**Fig. 6.1a**), essentially the inverse of the repetition rate, was 8 ms and 2 ms for a sample containing SA-BDPA and trityl-OX063,

respectively. The ^{1}H NMR signals were read out by a solid echo sequence using a Spincore NMR spectrometer. The data processing was done with Matlab. The enhancement is calculated from NMR signals obtained with and without microwave irradiation. The DNP-enhanced signals were measured at 3 T_B whereas the off signals were measured at 3 T_1 to ensure the enhancement is not biased due to the fact that T_1 is much longer than T_B.

Acknowledgements

This research was supported by grants to RGG from the National Institutes of Biomedical Imaging and Bioengineering, Grant Nos. EB-002804 and EB-002026 and to T.M.S from the National Institutes of Health of General Medical Sciences, Grant No. GM095843. We thank Ajay Thakkar and Jeff Bryant for assistant.

References

[1] A.W. Overhauser, Polarization of Nuclei in Metals, Physical Review, 92 (1953) 411.
[2] L. Becerra, G. Gerfen, R. Temkin, D. Singel, R. Griffin, Dynamic nuclear polarization with a cyclotron resonance maser at 5 T., Physical Review Letters, 71 (1993) 3561-3564.
[3] L.R. Becerra, G.J. Gerfen, B.F. Bellew, J.A. Bryant, D.A. Hall, S.J. Inati, R.T. Weber, S. Un, T.F. Prisner, A.E. McDermott, K.W. Fishbein, K. Kreischer, R.J. Temkin, D.J. Singel, R.G. Griffin, A Spectrometer for Dynamic Nuclear Polarization and Electron Paramagnetic Resonance at High Frequencies, Journal of Magnetic Resonance, A117 (1995) 28-40.
[4] V. Bajaj, C. Farrar, M. Hornstein, I. Mastovsky, J. Vieregg, J. Bryant, B. Elena, K. Kreischer, R. Temkin, R. Griffin, Dynamic nuclear polarization at 9T using a novel 250GHz gyrotron microwave source., J Magn Reson, 160 (2003) 85-90.
[5] M. Rosay, L. Tometich, S. Pawsey, R. Bader, R. Schauwecker, M. Blank, P.M. Borchard, S.R. Cauffman, K.L. Felch, R.T. Weber, R.J. Temkin, R.G. Griffin, W.E. Maas, Solid-state dynamic nuclear polarization at 263 GHz: spectrometer design and experimental results, Physical Chemistry Chemical Physics, 12 (2010) 5850-5860.
[6] A. Barnes, E. Markhasin, E. Daviso, V. Michaelis, E.A. Nanni, S.K. Jawla, E.L. Mena, R. DeRocher, A. Thakkar, P.P. Woskov, J. Herzfeld, R.J. Temkin, R.G. Griffin, Dynamic nuclear polarization at 700 MHz/460 GHz, J Magn Reson, 224 (2012) 1-7.
[7] Y. Matsuki, S. Nakamura, S. Fukui, H. Suematsu, T. Fujiwara, Closed-cycle cold helium magic-angle spinning for sensitivity-enhanced multi-dimensional solid-state NMR, Journal of Magnetic Resonance, 259 (2015) 76-81.
[8] E. Bouleau, P. Saint-Bonnet, F. Mentink-Vigier, H. Takahashi, J.F. Jacquot, M. Bardet, F. Aussenac, A. Purea, F. Engelke, S. Hediger, D. Lee, G. De Paepe, Pushing NMR sensitivity limits using dynamic nuclear polarization with closed-loop cryogenic helium sample spinning, Chemical Science, 6 (2015) 6806-6812.
[9] A. Henstra, P. Dirksen, J. Schmidt, W.T. Wenckebach, Nuclear Spin Orientation via Electron Spin Locking (NOVEL), J. Magn. Reson., 77 (1988) 389-393.
[10] A. Henstra, P. Dirksen, W.T. Wenckebach, Enhanced dynamic nuclear polarization by the integrated solid effect, Physics Letters A, 134 (1988) 134-136.
[11] C. Farrar, D. Hall, G. Gerfen, M. Rosay, J. Ardenkjaer-Larsen, R. Griffin, High-frequency dynamic nuclear polarization in the nuclear rotating frame., J Magn Reson, 144 (2000) 134-141.

[12] V. Weis, M. Bennati, M. Rosay, R.G. Griffin, Solid effect in the electron spin dressed state: A new approach for dynamic nuclear polarization, J. Chem. Phys., 113 (2000) 6795-6802.
[13] G.W. Morley, J. van Tol, A. Ardavan, K. Porfyrakis, J.Y. Zhang, G.A.D. Briggs, Efficient dynamic nuclear polarization at high magnetic fields, Physical Review Letters, 98 (2007).
[14] N. Khaneja, Switched control of electron nuclear systems, Physical Review A, 76 (2007) 032326.
[15] K. Tateishi, M. Negoro, S. Nishida, A. Kagawa, Y. Morita, M. Kitagawa, Room temperature hyperpolarization of nuclear spins in bulk, Proceedings of the National Academy of Sciences of the United States of America, 111 (2014) 7527-7530.
[16] T.R. Eichhorn, B. van den Brandt, P. Hautle, A. Henstra, W.T. Wenckebach, Dynamic nuclear polarisation via the integrated solid effect II: experiments on naphthalene-h(8) doped with pentacene-d(14), Molecular Physics, 112 (2014) 1773-1782.
[17] D. Mance, P. Gast, M. Huber, M. Baldus, K.L. Ivanov, The magnetic field dependence of cross-effect dynamic nuclear polarization under magic angle spinning, Journal of Chemical Physics, 142 (2015).
[18] T.V. Can, Q.Z. Ni, R.G. Griffin, Mechanisms of Dynamic Nuclear Polarization in Insulating Solids, Journal of magnetic resonance (San Diego, Calif. : 1997), 253 (2015) 23-35.
[19] K. Thurber, R. Tycko, Theory for cross effect dynamic nuclear polarization under magic angle spinning in solid state nuclear magnetic resonance: the importance of level crossings, J Chem Phys, 137 (2012) 084508-084501.
[20] F. Mentink-Vigier, U. Akbey, Y. Hovav, S. Vega, H. Oschkinat, A. Feintuch, Fast passage dynamic nuclear polarization on rotating solids, Journal of magnetic resonance (San Diego, Calif. : 1997), 224 (2012) 13-21.
[21] K.-N. Hu, G.T. Debelouchina, A.A. Smith, R.G. Griffin, Quantum mechanical theory of dynamic nuclear polarization in solid dielectrics, Journal of Chemical Physics, 134 (2011) 125105.
[22] Y. Hovav, A. Feintuch, S. Vega, Theoretical aspects of dynamic nuclear polarization in the solid state- The solid effect, Journal of Magnetic Resonance, 207 (2010) 176-189.
[23] T. Maly, G.T. Debelouchina, V.S. Bajaj, K.-N. Hu, C.-G. Joo, M.L. Mak-Jurkauskas, J.R. Sirigiri, P.C.A. van der Wel, J. Herzfeld, R.J. Temkin, R.G. Griffin, Dynamic nuclear polarization at high magnetic fields, The Journal of Chemical Physics, 128 (2008) 052211.
[24] H.J. Kim, E.A. Nanni, M.A. Shapiro, J.R. Sirigiri, P.P. Woskov, R.J. Temkin, Amplification of Picosecond Pulses in a 140-GHz Gyrotron-Traveling Wave Tube, Physical Review Letters, 105 (2010) 135101 (135101-135104).
[25] E.A. Nanni, S.M. Lewis, M.A. Shapiro, R.G. Griffin, R.J. Temkin, Photonic-Band-Gap Traveling-Wave Gyrotron Amplifier, Physical Review Letters, 111 (2013).
[26] T.V. Can, J.J. Walish, T.M. Swager, R.G. Griffin, Time domain DNP with the NOVEL sequence, The Journal of Chemical Physics, 143 (2015) 054201-054201.
[27] T.V. Can, R.T. Weber, J.J. Walish, T.M. Swager, R.G. Griffin, Ramped-Amplitude NOVEL, J. Chem. Phys., submitted for publication (2016).
[28] A. Henstra, W.T. Wenckebach, Dynamic nuclear polarisation via the integrated solid effect I: theory, Molecular Physics, 112 (2014) 1761-1772.
[29] O. Haze, B. Corzilius, A.A. Smith, R.G. Griffin, T.M. Swager, Water-Soluble Narrow-Line Radicals for Dynamic Nuclear Polarization, J. Am. Chem. Soc., 134 (2012) 14287-14290.
[30] N.S. Dalal, D.E. Kennedy, C.A. McDowell, EPR and ENDOR studies of hyperfine interactions in solutions of stable organic free radicals, The Journal of Chemical Physics, 61 (1974) 1689-1697.

[31] M. Bennati, C. Farrar, J. Bryant, S. Inati, V. Weis, G. Gerfen, P. Riggs-Gelasco, J. Stubbe, R. Griffin, Pulsed electron-nuclear double resonance (ENDOR) at 140 GHz., Journal of Magnetic Resonance, 138 (1999) 232-243.
[32] T.V. Can, M.A. Caporini, F. Mentink-Vigier, B. Corzilius, J.J. Walish, M. Rosay, W.E. Maas, M. Baldus, S. Vega, T.M. Swager, R.G. Griffin, Overhauser effects in insulating solids, Journal of Chemical Physics, 141 (2014) 064202.
[33] T. Reddy, T. Iwama, H. Halpern, V. Rawal, General synthesis of persistent trityl radicals for EPR imaging of biological systems., J Org Chem, 67 (2002) 4635-4639.
[34] S.N. Trukhan, V.F. Yudanov, V.M. Tormyshev, O.Y. Rogozhnikova, D.V. Trukhin, M.K. Bowman, M.D. Krzyaniak, H. Chen, O.N. Martyanov, Hyperfine interactions of narrow-line trityl radical with solvent molecules, Journal of Magnetic Resonance, 233 (2013) 29-36.
[35] Y. Hovav, A. Feintuch, S. Vega, D. Goldfarb, Dynamic nuclear polarization using frequency modulation at 3.34 T, Journal of Magnetic Resonance, 238 (2014) 94-105.
[36] E.A. Nanni, A.B. Barnes, Y. Matsuki, P.P. Woskov, B. Corzilius, R.G. Griffin, R.J. Temkin, Microwave field distribution in a magic angle spinning dynamic nuclear polarization NMR probe, Journal of Magnetic Resonance, 210 (2011) 16-23.
[37] D.E.M. Hoff, B.J. Albert, E.P. Saliba, F.J. Scott, E.J. Choi, M. Mardini, A.B. Barnes, Frequency swept microwaves for hyperfine decoupling and time domain dynamic nuclear polarization, Solid State Nuclear Magnetic Resonance, 72 (2015) 79-89.

Chapter 7: Time Domain DNP at 1.2 T

T.V. Can, R.T. Weber, and R.G. Griffin, In preparation

We present pulsed DNP study at 1.2 T (33.5 GHz/ 51 MHz of electron and proton Larmor frequency, respectively) on a sample of glycerol-d_8/D_2O/H_2O (60/30/10 v/v) doped with 5 mM trityl-OX063 at 80 K. Pulse sequences include constant-amplitude NOVEL (CA-NOVEL), ramped-amplitude NOVEL (RA-NOVEL) and frequency-swept integrated solid effect (FS-ISE) all of which were operated at the NOVEL matching condition, which matches the electron Rabi frequency with the proton Larmor frequency. To the best of our knowledge, this is the first pulsed DNP study carried out at field higher than X-band (0.35 T) using the NOVEL sequence. A combination of strong microwave power (~150 W) and microwave cavity with high quality factor Q (at least ~500) was needed to reach the NOVEL condition. The high Q of the cavity limits the concentration of the radical (5 mM). Nevertheless, we obtained very high DNP enhancements that are comparable to the results at X-band. These promising results will stimulate further study at even higher fields. Our study presents a major step towards pulsed DNP at high fields for NMR applications and has implications on the instrumentation needed to reach the NOVEL condition.

Introduction

The last two decades witness the rapid development of instrumentations for the application of dynamic nuclear polarization (DNP) in enhancing the sensitivity of NMR experiments. At the heart of the instrumentations is the gyrotron, a continuous wave (CW) microwave source operating in the sub-THz frequency regime. The first successful demonstration of DNP using gyrotron was performed at 5 T (140 GHz/211 MHz) in 1993[1-3]. Subsequently, with the first commercial DNP/NMR spectrometer operating at 9.4 T (263 GHz/ 400 MHz) coming online in 2010, the field has since rapidly expanded and matured. Commercial DNP/NMR spectrometers are now available at magnetic field up to 18.1 T (527 GHz/ 800 MHz)[4, 5]. Unfortunately, the DNP enhancement obtained at such high field is only a small fraction of the theoretical limit. This is due to the fact that current CW DNP mechanisms, including the solid effect and cross effect, decrease with increasing the B_0 field[6, 7]. It has become more and more pressing to develop new DNP mechanisms that do not suffer from the same issue. Recently, we demonstrated the performance of pulsed DNP using the NOVEL pulse sequence at 0.35 T[8]. Although our data showed very high efficiency, it is still skeptical whether it is possible to carry out this sequence at high fields used in contemporary NMR applications. Thus, it is important to pursue this experiment at higher fields.

Herein, we present our study of pulsed DNP at the NOVEL condition at 1.2 T. This is the first demonstration at field higher than X-band. We obtained DNP enhancement of ~100 to over 300 with various sequences including NOVEL, ISE and stretched SE. Our study utilized a combination of strong microwave power and high Q microwave cavity as well as an arbitrary waveform generator to reach the NOVEL condition and to modulate the microwave pulses. Our study suggests that it is entirely possible to perform these experiments at field as high as 9.4 T at which commercial EPR driver and gyroamplifer are available.

Experimental

EPR/NMR/DNP experiments were performed at Bruker BioSpin (Billerica, Massachusetts, USA) on a Q-band EPR spectrometer equipped with an ENDOR resonator (ER 5106QT-E). The spectrometer is an extension of a X-band (9.5 GHz) system. The microwave excitation and detection at Q-band (33.5 GHz) were achieved by up/down mixing of the baseband frequency (9.5 GHz) with a local oscillator (~24 GHz), a scheme that is widely used in modern NMR spectrometers. Specifically, the pulses are first formed and modulated by an arbitrary waveform generator (AWG) at X-band and then upconverted to Q-band frequency (33.5 GHz) by mixing with a local oscillator operating at 24 GHz. The resulting pulses are amplified by a traveling-wave tube (TWT) microwave amplifier with a gain of ~51 dB (~150 W maximum output), duty cycle of 10% and maximum pulse length of 100 μs. For EPR detection, the Q-band frequency is downconverted to X-band. For NMR/DNP experiments, the RF coil of the ENDOR resonator is connected to an external tuning/matching circuit (courtesy of Thorsten Marquardsen). The circuit provides excellent tuning range (40 to 60 MHz) with the Q factor of ~40 across that range. Typically, the coil was tune to ~51 MHz in our experiments. All experiments were performed at 80 K on a sample of glycerol-d_8/D_2O/H_2O (60/30/10 volume ratio) doped with 5 mM trityl-OX063. The radical concentration was chosen because higher radical concentrations gave rise to severely distorted EPR signals due to the interaction of the induced field with the high Q cavity.

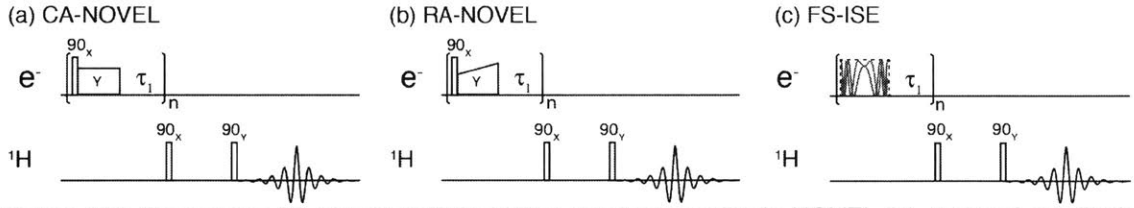

Figure 7.1: Sequences for pulsed DNP including constant amplitude NOVEL (a), ramped-amplitude NOVEL (b), and frequency-swept integrated solid effect (c). All sequences were performed at the NOVEL matching condition, which matches the Rabi frequency of electron with the Larmor frequency of proton. For demonstration purpose, the NMR signal of ^1H was measured using solid echo sequence. In principle, any NMR sequence can be used.

Results

Pulse sequences used in our study, including constant-amplitude NOVEL (CA-NOVEL), ramped-amplitude NOVEL (RA-NOVEL) and frequency-swept integrated solid effect (ISE), are summarized in **Figure 7.1**. In all cases, the electron Rabi frequency was set at or near the NOVEL condition $\omega_{1S}/2\pi = \omega_{0I}/2\pi = 51$ MHz. In order to achieve such a

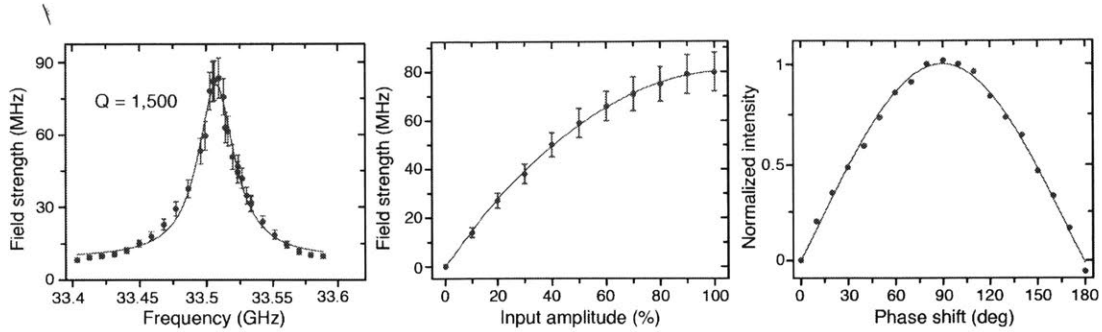

Figure 7.2: Instrumentation needed to reach the NOVEL conditions. A combination of high Q microwave cavity (a) and high power TWT amplifier results in Rabi frequency up to ~80 MHz (b). The maximum output power from the microwave amplifier is 150 W corresponding to 100% input amplitude. In (c) the phase of the locking pulse in CA-NOVEL was varied using the AWG function. The efficiency is maximum at 90° phase shift as expected.

strong microwave field, a combination of high Q microwave cavity and strong microwave power was employed. Shown in **Figure 7.2a** is the measurement of the Q factor of the cavity. The microwave field strength was measured as a function of the frequency, yielding a Q factor of ~1,500. **Figure 7.2b** showed the field strengths at varying TWT input amplitude. A Rabi frequency as high as ~80 MHz was achieved at maximum power level which correspond to ~150 W of microwave power. The inhomogeneity of the microwave field is ~10%. For experiments that require modulation of the microwave pulses such as RA-NOVEL and FS-ISE, an arbitrary waveform generator (AWG) was used. Even in the case of CA-NOVEL, **Figure 7.2c** demonstrates one of the benefits of the AWG, in which the phase of the locking pulse was incremented and the optimum performance of this sequence was obtained at 90° phase shift as expected.

Figure 7.3a compares the microwave field profile of the CA-NOVEL sequence at X- and Q-band. The normalized enhancements were measured at varying microwave field strength $\omega_{1S}/2\pi$ and plotted as functions of the ratio between the electron Rabi and the proton Larmor frequencies ω_{1S}/ω_{0I}. The data at both fields clearly show the NOVEL matching condition at $\omega_{1S}/\omega_{0I}=1$ [9]. In comparison, the matching condition appears to be narrower at higher field. **Figure 7.3b** shows the Zeeman field profiles obtained at the NOVEL condition at Q-band. The magnetic field was incremented while the microwave frequency and its strength were kept constant. The field profile was obtained with and without the 90° flip pulse. Without the flip pulse, the field profile resembles that a of the an unresolved solid effect as opposed to resolved solid effect in low power CW experiment. The field profile obtained with CA-NOVEL (with the flip pulse) shows a maximum at slight off

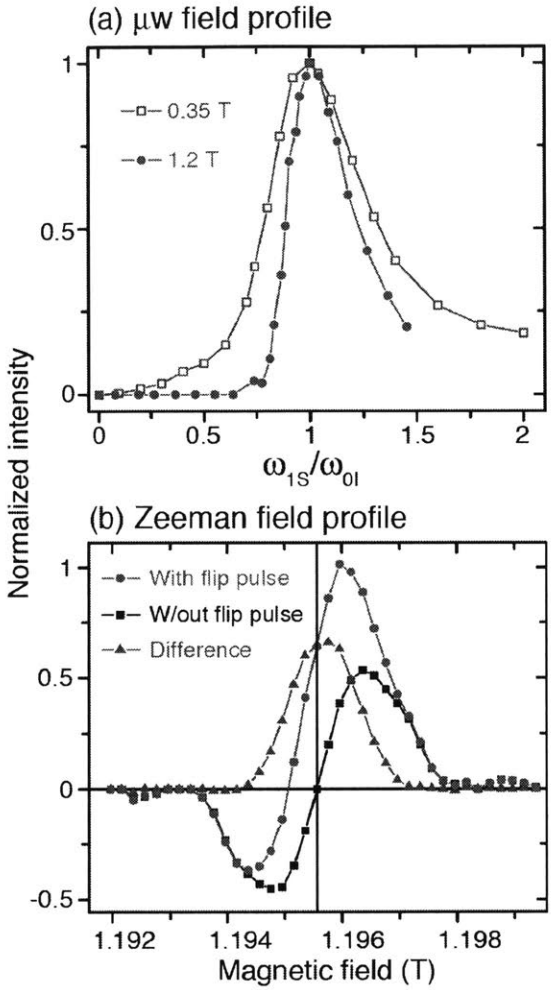

Figure 7.3: (a) Microwave field profile in CA-NOVEL experiment at 0.35 T (blue, open rectangle) an (red, solid circle). The Larmor frequency of ^{1}H was ~14.7 MHz and ~51 MHz, respectively. At higher fi matching condition becomes well defined. (b) The Zeeman DNP field profiles at 1.2 T using CA- sequence (red circle), only the locking pulse (black rectangle), and the difference of the two (blue resembles the EPR lineshape. Sample contains 5 mM trityl-OX063.

resonance. Subtracting the field profile obtained without the flip pulse from that obtained with the flip pulse yielded Gaussian like curve resembling the EPR lineshape.

Next we investigated the performance of RA-NOVEL sequence. The microwave frequency was set on resonant with the EPR spectrum. In **Figure 7.4a**, the length of the locking pulse was varied up to 80 μs which is an order of magnitude longer than what can be achieved at X-band thanks to the high duty cycle of the TWT amplifier at Q-band. This allows us not only confirm the improvement of RA-NOVEL over CA-NOVEL but also observe the decay of the enhancement at long locking pulse which is indicative of the relaxation of the electron in the rotating frame $T_{1\rho,e}$. Ramping the microwave field strength

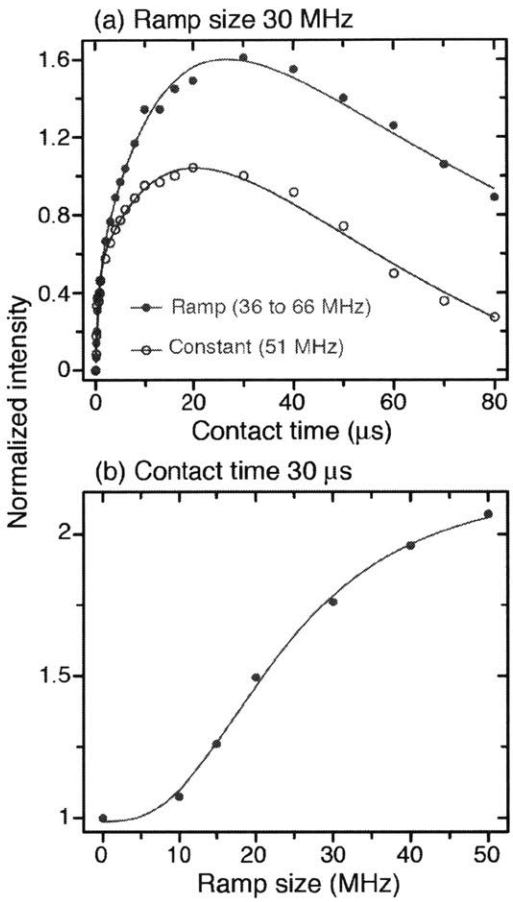

Figure 7.4: (a) Buildup of the DNP enhancement with respect to the contact time in CA-NOVEL (blue, open\circle) and in RA-NOVEL with 30 MHz of ramp size (red, solid circle). In both cases, the optimum enhancements were found at 30 μs of contact time. The efficiency decreases at longer contact time due to the $T_{1\rho}$. (b) The improvement factor as a function of the ramp size at 30 μs contact time.

from 36 to 66 MHz (30 MHz ramp size) improved the efficiency by a factor of 1.6 compared to CA-NOVEL at 51 MHz. Furthermore, the improvement factor reached ~2.1 at ~50 MHz of ramp size (ramp 26 to 76 MHz) which is the largest size possible keeping the center at 51 MHz given the maximum field strength of ~80 MHz.

We then studied the FS-ISE sequence at the NOVEL condition at 1.2 T. We note that a very high Q will lead to nonuniform field strength across the frequency range of the sweep. Thus, for this experiment we slightly overcoupled the microwave cavity to lower the Q factor. The degree of overcoupling was chosen so that the maximum field strength was slightly higher than the proton Larmor frequency. In particular, we used a Q factor of ~465 and the corresponding maximum field strength was ~ 55 MHz (**Figure 7.5a**). The Zeeman field profiles were measured with different sweep widths (**Figure 7.5b)**. At the sweep width of 0

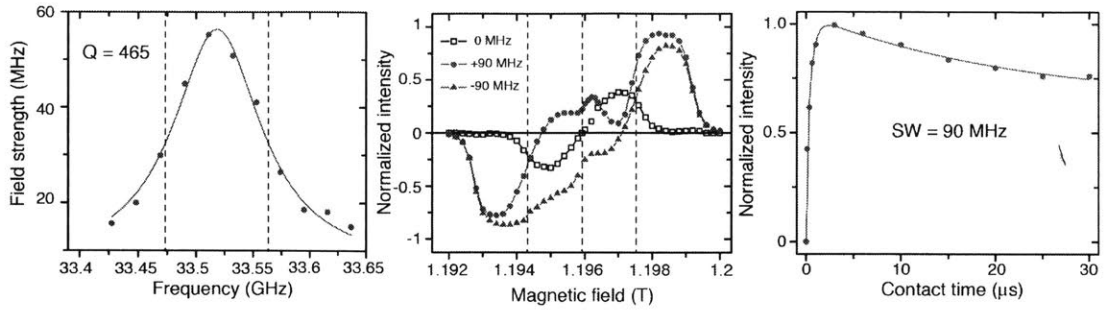

Figure 7.5: (a) In order to perform the FS-ISE sequence, the bandwidth of the cavity was lowered at the cost of a lower Q factor (465 vs. 15,00 in Fig. 2a). Nevertheless, the maximum field strength was ~ 55 MHz which still slightly above the NOVEL condition (~ 51 MHz). (b) Zeeman DNP field profiles obtained without frequency sweeping (0 MHz, black) and with frequency sweeping up (+90 MHz, red) or down (-90 MHz, blue). (c) The buildup curve shows maximum efficiency at 2 μs corresponding to sweep rate of 45 MHz/μs, indicative of the adiabatic nature of the FS-ISE sequence when operating at the NOVEL condition.

MHz (constant microwave frequency), the field profile is essentially the same as the data in **Figure 7.4b** (unresolved solid effect). As the sweep width became nonzero, we observed the characteristic field profiles of the FS-ISE consisting of the ISE part in the middle sandwiched by the negative and positive stretched solid effect field profile. We found that the sign of the stretched SE did not change with respect to the direction of the sweep, whereas the sign of the ISE enhancements flips as we changed the direction of the sweep. In **Figure 7.5c**, we varied the pulse length while keeping the sweep width constant at 90 MHz. The curve confirmed the adiabatic nature of the FS-ISE sequence at the NOVEL condition with an optimum sweep rate of 45 MHz/μs.

Discussion

The combination of high Q and high power requirement immediately explains the challenge to achieve the NOVEL matching condition at high frequency. Keeping the conversion factor and the Q factor the same, in order to reach the NOVEL condition at high field, for example 9 T (250 GHz/380 MHz), the microwave power is estimated to be ~ 3 kW (using 150 W for 80 MHz as the reference). However, from our experience it was possible to achieve electron Rabi frequency of $\omega_{1S}/2\pi \approx 200$ MHz on a similar Q-band spectrometer. Unfortunately, we did not make any effort to reproduce the result. Nevertheless, in that case the estimation for the microwave power at 250 GHz/ 380 MHz would be ~ 500 W which is within the reach of the gyroamplifier being developed by one of our collaborators at MIT. Recently, they demonstrated a circuit gain of ~45 dB using a photonic band gap resonant structure[10]. An input of ~15 mW at 250 GHz would suffice to provide 500 W at the output.

Furthermore, pulse EPR spectrometer operating in that frequency band (263 GHz) is commercially available from Bruker. Thus, we believe that all the technologies needed for the realization of high frequency pulsed DNP are available at the moment. We do expect it to be a large investment and time consuming effort.

The NOVEL microwave field profile (**Figure 7.3a**) appears to be sharper at higher field. This confirms that the NOVEL condition is a trick condition. At X-band one would think the sequence can be performed at relatively lower power level but at higher field it becomes clear that it is not the case. In particular, at Q-band we did not see any enhancement when $\omega_{1S}/\omega_{0I} < 0.75$, whereas at X-band the enhancement reached 50% that obtained at optimum condition with the same ω_{1S}/ω_{0I} ratio[8]. This is probably because of the contribution from the hyperfine coupling broadening out the matching condition gets truncated at higher field. Furthermore, the profile is also sharpened up at higher side of the profile. The broadening of this tail end is due to the hyperfine coupling and/or higher order processes involving one electron and multiple protons, both of which are perturbation effect and also get truncated at higher field. It is likely that at even higher field (>9T), the microwave field profile will be come more symmetric with small broadening effect from the hyperfine coupling and the proton-proton coupling[11].

The Zeeman field profiles in **Figure 7.3b** suggest that the NOVEL field profile can be decomposed into the field profile by the pulsed SE (only locking pulse) and that of an intrinsic NOVEL profile which resembles the EPR lineshape. As a result, the maximum enhancement was obtained at slightly off resonant. In this case, the off resonance is ~ 4 G and leads to ~50% higher enhancement compared to on resonance irradiation. We note that the pulsed SE field profile does not change with respect to the phase of the locking pulse, whereas inverting the phase of the locking pulse results in change in sign of the intrinsic NOVEL enhancement and the maximum enhancement is negative and appears at negative offset. Roughly speaking, the field profiles obtained with opposite phases of the locking pulse are point symmetry image of each other.

Our initial motivation of performing the FS-ISE sequence was to obtained enhancement when microwave irradiation is on resonant with the EPR line. However, the Zeeman field profile reveals also the stretched SE which actually even more efficient than the intrinsic ISE. The presence of stretched SE is now less of a surprise given the work from Shimon Vega group on frequency modulated CW DNP[12]. Nevertheless, it is still worth noting that such an effect was completely ignored in the previous pulsed DNP experiments

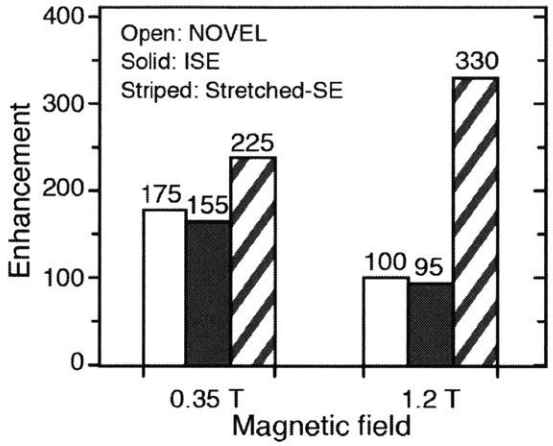

Figure 7.6: Comparison of the enhancements obtained at X-band (0.35 T) and Q-band (1.2 T) using CA-NOVEL, RA-NOVEL and FS-ISE. The same sample of glycerol-d_8/D_2O/H_2O (60/30/10 v/v) doped with 5 mM trityl-OX063 was used.

using photo-excited triplet state[13]. The reason for that was probable due to the requirement for very fast transfer in such experimental settings. For photo-excited triplet state, one needs to take into account the lifetime of the radical created by photo-excitation. We found that the transfer time is ~ 20 μs, which we think is still short enough for many photo-excited triplet state. Therefore, it is worth investigating the usefulness of this effect for photo-excited triplet state DNP. It might be good for high field DNP/NMR as well, because when operating at the NOVEL condition, the unfavorable B_0 field dependence found in CW SE, a consequence of first order perturbation theory is no longer valid.

Finally, we compared the enhancement factor obtained at X-band and Q-band on the same containing 5 mM of trityl-OX063. It is worth noting that, despite the analogy between CP and NOVEL at theoretical level, there is a fundamental difference between the two in practice. In CP the low gamma nuclei are often polarized by multiple surrounding protons. In NOVEL, each electron polarizes thousands of protons due to the order of magnitude difference in their relaxation times. Thus relaxation plays an important role in DNP or pulsed DNP in particular. The relaxation is, in turn, a function of the magnetic field B_0. Thus, it is tricky to know the exact field dependence of pulsed DNP experiments. In any case, we obtained very high DNP enhancements at 1.2 T. For NOVEL and ISE, the enhancements at 1.2 T were smaller than those obtained at 0.35 T (100 vs. 150). On the other hand, the stretched SE showed much higher enhancement at 1.2 T (330 vs. 240).

Conclusions

In summary, we have demonstrated the performance of various pulsed DNP sequences operating at or near the NOVEL condition at highest possible magnetic field at the moment. Our study utilized a Q-band (1.2 T or 33.5 GHz/ 51 MHz of electron and proton Larmor frequency, respectively) pulsed EPR spectrometer equipped with high Q (up to ~1,500) ENDOR resonator. Such a high Q cavity, in addition to a TWT amplifier, enables the NOVEL matching condition at this field. Our result shows that this is a strict condition with a sharp cut off. More importantly, it suggests that this condition can be met at field as high as 9 T with the available technologies including gyroamplifier and high frequency EPR spectrometer.

Acknowledgements

This research was supported by grants to RGG from the National Institutes of Biomedical Imaging and Bioengineering, Grant Nos. EB-002804 and EB-002026. We thank Ajay Thakkar and Jeff Bryant for assistant. Drs. Ivan Sergeyev, James Kempf and Kalina Ranguelova are gratefully appreciated for their help in setting up the instruments.

References

[1] L. Becerra, G. Gerfen, R. Temkin, D. Singel, R. Griffin, Dynamic nuclear polarization with a cyclotron resonance maser at 5 T., Phys. Rev. Lett., 71 (1993) 3561-3564.
[2] L.R. Becerra, G.J. Gerfen, B.F. Bellew, J.A. Bryant, D.A. Hall, S.J. Inati, R.T. Weber, S. Un, T.F. Prisner, A.E. McDermott, K.W. Fishbein, K. Kreischer, R.J. Temkin, D.J. Singel, R.G. Griffin, A Spectrometer for Dynamic Nuclear Polarization and Electron Paramagnetic Resonance at High Frequencies, J. Magn. Reson., A117 (1995) 28-40.
[3] G.J. Gerfen, L.R. Becerra, D.A. Hall, R.G. Griffin, R.J. Temkin, D.J. Singel, High frequency (140 GHz) dynamic nuclear polarization: Polarization transfer to a solute in frozen aqueous solution, J. Chem. Phys., 102 (1995) 9494-9497.
[4] M. Rosay, L. Tometich, S. Pawsey, R. Bader, R. Schauwecker, M. Blank, P.M. Borchard, S.R. Cauffman, K.L. Felch, R.T. Weber, R.J. Temkin, R.G. Griffin, W.E. Maas, Solid-state dynamic nuclear polarization at 263 GHz: spectrometer design and experimental results, Phys. Chem. Chem. Phys., 12 (2010) 5850-5860.
[5] M. Rosay, M. Blank, F. Engelke, Instrumentation for solid-state dynamic nuclear polarization with magic angle spinning NMR, J. Magn. Reson., 264 (2016) 88-98.
[6] Q.Z. Ni, E. Daviso, T.V. Can, E. Markhasin, S.K. Jawla, T.M. Swager, R.J. Temkin, J. Herzfeld, R.G. Griffin, High Frequency Dynamic Nuclear Polarization, Acc. Chem. Res., 46 (2013) 1933-1941.
[7] T.V. Can, Q.Z. Ni, R.G. Griffin, Mechanisms of Dynamic Nuclear Polarization in Insulating Solids, Journal of magnetic resonance (San Diego, Calif. : 1997), 253 (2015) 23-35.
[8] T.V. Can, J.J. Walish, T.M. Swager, R.G. Griffin, Time domain DNP with the NOVEL sequence, J. Chem. Phys., 143 (2015) 054201-054201.
[9] A. Henstra, P. Dirksen, J. Schmidt, W.T. Wenckebach, Nuclear Spin Orientation via Electron Spin Locking (NOVEL), J. Magn. Reson., 77 (1988) 389-393.
[10] E.A. Nanni, S.M. Lewis, M.A. Shapiro, R.G. Griffin, R.J. Temkin, Photonic-Band-Gap Traveling-Wave Gyrotron Amplifier, Phys. Rev. Lett., 111 (2013).

[11] A. Henstra, W.T. Wenckebach, The theory of nuclear orientation via electron spin locking (NOVEL), Mol. Phys., 106 (2008) 859-871.
[12] Y. Hovav, A. Feintuch, S. Vega, D. Goldfarb, Dynamic nuclear polarization using frequency modulation at 3.34 T, J. Magn. Reson., 238 (2014) 94-105.
[13] A. Henstra, P. Dirksen, W.T. Wenckebach, Enhanced dynamic nuclear polarization by the integrated solid effect, Phys. Lett. A, 134 (1988) 134-136.

\

\

\

Chapter 8: High Frequency Integrated Solid Effect

T.V. Can, J.E. McKay, R.T. Weber, T. Dubroca, J. van Tol, S. Hill, and R.G. Griffin,
In preparation

We investigate the frequency-swept integrated solid effect (FS-ISE), a pulsed DNP sequence, at 3.35 T (94 GHz/ 143 MHz of electron and proton Larmor frequency, respectively) on a glassy frozen sample of glycerol-d_8/D_2O/H_2O doped with 10 mM trityl-OX063 at 80 K. Our study utilized the HiPER, a high power, and broadband pulse EPR spectrometer at W-band. The system is equipped with a 1 kW EIK amplifier, resulting in an average microwave field strength of $\omega_{1S}/2\pi = 40$ MHz which amounts to ~30% of the ^{1}H Larmor frequency at this field. The broadband of the spectrometer enabled fast and automated measurement of the DNP frequency profile. Similar to previous study, the profile showed a combination of the ISE and the stretched solid effect. Despite the limitations in the pulse length (10 μs) and the repetition time (2 kHz), we obtained signal enhancements up ~70 for the stretched-SE and ~50 for the ISE. To the best of our knowledge, these are the first results of pulsed DNP at a frequency 10 times higher than all previous studies. Our study has direct implication on the instrumentation required for pulsed DNP at high field and paves the way to high frequency pulsed DNP for NMR applications.

Introduction

Recently, we have demonstrated the performance of frequency-swept integrated solid effect (FS-ISE) pulsed DNP sequence far below the NOVEL condition which matches the electron Rabi frequency with the nuclear Larmor frequency at 0.35 T. Our ultimate goal is to develop pulsed DNP for high field NMR, a task that has been stagnated mainly due to the challenges in generating and coherently controlling high power microwave pulses. This is especially true for the NOVEL experiment, the most promising sequence to date and probably most demanding field strength requirement[1-3]. Thus, the flexibility in power requirement of FS-ISE has motivated us to perform this sequence at highest magnetic field possible. Here, we investigate the feasibility of operating the FS-ISE below the NOVEL condition at three different magnetic fields including 0.35 T (X-band 9.5 GHz/14.7 MHz), 1.2 T (Q-band 33.5 GHz/ 51 MHz), and 3.35 T (W-band 94 GHz/ 143 MHz). In all cases, the same ratio between the electron Rabi frequency and the proton Larmor frequency ω_{1S}/ω_{0I} was kept at 30% corresponding to less than 10% of the microwave power level needed for NOVEL experiments, keeping everything else the same. Specifically, the microwave field strength was set to 4 MHz, 14 MHz, and 40 MHz at X-band, Q-band, and W-band, respectively. Our results at 3.35 T suggest that FS-ISE is a strong candidate for pulsed DNP at high fields.

Experiments

Experiments at 3.35 T (94GHz/143 MHz of electron and proton Larmor frequency, respectively) were performed at the National High Magnetic Field Laboratory (Tallahassee, Florida, USA). In particular, we employed the state-of-the-art high power pulsed EPR (HiPER) spectrometer with 1 kW of microwave power[4, 5]. The microwave pulses were formed at 7.833 GHz and converted to 94 GHz by a 12-fold frequency multiplier. At 94 GHz, the spectrometer can operate in either CW mode with ~200 mW of power or pulsed mode with 1 kW of peak power. In the pulsed mode operation, the microwave power was amplified by an extended interaction klystron (EIK) amplifier with 60 dB of gain and 1 GHz of bandwidth[4, 5]. For EPR detection, induction scheme is used. The transmitting and duplexing of the microwave is achieved by a quasi-optic bridge. The isolation is obtained based on the orthogonal polarizations of the reflected microwave and the signals of interest. The microwave is coupled to the sample via a specially designed waveguide starting out at 50 mm ID and tapering down to 3 mm ID. The cross section of the down taper was carefully designed by computer simulation to maximize the efficiency. The sample container is located inside the 3 mm ID German silver waveguide. We note that this instrumentation does not use a high Q cavity to permit broadband excitation and short dead time needed for pulsed EPR experiments.

For NMR excitation and detection the 3 mm ID waveguide was wrapped with a saddle coil (6 turns, 6 mm in diameter, 10 mm in length). The inductance of the coil was ~ 400 nH. The coil is electrically isolated from the German silver waveguide by a thin Macor sleeve (~1 mm thick). We note that the sample is residing inside a metallic waveguide which effectively shields the sample from the RF field generated by the NMR coil. Thus, the waveguide needs slotting on both sides by electrical discharge machining (EDM) wire cutting similar to the structure used by Burghaus *et al.*[6]. A ceramic capacitor of 2.7 pF (NP0 700 series from ATC) was put in parallel to with the coil. The resulting LC circuit was connected to tuning and matching capacitors on the top of the magnet by a set of two semi-rigid coaxial cables (3.58 mm in outer conductor diameter, 0.91 mm in inner conductor diameter, and 1.3 m in length) to allow convenient adjustment of the RF resonance from outside.

In addition, to modulate the microwave frequency, we used a 2-channel arbitrary waveform generator (AWG) model DAx22000-8M (Chase Scientific, Langley, WA 98260) with 2.5 GSa/s, 12-bit vertical resolution, and 8 MSa of memory per channel. The waveform

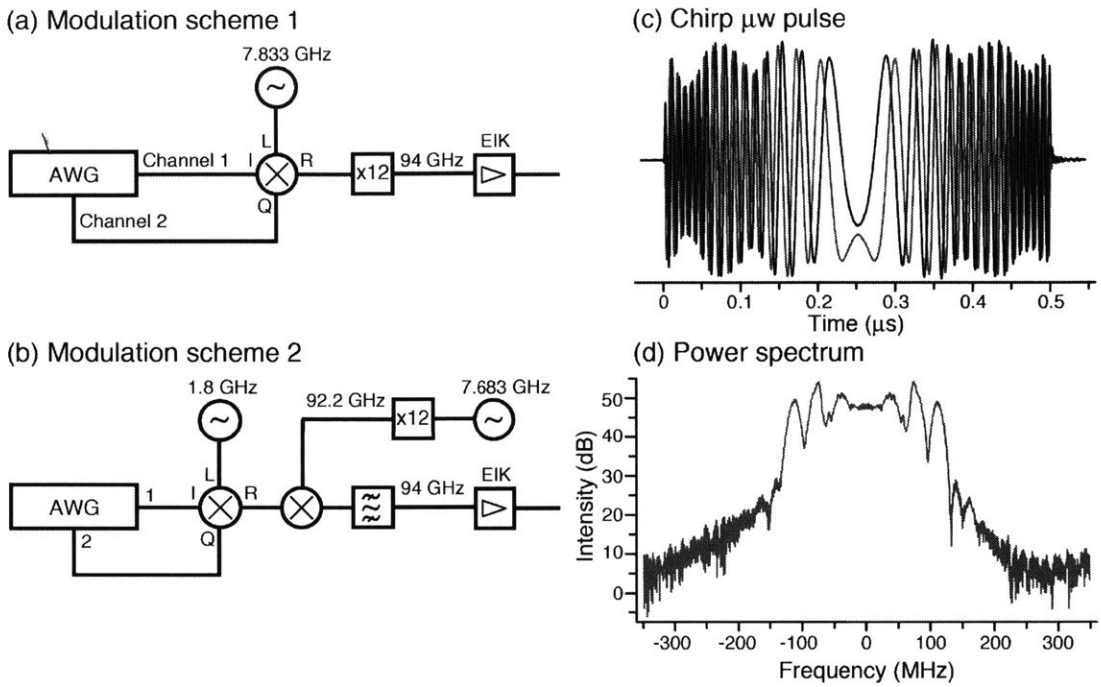

Figure 8.1: (a) and (b) Modulation of the microwave pulses at 94 GHz. In (a), the pulses are first formed and modulated at 7.833 GHz by up-conversion mixing with signals from a 2-channel AWG using an IQ mixer operating at LO frequency in the range of 2-18 GHz. The frequency was then multiplied by 12 to reach 94 GHz. The power was amplified by an EIK to obtained ~1kW output power at 94 GHz. The average $\gamma B_1/2\pi$ was ~40 MHz. (c) An example of a chirp microwave pulse used in ISE experiment. The sweep width was 250 MHz as seen in the corresponding power spectrum in (d). The waveform at 94 GHz was recorded upon down mixing with a reference signal at 92.2 GHz.

from the AWG was mixed with the carrier frequency of 7.833 GHz using an IQ mixer (model MLIQ0218 from Marki Micrrowave) as shown in **Figure 8.1a**. The IQ mixing scheme allows upconversion of the carrier frequency by the AWG signals, resulting in only the sum of the two frequencies as opposed to both sum and difference of the two frequencies in normal mixer. Frequency modulated pulses at 94 GHz were then obtained by a 12-fold frequency multiplier. **Figure 8.1c** features a typical chirp waveform detected at 94 GHz upon downmixing to 1.8 GHz. The waveform shows excellent quality, further error correction can be done by applying transfer functions to the output of the AWG.

Results

Experiments at 3.35 T were performed on a sample consisting of 10 mM trityl-OX063 doped in glycerol-d_8/D_2O/H_2O (60/30/10 volume ratio) glassy matrix at 80 K. Shown in **Figure 8.2a** is the echo detected EPR spectrum together with the solid effect DNP frequency profile. A series of microwave pulses at constant frequency was applied and the DNP frequency profile was obtained by incrementing the microwave frequency. The EPR

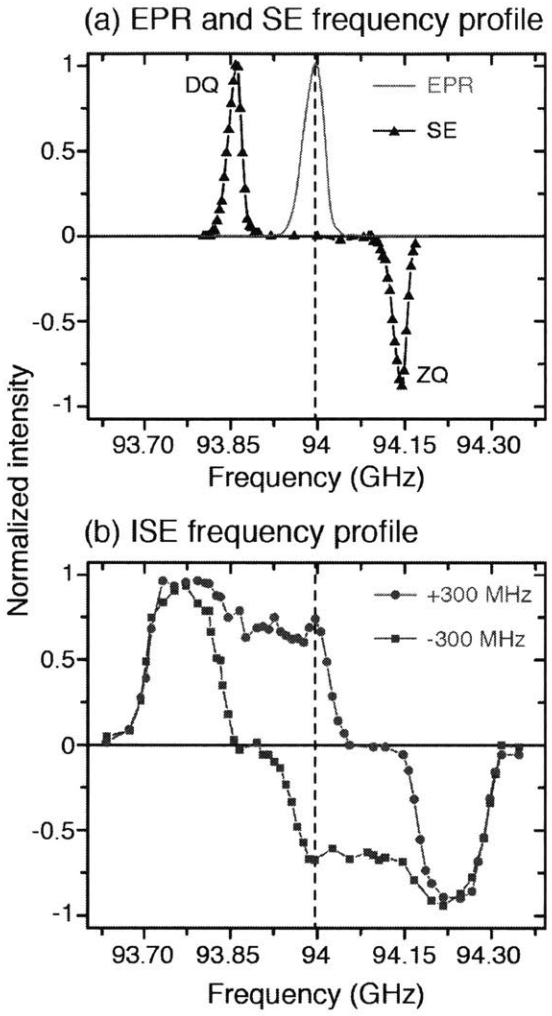

Figure 8.2: (a) Echo detected EPR spectrum and SE frequency profile (constant microwave frequency). (b) ISE frequency profile with sweep width +300 MHz (red) and -300 MHz (blue). Data were taken on a sample of glycerol-d_8/D_2O/H_2O (60/30/10 volume ratio) doped with 10 mM trityl-OX063 at 80K. The average microwave $\gamma B_1/2\pi$ was ~40 MHz. The maximum enhancement for ISE was ~50 due to the restriction in the contact time, the repetition rate (**Figure 8.3**).

spectrum exhibits nearly Gaussian lineshape, indicative of a small anisotropy in the *g*-tensor of trityl-OX063. The DNP field profile consists of the positive and negative peaks displaced from the EPR spectrum by exactly the Larmor frequency of ^{1}H[7, 8]. It is worth noting that the broad bandwidth of the spectrometer facilitates quick and automated acquisition of the field profile by steeping the microwave frequency at constant B_0 thus bypassing the need of adjusting RF tuning/matching.

Shown in **Figure 8.2b** is the DNP frequency profile of the FS-ISE in which microwave chirp pulses were applied repeatedly at repetition rate up to 2 kHz (repetition time of 0.5 ms) and pulse length up to 10 μs. The sweep width of the chirp pulses were +300

MHz or -300 MHz, in which the positive and negative signs correspond to sweeping up and down, respectively. The frequency profile was obtained by incrementing the center frequency of the chirp. The profile consists of the stretched solid effect and the intrinsic ISE. The ISE part is on resonant with the EPR spectrum. The stretched SE is broadened and displaced away from the SE shown in **Figure 8.2a**. Furthermore, the sign of the ISE enhancement change with changing the direction of the sweep as opposed to the stretched SE.

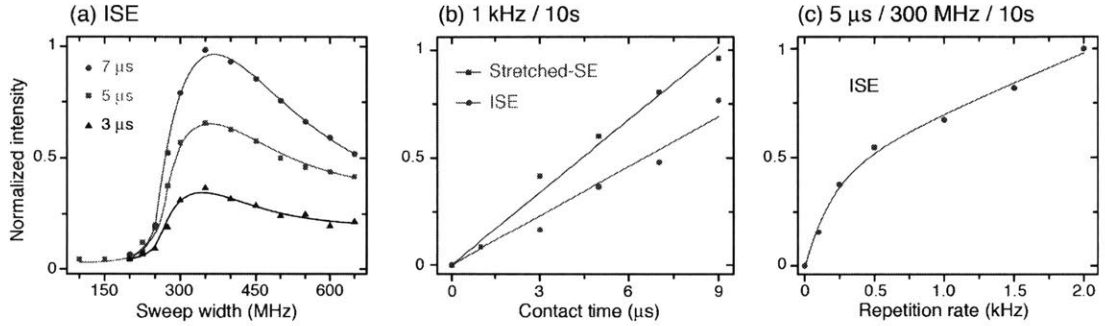

Figure 8.3: (a) ISE DNP enhancement as a function of the sweep width (SW) at different contact time of 3, 5 and 7 µs. Essentially no enhancement was obtained at SW below 225 MHz because such SW was not broad enough to hit the DQ and ZQ transitions separated by twice the ^{1}H Larmor frequency (2*143 MHz) (**Figure 8.2a**). The optimum SW was ~350 MHz which enough to cover the entire SE field profile obtained with SW=0 (**Figure 8.2a**). The enhancement decreases at broader SW, probably because the sweep rate becomes larger and unfavorable. (b) Enhancement as a function of the contact time at SW of 300 MHz. The enhancements obtained at both the center and the displaced-SE+ field position exhibit linear relationships and far away from saturation. (c) ISE enhancement as a function of repetition rate. The enhancement is still growing at fastest repetition allowed by the power supply modulator to the EIK.

In **Figure 8.3a**, we did not see any ISE enhancement when the sweep width is below ~250 MHz. This is because such sweep width is not enough to cover the DQ and ZQ of the SE frequency profile shown in **Figure 8.2a**. The enhancement is maximized at ~350 MHz of sweep width which cover the entire SE frequency profile in **Figure 8.2a**. Broader sweep width lowers the enhancement. **Figure 8.3b** and **c** shows the growth of the enhancement with increasing pulse length and repetition rate. At longest pulse length and highest repetition rate, the enhancement is still far from optimum at this microwave field strength. Nevertheless, we obtained enhancements of up to 70 for the stretched SE and 50 for the ISE. We believe that the enhancements could have been higher given more power, longer pulse length, and repetition rates.

Discussion

Beside the scheme shown in **Figure 8.1a**, it is also possible perform the modulation directly at 94 GHz (**Figure 8.1b**) by mixing the AWG waveform at 1.8 GHz with the carrier frequency at 92.2 GHz. The output would include both the sum (94 GHz) and the difference (90.6 GHz). The low frequency component can be eliminated by a bandpass filter. This scheme has been utilized by Guy *et al.*[9]. In comparison, direct mixing has broader dynamic range and smaller error. However, using a frequency multiplier is more cost effective in out case. Furthermore, such scheme is more practical at higher frequency. For example, commercial pulse EPR spectrometer operating at 263 GHz generated from Q-band frequency via a 8-fold frequency multiplier. Direct modulation at such a high frequency is not available at the moment due to the lack of microwave mixer. On the other hand, modulating at Q-band and multiply the frequency to 263 GHz is entirely feasible. The modulated high frequency microwave pulses can then drive a gyroamplifier to generate strong microwave pules for FS-ISE at high field. This is currently an ongoing project in our laboratory.

To fully employ the advantages of pulsed DNP, in particular the FS-ISE, requires high microwave fields ideally at or near the NOVEL condition. The original goal of HiPER is to perform high power pulsed EPR with short dead time. In our study, the microwave B_1 is ~30% of the ^1H Larmor frequency and we found that at this microwave power level, the contact time needs to be quite long (**Figure 8.3b**). For DNP one does not have to pay as much attention to the dead time thus the Q can be higher for stronger microwave fields that are closer to the NOVEL condition. To increase the B_1, we would need a microwave cavity. At the same time, the quality factor of the cavity cannot be too high because of the requirement of a broadband excitation for the FS-ISE sequence. Note that the sweep width is $\sim 2\omega_{0I}$, thus the Q of the cavity should not be much larger than $\frac{\omega_{0S}}{2\omega_{0I}} \approx 330$.

The current setup has microwave waveguide inside the NMR coil, making it less efficient for RF excitation/detection. Furthermore, the presence of metallic material inside the NMR coil distorts the B_0 field, hampering the NMR resolution. A strategy to overcome this is to integrate the microwave structure (waveguide or cavity) with the NMR coil, an approach that has been used in our design for ENDOR resonator operating at 140 GHz[10]. In this design a helical cavity serves as both an essentially a cylindrical microwave cavity as well as an NMR coil. This can be implemented similar to the design used in micro coil NMR developed in the group of Arno Kentgens[11]. In this design, the sample is contained in a

tiny capillary attached to the end cap of a 4 mm or 2.5 mm rotor. The rotor contains no sample and only served as a mechanical mechanism for the sample spinning.

The disadvantage of the using a microwave cavity is the low filling factor. Typically, the size of the sample has to scale with the wavelength of the microwave, which scales down with frequency. In comparison, the current design of the HiPER has a clear advantage. Specifically, a sample of 10 mm long, 3 mm diameter is use[4, 5]. Current MAS DNP/NMR spectrometer delivers microwave to the sample from the side and perpendicular to the rotor axis. We think that it is worth considering delivering the microwave along the rotor axis with the NMR coil also serves as microwave waveguide. Furthermore, the relatively large waveguide can accommodate various rotor sizes that are being used in MAS NMR (below 3.2 mm), which makes it readily transferable to DNP/NMR applications.

Despite operating far below the optimum condition in term of the pulse length and repetition rate (**Figure 8.3b** and **c**), the enhancements obtained at 3.35 T are only about 2 to 4 times lower compared to the results at lower fields. We have performed experiment at

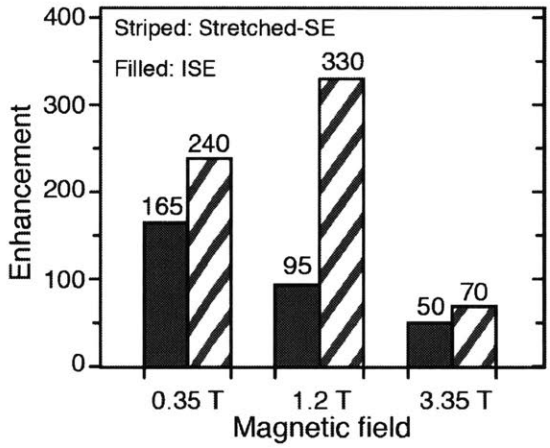

Figure 8.4: Comparison of the FS-ISE enhancement at X-, Q-, and W-band. The corresponding magnetic fields were 0.35 T, 1.2 T and 3.35 T. The data were taken on samples of glycerol-d_8/D_2O/H_2O (60/30/10) doped with trityl-OX063. The data at X- and Q-band were taken on a sample containing 5 mM trityl-OX063, whereas the data at W-band were taken on a sample containing 10 mM trityl-OX063. In all cases, the microwave field strength was set to ~30% of the ^1H Larmor frequency (4 MHz at X-band, 14 MHz at Q-band and 40 MHz at W-band).

three different magnetic fields 0.35 T, 1.2 T and 3.35 T on similar sample conditions and with the same ratio between the electron Rabi frequency and the proton Larmor frequency of ~30% (**Figure 8.4**). We believe that much higher enhancements are entirely possible at optimum conditions. This is the first demonstration of pulsed DNP at frequency 10 times higher than all previously studies.

Conclusions

In summary, we have demonstrated the performance of pulsed DNP at highest microwave frequency (94 GHz) and field strength possible at the moment (40 MHz or 30% of the Larmor frequency of ^{1}H). At this power level, the contact time for the FS-ISE sequence is quite long. Thus the enhancements that we obtained were limited by the pulse length (10 μs) as well as the repetition rate (2 kHz). Nevertheless, enhancements up to 70 and 50 were obtained with the stretched SE and ISE, respectively. It is highly possible that the enhancements can be comparable to results at lower fields (9.5 GHz and 34 GHz). Our findings mark a major step towards pulsed DNP at high frequency and help guide further effort and strategy to perform these experiments at higher fields (> 5 T).

Acknowledgements

A portion of this work was performed at the National High Magnetic Field Laboratory, which is supported by National Science Foundation Cooperative Agreement No. DMR-1157490 and the State of Florida. This research was supported by grants to RGG from the National Institutes of Biomedical Imaging and Bioengineering, Grant Nos. EB-002804 and EB-002026. We thank Peter Gorkov, Bianca Trociewitz, Ajay Thakkar, Jeff Bryant, and Qing Zhe Ni for assistant.

References

[1] A. Henstra, P. Dirksen, J. Schmidt, W.T. Wenckebach, Nuclear Spin Orientation via Electron Spin Locking (NOVEL), J. Magn. Reson., 77 (1988) 389-393.

[2] T.V. Can, J.J. Walish, T.M. Swager, R.G. Griffin, Time domain DNP with the NOVEL sequence, J. Chem. Phys., 143 (2015) 054201-054201.

[3] T.V. Can, Q.Z. Ni, R.G. Griffin, Mechanisms of Dynamic Nuclear Polarization in Insulating Solids, Journal of magnetic resonance (San Diego, Calif. : 1997), 253 (2015) 23-35.

[4] P.A.S. Cruickshank, D.R. Bolton, D.A. Robertson, R.I. Hunter, R.J. Wylde, G.M. Smith, A kilowatt pulsed 94 GHz electron paramagnetic resonance spectrometer with high concentration sensitivity, high instantaneous bandwidth, and low dead time, Rev. Sci. Instrum., 80 (2009) 103102.

[5] R.I. Hunter, P.A.S. Cruickshank, D.R. Bolton, P.C. Riedi, G.M. Smith, High power pulsed dynamic nuclear polarisation at 94 GHz, Phys. Chem. Chem. Phys., (2010).

[6] O. Burghaus, M. Rohrer, T. Gotzinger, M. Plato, K. Mobius, A novel high-field/high-frequency EPR and ENDOR spectrometer operating at 3 mm wavelength, Meas. Sci. Technol., 3 (1992) 765-774.

[7] T.V. Can, M.A. Caporini, F. Mentink-Vigier, B. Corzilius, J.J. Walish, M. Rosay, W.E. Maas, M. Baldus, S. Vega, T.M. Swager, R.G. Griffin, Overhauser effects in insulating solids, J. Chem. Phys., 141 (2014) 064202.

[8] B. Corzilius, A.A. Smith, R.G. Griffin, Solid effect in magic angle spinning dynamic nuclear polarization, J. Chem. Phys., (2012).

[9] M.L. Guy, L. Zhu, C. Ramanathan, Design and characterization of a W-band system for modulated DNP experiments, J. Magn. Reson., 261 (2015) 11-18.

[10] A.A. Smith, B. Corzilius, J. Bryant, R. DeRocher, P.P. Woskov, R.J. Temkin, R.G. Griffin, A 140 GHz pulsed EPR/212 MHz NMR spectrometer for DNP studies, J. Magn. Reson., 223 (2012) 170-179.
[11] A.P.M. Kentgens, J. Bart, P.J.M. van Bentum, A. Brinkmann, E.R.H. van Eck, J.G.E. Gardeniers, J.W.G. Janssen, P. Knijn, S. Vasa, M.H.W. Verkuijlen, High-resolution liquid- and solid-state nuclear magnetic resonance of nanoliter sample volumes using microcoil detectors, J. Chem. Phys., 128 (2008) 052202-052217.